

Master Thesis - Time domain modeling of a point absorber

Master Offshore Engineering and Dredging Technology

TU Delft &

Dutch Wave Power

Autor: Wouter Grolman

Chairperson: Dr.ir. A. Jarquin Laguna

First supervisor: J. Tan Msc

Second supervisor: Dr.-Ing. S. Schreier

June 24, 2022

Abstract

The demand for renewable energies is rising due to climate goals and high oil prices. Not only the established renewable sources like wind and solar are interesting to exploit. There is a vast amount of energy stored in the world's oceans. To harvest this energy, one needs a Wave Energy Converter (WEC). There are already some prototype WECs tested around the world but there is no leading design that proves to be a cost-effective way to convert this energy to electricity.

A company from the Netherlands, Dutch Wave Power, also tries to build a cost-effective device to harvest the ocean's energy. Their design consists of a floating tube or cylinder that converts the heave and sway motion into a pitch motion. This pitch motion drives a generator which generates electrical power. The generator is connected to the outer wall of the float and rotates as the float pitches. Inside the generator is a shaft that is kept in place by an inside pendulum. Dutch Wave Power validated their concept with experimental tests in a wave flume. The next step in the development is a numerical model. This model gives insight into the effects that influence the dynamics and power production of the WEC. Secondly, a numerical model eliminates the need for new experimental tests each time a design parameter is changed.

The numerical model estimates the dynamics of the WEC. The BEM software NEMOH is used to estimate the diffraction and radiation forces coefficients. A state-space approximation of the Cummins equation is used to capture the memory effect of the radiation forces. The Froude-Krylov forces are fully non-linear and are evaluated for each time step. Lastly, some friction and drag forces are included. The PTO system is described as a linear damper. The numerical model is validated with experimental tests executed by Dutch Wave Power.

Next, the numerical model is adapted to also estimate the hydrodynamics in irregular waves. The irregular waves used in this thesis are based on a JONSWAP spectrum. Using the parameters of the JONSWAP spectrum, a sea-state with the desired significant wave height and peak period can be generated. The Froude-Krylov and the diffraction forces are estimated based on the principle of superposition. With this irregular wave model, a power matrix is constructed for a WEC with twice the size that was used in the experimental tests. This power matrix gives an indication of the ideal operational wave conditions, where the efficiency of the WEC is the highest, and it makes it enables the possibility to compare the performance of the WEC at different sea-states.

Contents

1	Introduction	1
1.1	Wave Energy	1
1.2	The Wave Energy Converter developed by Dutch Wave Power	1
1.3	Objective & Scope	4
1.3.1	Objective	4
1.3.2	Research questions	4
1.3.3	Scope	4
1.4	Structure of this thesis	5
2	Theoretical model	6
2.1	System description	6
2.2	Model derivation	8
2.2.1	Equations of motion	8
2.2.2	Hydrostatic force	9
2.2.3	Excitation force	9
2.2.4	Radiation force	10
2.2.5	Drag force	10
2.2.6	Ballast force	10
2.2.7	Tension force	11
2.2.8	PTO moment & electrical power generation	12
2.3	Calculation method	13
2.3.1	ODE45 solver	13
2.3.2	Non-linear buoyancy and Froude-Krylov force	14
2.3.3	NEMOH	15
2.3.4	State-space approximation of the radiation force	17
2.4	Model verification	18
2.4.1	Free decay tests	19
2.4.2	Free decay test - surge	21
2.4.3	Response of regular waves	22
2.5	Discussion & limitations	24
3	Experimental scale tests	27
3.1	Test setup	27
3.1.1	Scale model	27
3.1.2	Wave flume	29
3.1.3	Test parameters & wave characteristics	29
3.2	Data processing	30
3.2.1	Correction of the raw data	30
3.2.2	Clean wave selection	30
3.2.3	Angular velocities	32
3.3	Observations during the tests	34
3.3.1	Overtopping	35
3.3.2	Slack in the ballast line	36
3.3.3	Full rotation of the pendulum	36
3.3.4	Wave reflection	36
3.4	Discussion	36

4	Validation of the model	37
4.1	Comparison of the numerical model and the experimental tests	37
4.1.1	Input parameters for the numerical model	37
4.1.2	Find the PTO-damper value to match the experiments	38
4.2	Compare dynamics	39
4.2.1	Pitch angle	39
4.2.2	Pendulum angle	40
4.2.3	Surge motion	40
4.3	Compare Produced Power	42
4.4	Validation of the ideal damper as a PTO-system	42
4.5	Compare generator settings with the numerical maximum	44
4.6	Improving the WEC performance	46
4.6.1	Pendulum Weight	46
4.6.2	Winding diameter	48
4.7	Discussion and conclusion	50
5	Irregular wave model prediction	52
5.1	Irregular waves	52
5.1.1	Wave spectrum	52
5.1.2	JONSWAP spectrum	53
5.2	Adaptation of the model for irregular waves	54
5.2.1	Wave input and ramp-up time	54
5.2.2	Froude-Krylov force	54
5.2.3	Diffraction force	55
5.2.4	Results	55
5.3	Optimizing the PTO damper for irregular waves	57
5.4	1:2 Scale model predictions	59
5.4.1	Froude scaling	59
5.4.2	Power matrix	60
5.4.3	Discussion	61
6	Conclusions & Recommendation	63
6.1	Conclusions	63
6.2	Recommendations	64
6.2.1	Recommendations - numerical model	64
6.2.2	Recommendations - Further research	64
APPENDICES		
A	Equations of motion of the WEC	68
B	Derivation of the pendulum angle θ	69
C	Derivation Line Tension	71
D	Experimental Test results - Unprocessed data	72
E	Experimental Test results - Comparison with the theoretical model	77

List of Figures

1.1	Concept of Dutch Wave Power	2
1.2	Dutch Wave Power concept - Components	3
1.3	Working principle of the inside pendulum	3
2.1	Free body diagram	7
2.2	Forces acting on the system	8
2.3	Simplified free body diagram to solve the line tension	11
2.4	Theoretical generator efficiency	13
2.5	Derivation of the pressure integral	15
2.6	3D model of the WEC at still water draft in SALOME	16
2.7	Mesh of the SALOME model	16
2.8	Diffraction force coefficients and phase shifts	17
2.9	Theoretical model at SWL	19
2.10	Free decay test: Heave displacement	20
2.11	Free decay test: Resulting forces on the WEC	21
2.12	Free decay test in surge: surge motion	22
2.13	Free decay test in surge: Resulting forces on the WEC	22
2.14	Dynamic response of a test with $H=1\text{m}$ and $T=6.5\text{s}$	23
2.15	Resulting forces of a test with $H=1\text{m}$ and $T=6.5\text{s}$	24
2.16	Resulting forces, with linear FK force in surge $H=1\text{m}$ and $T=6.5\text{s}$	25
2.17	Heave displacement and velocity of the WEC $H=1, T=6.5\text{s}$	26
3.1	Test setup in the wave flume	28
3.2	Generator efficiency curve	28
3.3	Schematic side- and top view of the experimental setup	29
3.4	Test 4: Time series results and selected waves	31
3.5	Test 4: 5 Clean waves corrected for the mean	32
3.6	Test 4: Compare the original signal with the re-sampled signal	33
3.7	Test 4: Velocities computed with the function gradient	33
3.8	Test 4: Filtered velocities	34
3.9	Integrated velocity signal compared with the original positions	34
3.10	Unwanted behaviour during the experimental scale tests: Complete submersion 1	35
3.11	Unwanted behaviour during the experimental scale tests: Complete submersion 2	35
4.1	Compare the dynamic response for different PTO-damper values	38
4.2	Comparison between the numerical model and the experiments	39
4.3	Comparison between numerical model and experiments $H=1\text{m}, P=7\text{s}$	40
4.4	Test 1: Minimum surge	41
4.5	Test 7: Minimum surge	41
4.6	Test 1: Maximum surge	41
4.7	Test 7: Maximum surge	41
4.8	Relative velocity plotted against mechanical power $H=1\text{m } T=7\text{sec}$	43
4.9	Relative velocity plotted against torque inside the generator $H=1\text{m } T=7\text{sec}$	44
4.10	Mean power compared to different PTO-damper values	45
4.11	Efficiency compared to different PTO-damper values	46
4.12	Mean produced power for different pendulum weights with a sea-state of 1m and 7sec	47

4.13	Dynamic response for different pendulum weights	48
4.14	Mean produced powers for different r_{in} against different PTO damper values	49
4.15	Dynamics of the WEC for different PTO damper values	50
5.1	Irregular waves from the sum of regular waves	52
5.2	Wave spectrum	53
5.3	Example of a JONSWAP spectrum	54
5.4	Irregular waves: Heave motion and Wave elevation $H_s = 1m$ $T_p = 6.5sec$	55
5.5	Irregular waves: model output $H_s = 1m$ $T_p = 6.5sec$	56
5.6	Irregular waves: Heave motion and Wave elevation $H_s = 2m$ $T_p = 8.5sec$	56
5.7	Irregular waves: model output $H_s = 2m$ $T_p = 8.5sec$	57
5.8	Mean power for different PTO-damper values for regular and irregular waves	58
5.9	Compare two PTO settings	59
5.10	Wave scatter data for the L9 platform in the North Sea	60
5.11	Mean produced power and the energy capture ratios for an irregular sea-state and different scale factors	61
B.1	Pendulum on a moving support	69
C.1	Solve the F_T in 2D	71
D.1	Unprocessed data Test 1: $H=1m$ $T=6sec$ $Load=80\Omega$	73
D.2	Unprocessed data Test 2: $H=1m$ $T=6sec$ $Load=120\Omega$	73
D.3	Unprocessed data Test 3: $H=1m$ $T=7sec$ $Load=80\Omega$	74
D.4	Unprocessed data Test 4: $H=1m$ $T=7sec$ $Load=120\Omega$	74
D.5	Unprocessed data Test 5: $H=1m$ $T=8sec$ $Load=80\Omega$	75
D.6	Unprocessed data Test 6: $H=1m$ $T=8sec$ $Load=120\Omega$	75
D.7	Unprocessed data Test 7: $H=1m$ $T=9sec$ $Load=80\Omega$	76
E.1	Comparison of Test 1 with the theoretical model	78
E.2	Comparison of Test 2 with the theoretical model	79
E.3	Comparison of Test 3 with the theoretical model	80
E.4	Comparison of Test 4 with the theoretical model	81
E.5	Comparison of Test 5 with the theoretical model	82
E.6	Comparison of Test 6 with the theoretical model	83
E.7	Comparison of Test 7 with the theoretical model	84

List of Tables

- 2.1 Suggested drag coefficients 10
- 2.2 Coefficients of the generator efficiency polynomial 12
- 2.3 Theoretical model outputs 18
- 2.4 Parameters used in the theoretical model 19

- 3.1 List of experiments and parameters 30
- 3.2 Changes made in the raw data 30

- 4.1 Errors in the dynamics with the tuned damper 39
- 4.2 Observed surge motions 41
- 4.3 Comparison between the mean power and maximum power of the numerical model 42
- 4.4 The optimal PTO-damper values 46

- 5.1 Froude Scaling Laws 60

- D.1 List of experimental tests, parameters and corresponding figures 72

List of Symbols

A_{∞}	Added mass at infinite wave frequency
B_{PTO}	Linear PTO damper
C_d	Drag coefficient
c_g	Group velocity
C_{diff}	Diffraction force coefficient
d	Water depth
E_{wave}	Energy stored in the wave
$F_{Ballast}$	Ballast line force
F_{Diff}	Diffraction force
F_{Drag}	Drag force
$F_{Excitation}$	Excitation force
$F_{External}$	External force
F_{FK}	Froude-Krylov force
F_g	Gravity force
F_{HS}	Hydrostatic force
$F_{Mooring}$	Mooring line force
F_{PTO}	Power take-off force
F_{rad}	Radiation force
$F_{Tension}$	Line tension force
g	Gravitational acceleration
h	Water depth
J	Mass moment of inertia of the WEC
k	Wave number
k_r	Impulse response function
$l(t)$	Length of the mooring line
L_{pen}	Length of the pendulum
\bar{M}	Mass matrix
$M_{External}$	PTO moment
M_{PTO}	PTO moment
m_1	Mass of the WEC
m_2	Mass of the inside pendulum
m_3	Mass of the ballast weight
n	Number of wave components
$P_{dynamic}$	Dynamic water pressure
P_{static}	Static water pressure
$P_{Electrical}$	Electrical power
$P_{Mechanical}$	Mechanical power
P_{wave}	Energy flux moving through a vertical plane
\bar{q}	State vector of the ODE function
r_{in}	Radius of the inner part of the WEC
r_{out}	Radius of the WEC
S	Wet hull surface
S_{ζ}	Wave spectrum
t	Current time
T	Still water draft of the WEC
$T_{simulation}$	Total simulation time
$x(t)$	Surge position of the WEC
\bar{X}	3x1 position vector

$\bar{\dot{X}}$	3x1 velocity vector
$\bar{\ddot{X}}$	3x1 acceleration vector
x_r	State space of the radiation force approximation
$z(t)$	Heave position of the WEC
$\alpha(t)$	Angle of the mooring line with the sea floor
Δf	Frequency bandwidth in hertz
$\Delta\sigma$	Frequency bandwidth in radians
ζ_a	Wave amplitude
η	Surface elevation
$\eta_{generator}$	Generator efficiency
ϵ	Phase shift
$\theta(t)$	Angle of the pendulum
ρ	Water density
$\sigma(t)$	Pitching angle of the WEC
ω	Wave frequency

Chapter 1

Introduction

1.1 Wave Energy

Intending to become a carbon-neutral society, the interest in renewable energies only grows. To achieve this, we need more sources than only wind and solar. One mostly neglected source with huge potential is the world's oceans. The oceans hold a vast amount of energy that could add a significant portion to our energy demand. The amount of potential power stored in the open oceans is estimated to be ($\sim 10^{13}W$) [1] [2]. A device that harvests the energy in ocean waves is called a Wave Energy Converter (WEC).

There are already many concepts of WECs based on different conversion types. There is a lot of progress in theoretical studies, experiments and model testing of WEC prototypes. Some small scale prototypes are deployed and tested [3] [4] [5]. However, to become economically viable, significant cost reductions are necessary, especially when compared to much more developed alternatives of solar and wind [6]. The challenges identified for wave energy converters range from techno-economic problems to issues affecting their operation and maintenance. One of the major challenges militating against the use of WECs is that the technologies are still in an early stage of development in comparison to wind and solar [7] [8] [7] [9].

1.2 The Wave Energy Converter developed by Dutch Wave Power

One of the companies looking to build a cost-effective WEC is the Dutch-based company Dutch Wave Power, founded in 2020. They have developed a new concept with the promise to be cost-effective, efficient and robust. Their concept consists of a floating tube with all the components stored inside the tube/cylinder. The tube, also called "float", can move freely in surge and heave. But due to a cable wind around the float, the pitch motions are coupled to surge and heave, see figure 1.1.

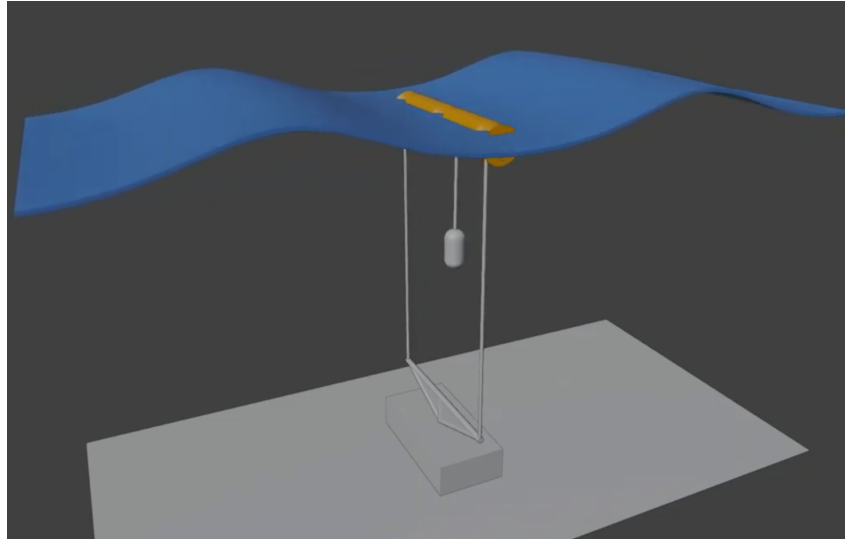


Figure 1.1: Concept of Dutch Wave Power

To better understand the working principle of the WEC, figure 1.2 shows its main components, as indicated by numbers. The WEC consists of the float (1), the mooring line (2), the ballast weight (3) and the ballast line (4). The WEC of Dutch Wave Power captures the wave energy in the following way. The float provides enough buoyancy force for the device to float. The WEC gets pushed up and sideways due to the incoming waves. The mooring line is wound around the ends of the float. This means that the WEC starts rotating, pitching, if it moves in heave or sway, just like an upside-down JoJo-toy. Due to the pitching motion, the ballast weight is lifted. Because the ballast line is wound around the float in the other direction, it ensures that the floater returns to its original position after a wave has passed.

The WEC moves due to the wave excitation forces. A part of the mechanical energy gets converted into electricity with a rotational generator that is connected to the hull of the float. Normally a shaft is rotated inside the generator, but in this concept the generator is connected to the float. This means that the generator rotates while this shaft is kept as steady as possible. The energy is generated by the rotational speed difference in the shaft and the float.

Seeing that the shaft is also located inside the float, the challenge is to decouple the shaft's movement from the float's movement. To keep the shaft steady, a pendulum is connected to the shaft inside the float. The inside pendulum ensures that the shaft is kept steady and that electricity gets generated. If a wave initiates a rotational movement of the float, the generator enforces a moment on the shaft. This turns the pendulum out of its neutral position, which creates a moment in counter direction of the one created by the generator. This moment is what keeps the shaft from rotating. If the float changes pitching direction and starts rotating in the opposite direction, the pendulum swings to the other side and generates a moment using the same principle. Figure 1.3 shows the working principle of the inside pendulum.

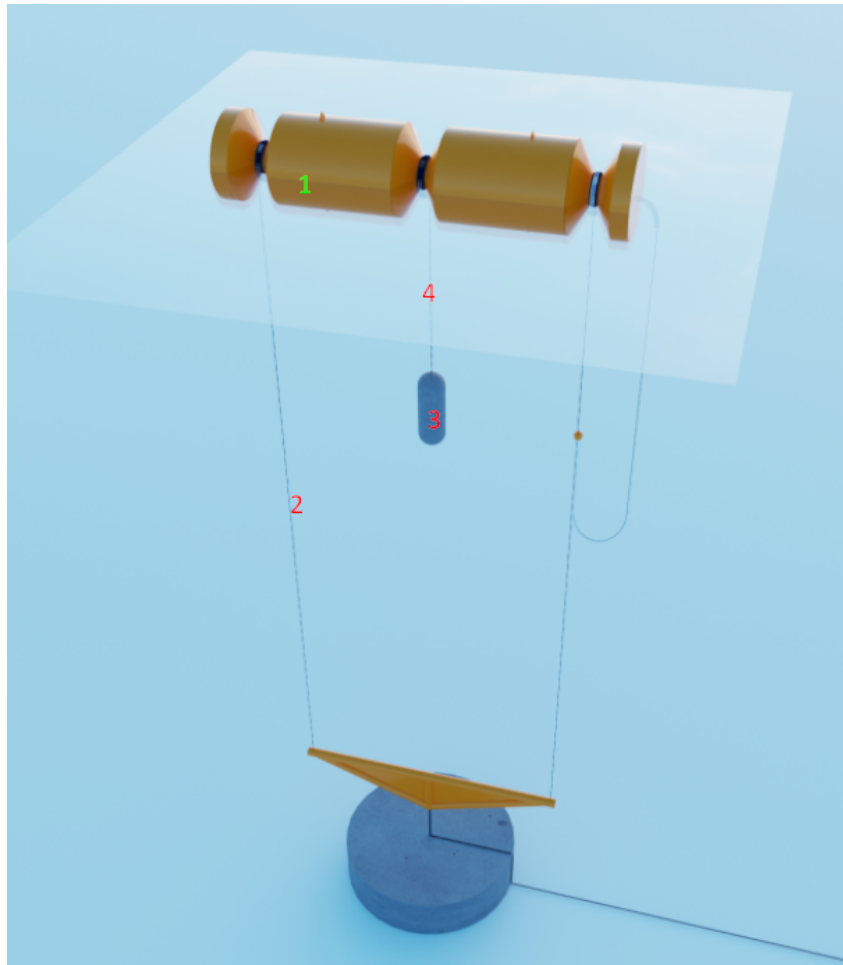


Figure 1.2: Dutch Wave Power concept - Components

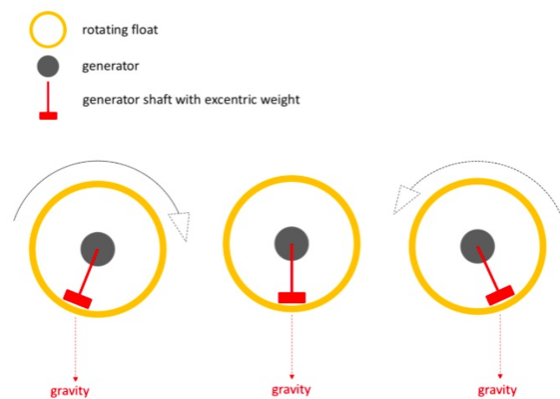


Figure 1.3: Working principle of the inside pendulum

Dutch Wave Power tested this concept first in their own build wave flume. To validate their concept, they got the chance to build a 1:3 scale model and tested this model in the wave flume at Deltares. This validated their idea but also increased the need for more research on the working principle of their WEC. One of the ways to research this is the development of a numerical model. With a numerical model, the influence of different forces and effects can be studied. A numerical model can be either built in the frequency domain or in the time-domain. For this thesis, it is chosen to build the numerical model in

the time domain. Time-domain models are usually better in estimating non-linear forces. For this WEC some non-linear forces are expected to influence the performance of the WEC. For example, during the experimental tests, a large change in draft was observed. To capture this change in draft, an analytical method is used to calculate the Froude-Krylov force acting on the WEC. This thesis includes all the work done while developing a numerical time-domain model of the WEC developed by Dutch Wave Power.

1.3 Objective & Scope

1.3.1 Objective

The objective of this master thesis is to gain a better understanding of the forces and effects that influence the hydrodynamic behaviour of the WEC developed by Dutch Wave Power. To achieve this a numerical model will be constructed. This numerical model will be validated with experimental test results executed by Dutch Wave Power. After validation with the experimental data, recommendations will be given to improve the energy production of the WEC based on the results of numerical model.

1.3.2 Research questions

Now that the objective is defined, the following research questions can be formulated. These will help guide the thesis in the right direction.

- What is the hydrodynamic response, of the WEC of Dutch Wave Power, in a 2D the time-domain model?
- How are the non-linearity's, associated with the large change in draft, captured in a numerical model?
- How is the performance of the WEC influenced by changes in the parameters of the novel PTO system?
- What is the estimated response in irregular waves?
- Can the numerical model estimate the produced power?

1.3.3 Scope

To simplify, the model will be in 2D with only unidirectional waves. This approximation holds when the WEC is small with respect to wave lengths. First, the equations of motions will be derived. Next for each force component, an estimation is made based on the estimations available in the literature. The goal is to find an analytical expression for the non-linear Froude-Krylov and hydrostatic forces. Secondly, a BEM solver, NEMOH, will be used to obtain the radiation and diffraction terms. A simplified model of the PTO system will be used in the form of a linear damper. The mooring lines will be considered as an analytical expressed force based on the dynamics. This means that there is no slack possible in the lines. Lastly, the ballast weight is estimated by a downward pulling force. While in the concept, the ballast weight is free to move. The simplifications of the lines are made because there is no data available on the forces or angles of the lines. The same holds for the PTO-system. There is not enough data available on the generator to make a more detailed PTO-system. With estimations for all the different force components, an ordinary differential equation solver will estimate the dynamic response of the system.

The results of the numerical model will be validated with the test results of Dutch Wave Power. To do this, the results need to be analyzed and post-processed. From all the test data there is video material available. This will be reviewed to spot any noticeable effects. Secondly, there is data available from the experimental tests. During the tests, there is time-series data from the pitch angle, the angle of the inside pendulum and the produced electrical power. This data will be compared with results from the numerical model.

The experimental tests executed by Dutch Wave Power, are done with regular waves. This is why the numerical model will first only include regular waves. After the numerical results are validated with the experimental tests. The model is adapted to also estimate the response in irregular waves.

1.4 Structure of this thesis

The first part of this thesis, chapter 2, describes the numerical model. The equations of motion are derived and described. Next, an approximation is given for all the different force components. The chapter is concluded with a discussion and the limitations of the model.

Chapter 3 describes the experimental tests executed by Dutch Wave Power prior to this thesis. The test setup and results are described. In the second part of this chapter, the data is reviewed and it is described how this data is processed to be able to compare and validate the numerical model.

The comparison between the numerical model and the experimental tests is done in chapter 4. This chapter explains the shortcomings of the numerical model and how the numerical model can be tuned to best reproduce the experimental tests on the computer. This chapter also gives an idea of the ideal PTO settings and shows the potential of the WEC if it is tuned to the wave conditions.

In the last part of this thesis, chapter 5, the numerical model is adapted for irregular waves. With this model not only the performance of this WEC can be estimated, but it can also be scaled. This is done for a scale factor of 2. The performance of this scaled WEC is shown in a power matrix. This power matrix can be used to estimate the performance of the WEC if the wave climate at a site is known.

The thesis will be concluded with a final discussion and conclusion. Here the overall findings of this thesis are summarized.

Chapter 2

Theoretical model

In this chapter, the time-domain model of the WEC of Dutch Wave Power is described. In chapter 3 is the working principle of the WEC described. In chapter 3 are also the experimental tests described that are used to validate the theoretical model. In the first part of the thesis, a 2D simplification of the WEC is made. The equations of motion, the constraints and some conventions are described. In the second part of this chapter, an approximation for all the different force components is given. Next, the integration method to solve the differential equations is described. The chapter is concluded with an example of the output of the model and discusses its limitations.

2.1 System description

For this numerical model, it is assumed that the WEC is a ridged body and the equations of motion can be described according to the numerical models that have been used frequently in the offshore and ship industry, see equation 2.1 [4] [10] [11] [12] [13] [14] [15]. For the 2D case, this corresponds with the free-body diagrams in figures 2.1 and 2.2. \bar{M} is a 3x3 mass matrix for surge, heave and pitch. $\bar{\ddot{X}}$ is a 3x1 acceleration matrix containing the accelerations in surge, heave and pitch. F_{Rad} are the radiation forces. F_{Diff} are the diffraction forces. F_{HS} are the hydrostatic forces. F_{FK} are the Froude-Krylov forces. F_{drag} are the drag forces. F_{PTO} are the PTO forces and $F_{Mooring}$ are the mooring forces. The mass of the WEC, the mass of the pendulum and the mass of the ballast weight are respectively m_1 , m_2 and m_3 . The diameter of the WEC is r_{out} and inertia moment J around the y -axis. The part where the lines are connected has a diameter of r_{in} and the length of the pendulum is L_{pen} . The draft is described with T and the water depth with d . The WEC can move in surge ($x(t)$) and in heave ($z(t)$) and pitch ($\sigma(t)$). The angle of the pendulum is described by $\theta(t)$. These motions change length of the mooring line ($l(t)$) and the angle of the mooring line at the seafloor $\alpha(t)$. In the model, the waves are propagating from left to right.

$$\bar{M}\bar{\ddot{x}} = \bar{F}_{Rad} + \bar{F}_{Diff} + \bar{F}_{HS} + \bar{F}_{FK} + \bar{F}_{Drag} + \bar{F}_{PTO} + \bar{F}_{Mooring} \quad (2.1)$$

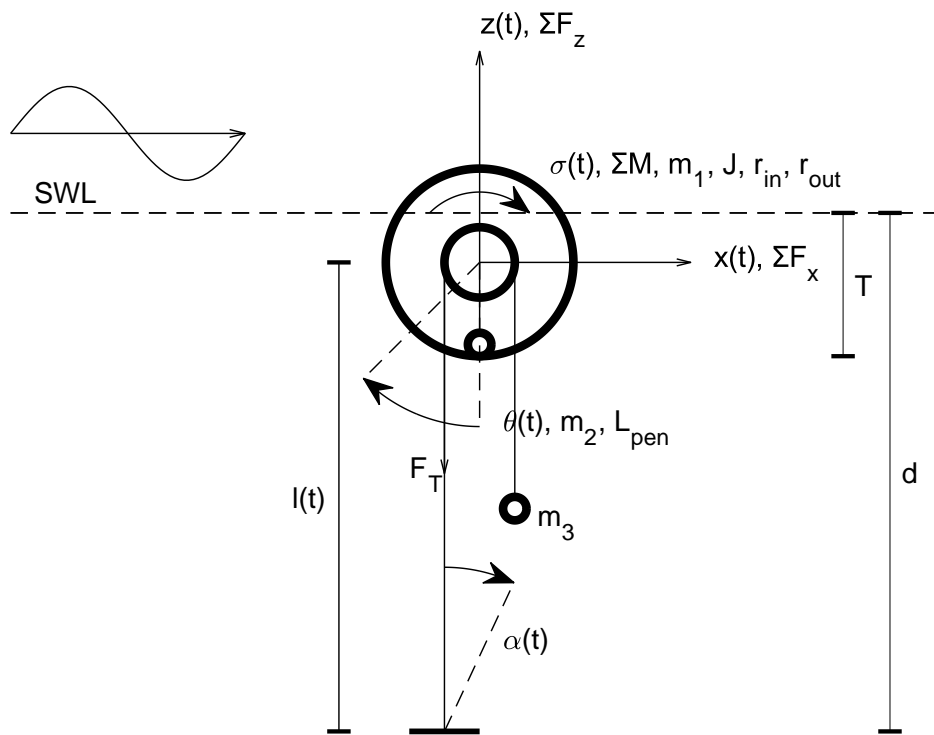


Figure 2.1: Free body diagram

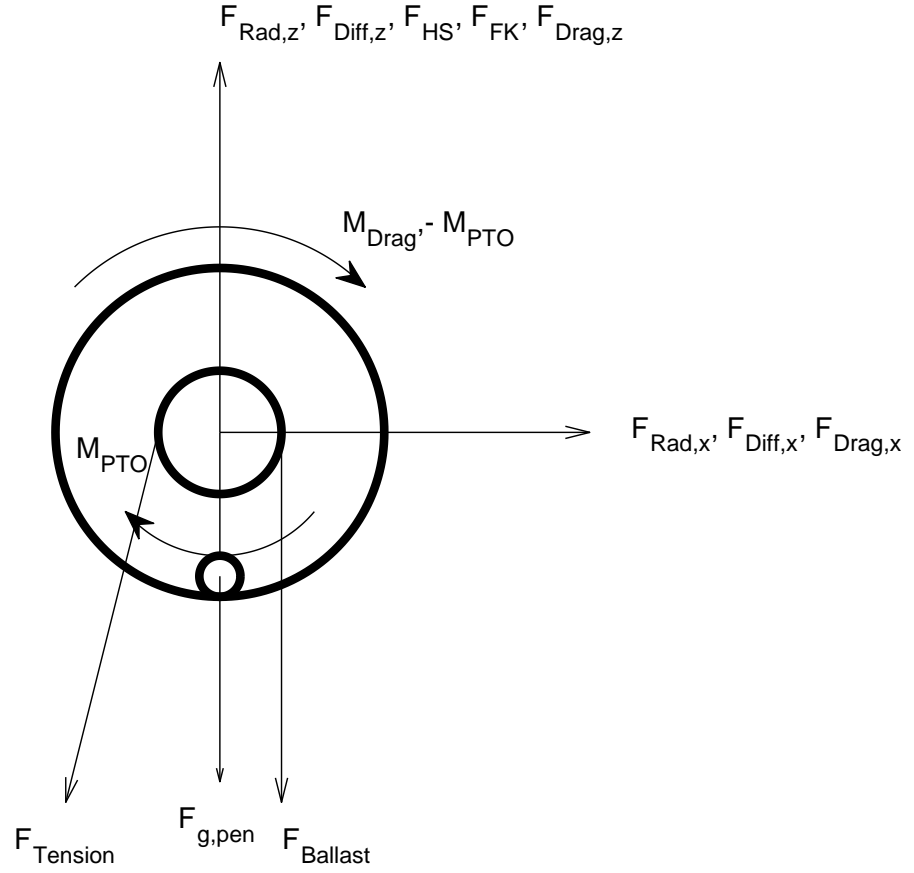


Figure 2.2: Forces acting on the system

2.2 Model derivation

2.2.1 Equations of motion

In the model, there are only three degrees of freedom. These are the x position of the WEC, the z position of the WEC and the angle of the pendulum θ . All the other variables are constrained by these 3 degrees of freedom. Equations 2.2, 2.3 and 2.4 are the equations of motions for surge, heave and pitch. But due to the mooring line, the pitch angle is constrained by the surge and heave displacements. The pitch angle can be described as the change in length of the mooring line multiplied by r_{in} . The length of the mooring line is defined by the original length at the still water level (l_0) and the displacements in surge and heave. This means that the pitch acceleration can be described as the acceleration of the length of the mooring line multiplied by r_{in} . This is given in equation 2.6 and 2.7. Furthermore, the pendulum inside the WEC has its own equation of motion described in equation 2.8. The derivation of the equation of motion of the pendulum is based on a pendulum on a moving support. The derivation is solved using Lagrangian mechanics and can be found in appendix B.

$$m_1 \ddot{x} = F_{Excitation} + F_{Radiation} + F_{External} + F_{Drag} \quad (2.2)$$

$$m_1 \ddot{z} = F_{Hydrostatic} + F_{Excitation} + F_{Radiation} + F_{External} + F_{Drag} \quad (2.3)$$

$$J \ddot{\sigma} = M_{External} + M_{PTO} \quad (2.4)$$

$$\tan(\alpha) = \frac{x(t)}{l_0 + z(t)} \quad (2.5)$$

$$\ddot{\sigma} = -\ddot{l} r_{in} \quad (2.6)$$

$$l(t) = \sqrt{x(t)^2 + (l_0 + z(t))^2} \quad (2.7)$$

$$\ddot{\theta} = \frac{\ddot{x} \cos(\theta)}{L_{pen}} + \frac{(g - \ddot{z}) \sin(\theta)}{L_{pen}} - \frac{M_{PTO}}{m_2 L_{pen}} \quad (2.8)$$

2.2.2 Hydrostatic force

The hydrostatic force is the result of the buoyancy force and the gravity force summed. The gravity force is the mass of the float (m_1) and the pendulum (m_2) multiplied by the gravitational acceleration (g). The buoyancy force is the static water pressure (P_{static}) integrated over the wet hull surface (S). A non-linear method is used to obtain the buoyancy force. This means that the buoyancy force is computed at each time step and corrected for the change in draft. The method is described in section 2.3.2 [16] [17] [18] [19].

$$F_{Hydrostatic} = F_g + F_{Buoyancy} \quad (2.9)$$

$$F_g = -(m_1 + m_2)g \quad (2.10)$$

$$F_{Buoyancy} = - \iint_S P_{static} n dS \quad (2.11)$$

2.2.3 Excitation force

The excitation force has two components the Froude-Krylov force and the diffraction force. The Froude-Krylov force is the pressure field in the incoming wave integrated over the wet surface of the WEC. The diffraction is the pressure field of the diffracted wave integrated over the wet surface.

$$F_{ex} = F_{FK} + F_{diff} \quad (2.12)$$

Froude-Krylov

The Froude-Krylov force is the force associated with the pressure field of the incident wave ($P_{dynamic}$) integrated over the hull surface (S) multiplied by a normal vector n . See equation 2.13. The Froude-Krylov force is mostly estimated with the use of BEM software like NEMOH [9] [13]. But one of the limitations of this software is that it assumes small changes in draft. In the videos from the experimental testing, it is clear that there is a large change in draft. This means that it is expected that there is a need for a non-linear Froude-Krylov force. A non-linear Froude-Krylov force is the most important non-linear force acting on the WEC [20]. To do this at each time-step integration the draft and wet surface need to be computed [18] [19]. The method used to solve the Froude-Krylov forces is described in section 2.3.2.

$$F_{FK} = - \iint_S P_{dynamic} n dS \quad (2.13)$$

Diffraction force

The diffraction forces are the forces due to the diffracted waves of the hull surface of the WEC. The diffraction force is assumed linear and is computed by the BEM software NEMOH. The output of NEMOH are the hydrodynamic coefficients that describe the diffraction forces (C_{diff}) and a phase shift wrt the incoming wave (ϵ_{diff}) as a function of the wave frequency (ω) and the wave amplitude (ζ_a). The force can be calculated by multiplying the diffraction coefficient by the wave amplitude and the cosine of the wave number (k), the surge displacement (x), the wave frequency (ω) and the current time (t), using equation 2.14.

$$F_{diff} = \zeta_a C_{diff} \cos(kx - \omega t + \epsilon_{diff}) \quad (2.14)$$

2.2.4 Radiation force

The radiation force F_{rad} is the force associated with the radiating waves due to the movement of the WEC. The radiation force is described by the Cummins equation [21]. This equation includes a convolution integral to describe the memory effect of the fluid. See equation 2.15 where A_∞ is the added mass at infinite frequency and k_r is the impulse response for the radiation force.

$$F_{rad} = A_\infty \ddot{x}(t) + \int_0^t k_r(t - \tau) \dot{x}(\tau) d\tau \quad (2.15)$$

The convolution term in equation 2.15 takes a lot of computation time to calculate at each time step. That is why a linear state-space model is used to approximate this convolution term [22] [23] [24] [25]. How this state-space approximation is constructed is described in section 2.3.4

2.2.5 Drag force

The drag force is the viscous force between the float and the water. The viscous drag force is expected to have a small influence on a heaving point absorber and can be approximated by using the semi-empirical Morison equation [17] [26]. This force is described by equation 2.16 [16] [27]. At each time-step the characteristic surface area (A) is calculated.

$$F_{drag} = -\frac{1}{2} \rho A C_d \dot{x} |\dot{x}| \quad (2.16)$$

From this expression choosing the right value for the drag coefficient C_d is challenging. From the literature, there are suggestions given for a circular shaped floating object. The suggested values are given in table 2.1 [28].

	C_d
Surge	0.5
Heave	0.5

Table 2.1: Suggested drag coefficients

2.2.6 Ballast force

The ballast force is the force on the WEC due to the ballast weight m_3 . This weight ensures that the WEC winds itself up. The buoyancy force is a constant on the ballast weight. m_3 is the weight of the ballast corrected for the buoyancy. See equation 2.17.

$$F_{ballast} = m_3 g \quad (2.17)$$

This simplification does not hold when the movements of the ballast weight are big. This could be the case if the wave period is near the natural frequency of the ballast weight connected to the WEC. The length of the line with which the ballast weight is connected to the WEC varies. This means that there is not one natural frequency but a range. The length of the line connected to the ballast is dependent on the starting length and the overall movement of the WEC. Secondly, there are lift and drag forces acting on the ballast weight. These forces are also neglected. And lastly, it is assumed that there is no slack in the ballast line connecting the ballast weight to the WEC. It is expected that these effects only significantly influence the WEC at higher speeds, outside of the operational conditions. The acceleration of the WEC can be used to check if slack occurs in the ballast line. The acceleration of the WEC in heave must be bigger than the ballast force divided by the mass of the ballast weight. See equation 2.18.

$$\ddot{z} > \frac{F_{ballast}}{m_3} \quad (2.18)$$

2.2.7 Tension force

The tension force is the force in the line that is wound around the WEC and connects the WEC to the seafloor. The length of this line is variable because the length changes as the WEC pitches. In the theoretical model, it is assumed that the line is always under tension. This means that there is no slack in the line. This simplification assumes that the tension in the line can be calculated using basic dynamics. A 1D example for the line tension is given in equations 2.19, 2.20, 2.21, 2.22 and 2.23. This is an example where the WEC is only heaving. A detailed derivation for the tension force in a 2D configuration where the surge is included can be found in appendix C. Consider the 1D example of the WEC in figure 2.3. This figure gives insight into the method used to solve the line tension in both surge and heave.

The WEC in figure 2.3 can only move in heave $z(t)$ and pitch $\sigma(t)$. The forces acting in the heave direction and the moments acting in pitch can be summed to gain $\sum F_z$ and $\sum M_\sigma$ respectively. The mooring line is attached to the inner part of the WEC with radius r_{in} . The WEC itself has a mass of m_1 and a moment of inertia J .

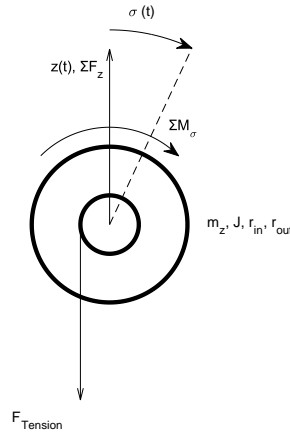


Figure 2.3: Simplified free body diagram to solve the line tension

The equation of motion for the heave motion is given in equation 2.19.

$$m_1 \ddot{z} = \sum F_z - F_{Tension} \quad (2.19)$$

The equation of motion for the pitch motion is given in equation 2.20.

$$J \ddot{\sigma} = \sum M_\sigma - F_{Tension} r_{in} \quad (2.20)$$

The pitch motion is constrained by the heave motion due to the line wind around the WEC. This means that if the WEC moves 1m up it also has to rotate by a rate of $-\frac{1m}{r_{in}} rad$. This gives the following kinetic constraint for the pitch motion, see equation 2.21:

$$\ddot{\sigma} = -\frac{\ddot{z}}{r_{in}} \quad (2.21)$$

Filling in the equations of motion into the constraint gives the expression given in equation 2.22.

$$\frac{\sum M_\sigma - F_{Tension} r_{in}}{J} = -\frac{(\sum F_z - F_{Tension})}{m_1 r_{in}} \quad (2.22)$$

Isolate F_T from equation 2.22 to get an expression for the tension in the line, see equation 2.23.

$$F_T = \frac{\sum M_\sigma}{r_{in} + \frac{J}{r_{in}}} + \frac{\sum F_z J}{(m_1 r_{in})(r_{in} + \frac{J}{r_{in}})} \quad (2.23)$$

2.2.8 PTO moment & electrical power generation

The PTO moment is the moment associated with the torque inside the generator. The PTO moment is estimated by an ideal rotational damper see equation 2.24 [4] [10] [13]. Also, the mechanical power production is estimated with the use of this ideal damper 2.25. The damping coefficient (B_{PTO}) of this damper is uncertain and a point of discussion. If the value is too low, this means that the torque will be underestimated and there is no electricity production. And if the damping coefficient is too high the shaft will follow the pitch movement of the float. This means that there is no relative velocity so also no electricity production. The value of the ideal damping coefficient gets discussed in chapter 4.

$$M_{PTO} = B_{PTO}(\dot{\sigma} - \dot{\theta}) \quad (2.24)$$

$$P_{mechanical} = M_{PTO}|(\dot{\sigma} - \dot{\theta})| \quad (2.25)$$

To estimate the produced electrical power ($P_{electrical}$) the efficiency of the generator ($\eta_{generator}$) is subtracted from the mechanical power ($P_{mechanical}$). See equation 2.26. The efficiency of the generator is dependent on the relative velocity inside the generator. The efficiency of the generator is given at 8 points. The efficiency gets approximated with a polynomial to gain a continuous curve. The original efficiency curve can be found in figure 3.2 in chapter 3. Figure 2.4 shows the original points and a 3rd, 4th and 5th order approximation of the efficiency curve. The norm of the residuals for the approximations are 0.148, 0.105 and 0.104 respectively. There is a less than 1% increase in accuracy between the 4th and 5th order approximations. That is why a 4th order approximation seems sufficient. The efficiency of the generator is estimated by the polynomial in equation 2.27 with the coefficients from table 2.2.

$$P_{electrical} = P_{mechanical}\eta_{generator} \quad (2.26)$$

$$\eta_{generator} = C_1 v_{rel}^4 + C_2 v_{rel}^3 + C_3 v_{rel}^2 + C_4 v_{rel} + C_5 \quad (2.27)$$

C_1	-3.2997e-4
C_2	0.0075
C_3	-0.0646
C_4	0.2499
C_5	0.6198

Table 2.2: Coefficients of the generator efficiency polynomial

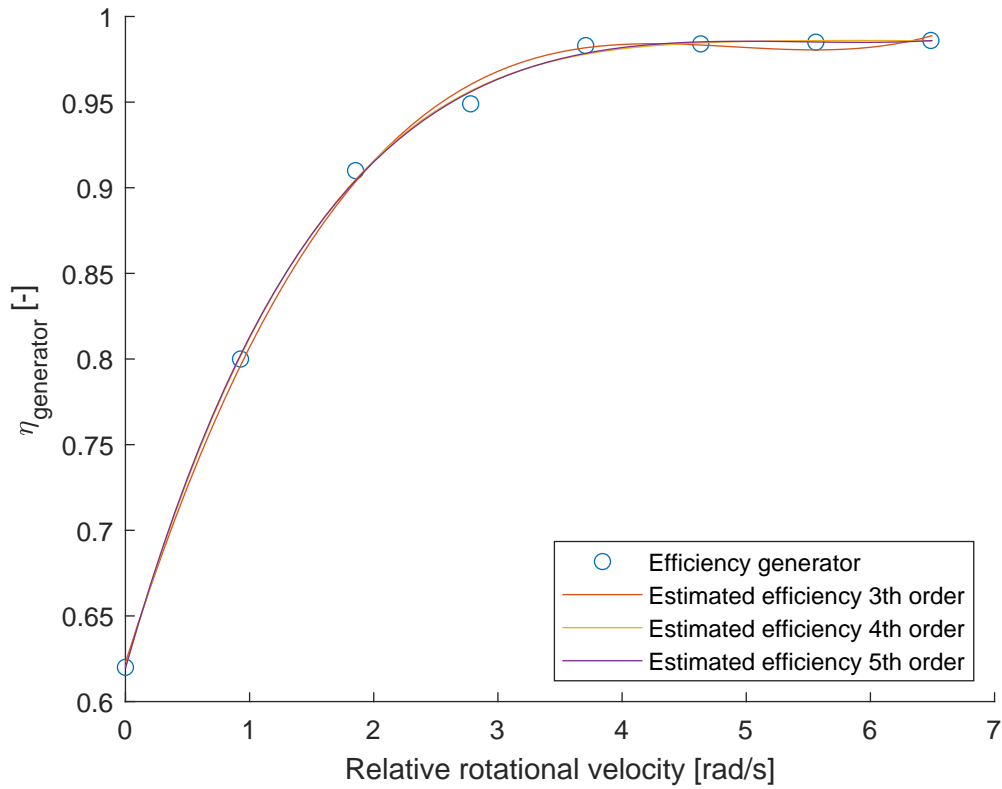


Figure 2.4: Theoretical generator efficiency

2.3 Calculation method

2.3.1 ODE45 solver

The theoretical results are obtained by using the Matlab function ODE45. This function is a solver for ordinary differential equations (ODEs). This specific ODE solver uses the Runge-Kutta method with a variable time step. The function is designed to handle the problem shown in equation 2.28 [29]. In equation 2.28 \bar{q} is the state of the system. At each time step the derivative of the state vector $\frac{d\bar{q}}{dt}$ gets calculated. This derivative is a function of the state vector q and the current time t .

$$\frac{d\bar{q}}{dt} = f(t, \bar{q}), \quad \bar{q}(t_0) = \bar{q}_0 \quad (2.28)$$

The state vector \bar{q} and its derivative $\frac{d\bar{q}}{dt}$ are shown in 2.29. To calculate the acceleration components in $\frac{d\bar{q}}{dt}$ equations 2.2, 2.3, 2.4 and 2.8 are used.

$$\bar{q} = \begin{bmatrix} x \\ \dot{x} \\ z \\ \dot{z} \\ \sigma \\ \dot{\sigma} \\ \theta \\ \dot{\theta} \end{bmatrix}, \quad \frac{d\bar{q}}{dt} = \begin{bmatrix} \dot{x} \\ \ddot{x} \\ \dot{z} \\ \ddot{z} \\ \dot{\sigma} \\ \ddot{\sigma} \\ \dot{\theta} \\ \ddot{\theta} \end{bmatrix} \quad (2.29)$$

2.3.2 Non-linear buoyancy and Froude-Krylov force

To obtain the non-linear buoyancy and Froude-Krylov force the expression given by [18] and [19] is improved to suit the geometry of the WEC of Dutch wave power.

The pressure in waves is divided into two parts. The static part and the dynamic part. The static part integrated over the hull surface is the buoyancy force and the dynamic part is the Froude-Krylov force. See equation 2.11, 2.13 and 2.30.

$$P = P_{static} + P_{dynamic} = \rho gh + \rho g \zeta_a e^{kh} \cos(kx - \omega t) \quad (2.30)$$

This pressure needs to be integrated over the hull surface. The outline of the hull surface is described in the cylindrical coordinate σ . The water depth h in equation 2.31 is dependent on the angle σ , the still water draft T , the radius of the WEC r_{out} and the heave displacement of the WEC $z(t)$.

$$h = r_{out} \sin(\sigma) + z(t) + r_{out} - T \quad (2.31)$$

The normal vector n is easy to calculate because the hull has a cylindrical shape. This means that n can be written as in equation 2.32.

$$n = \begin{bmatrix} n_x \\ n_z \end{bmatrix} = \begin{bmatrix} \cos(\sigma) \\ \sin(\sigma) \end{bmatrix} \quad (2.32)$$

In [18] the pressure gets integrated around the z-axis. This method works for an axis symmetrical WEC. But, because the hull of is vertical at the sides there is no need to integrate around the z-axis. Instead, the FK force per meter gets calculated. To account for both the waveward and leeward sides of the WEC the formula has to be multiplied by a factor of 2. This simplification also means that the resulting force in the surge direction on the waveward and leeward of the float cancels each other out. This means that the resulting hydrostatic and Froude-Krylov forces only have a component in the heave direction. To calculate this the resulting integral is shown in equation 2.33. With the integration boundaries σ_1 and σ_2 . This implies that there is no FK force in the surge direction. This simplification is discussed in section 2.5

$$F_{FK} = - \iint_S P_{dynamic} n dS \approx 2 \int_{\sigma_1}^{\sigma_2} (\rho g r_{out} \sin(\sigma) + z(t) + r_{out} - T + \rho g \zeta_a e^{kr_{out} \sin(\sigma) + z(t) + r_{out} - T}) \sin(\sigma) d\sigma \quad (2.33)$$

σ_1 and σ_2 are the boundaries of the integral. σ_1 is the bottom of the WEC and σ_2 is the wave height wrt the centre of the WEC. this results in the following expressions for σ_1 and σ_2 . As shown in equation 2.34 and figure 2.5.

$$\sigma_1 = -\frac{\pi}{2}, \quad \sigma_2 = -\arcsin\left(\frac{z(t) + r_{out} - T - \eta}{r_{out}}\right) \quad (2.34)$$

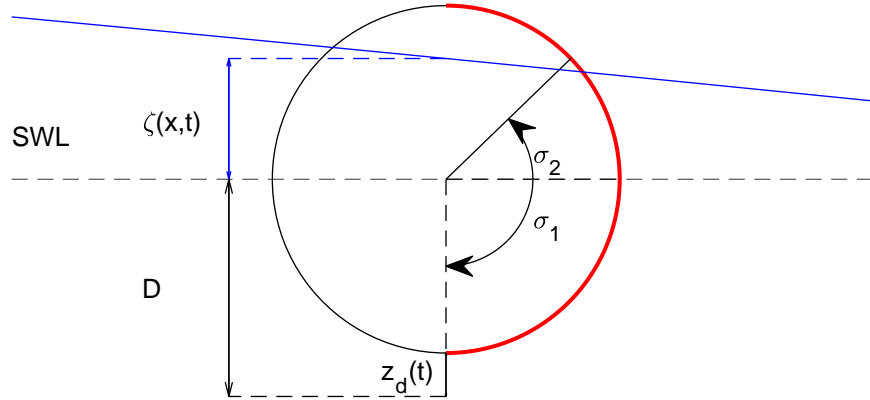


Figure 2.5: Derivation of the pressure integral

2.3.3 NEMOH

The diffraction forces and radiation forces are derived based on the hydrodynamic coefficients obtained from the BEM software NEMOH. This software calculates the first-order wave loads on offshore structures (added mass, radiation damping and diffraction forces). To obtain these coefficients a 3D model at still water draft is built in SALOME. The length of the model is 3m, the radius is 0.4m and the still water draft is 0.491m. A mesh is made from the wet hull surface. For the meshing the NETGEN 2D hypothesis and the NETGEN 1D-2D algorithm were used [30] [31]. This mesh is used as input for NEMOH. These algorithms discretise the hull by a specified maximum and minimum size for the mesh cells. Secondly, the shape of the cells are specified. See figures 2.6 and 2.7.

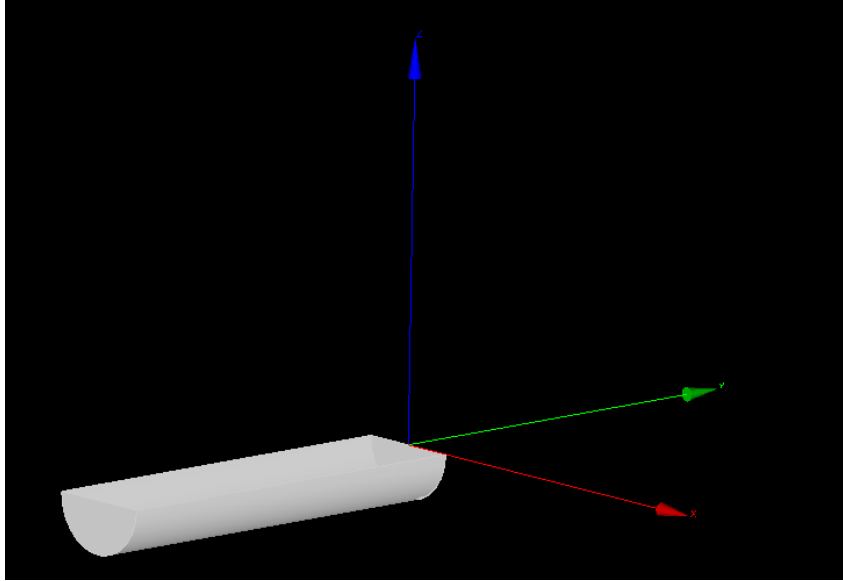


Figure 2.6: 3D model of the WEC at still water draft in SALOME

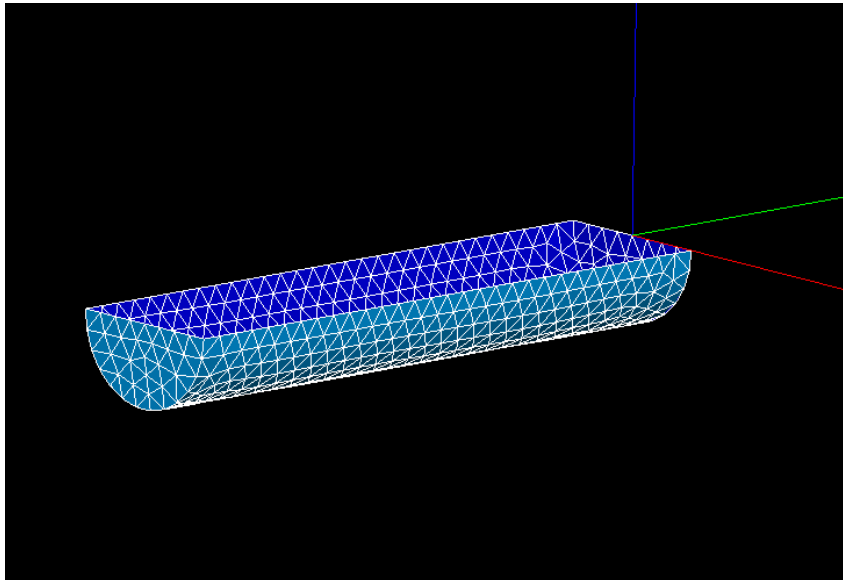


Figure 2.7: Mesh of the SALOME model

NEMOH calculates the hydrodynamic coefficients for all 6 degrees of freedom, but for this thesis only surge, heave and pitch are coincided. The hydrodynamic coefficients are calculated for 81 different wave frequencies from $0.1 \frac{rad}{s}$ to $4.0 \frac{rad}{s}$. Which corresponds to a wave period of $62.83sec$ to $1.57sec$. The only wave direction that is considered are waves propagating along the positive x-axis (0 deg).

Diffraction forces

The results of the BEM software NEMOH are the diffraction forces coefficients and phase shifts for surge, heave and pitch at different frequencies in the form shown in equation 2.35. ζ_a is the wave amplitude, $C_{diff,1,2,3}$ are the diffraction force coefficients for surge, heave and pitch respectively and $\epsilon_{1,2,3}$ are the phase shifts for surge, heave and pitch respectively. The diffraction force can be calculated using equation 2.35. diffraction force coefficients and phase shifts can be obtained by interpolating the values from figure 2.8

$$F_{diff,123} = \zeta_a C_{diff,1,2,3} \cos(kx(t) - \omega t + \epsilon_{1,2,3}) \quad (2.35)$$

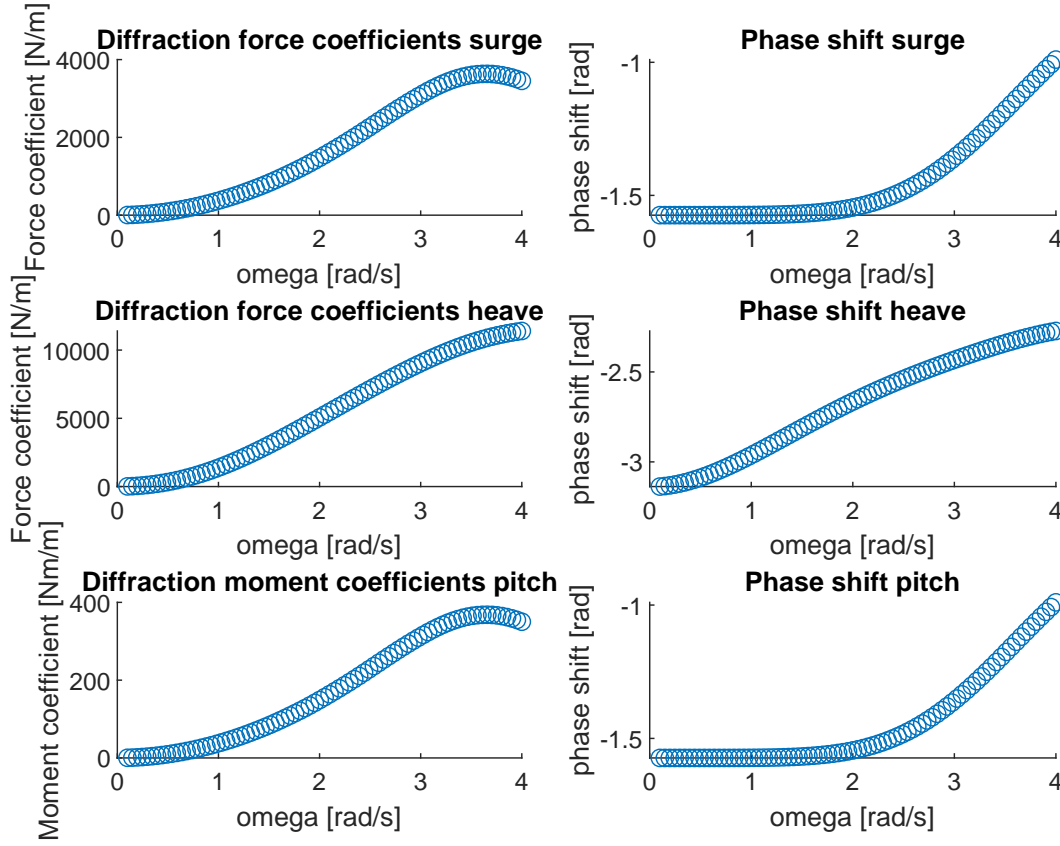


Figure 2.8: Diffraction force coefficients and phase shifts

2.3.4 State-space approximation of the radiation force

As discussed in section 2.2.4, the radiation forces are calculated by solving the Cummins equation (equation 2.36) at each time step [21]. It takes a lot of computation time to solve this equation [23]. That is why an alternative method is used to estimate the radiation forces in the time domain. This method substitutes the convolution integral in equation 2.37 by a state vector \bar{x}_r to estimate the radiation force F_r . The state-space vector gets updated each time step by its using $\dot{\bar{x}}_r(t)$ in equation 2.38. See equations 2.37 and 2.38.

$$(M + A)\ddot{x}(t) + \int_{-\infty}^t B(t - \tau)\dot{x}(\tau)d\tau + Cx(t) = X(t) \quad (2.36)$$

$$F_{rad}(t) = \int_0^t k_t(t - \tau)\dot{x}(t) \approx \bar{C}_r \bar{x}_r(t) \quad (2.37)$$

$$\dot{\bar{x}}_r(t) = \bar{A}_r \bar{x}_r(t) + \bar{B}_r \dot{x}(t) \quad (2.38)$$

In this approximation are \bar{A}_r , \bar{B}_r and \bar{C}_r are $m \times m$, $m \times 1$ and $1 \times m$ state matrices, respectively. $\bar{x}_r(t)$ is a $m \times 1$ state of the radiation subsystem. To obtain the coefficients used in the state space approximation. The Matlab toolbox Marine Systems Simulator (MSS) is used. The hydrodynamic coefficients of NEMOH are loaded into the MSS Matlab toolbox. The toolbox uses the radiation coefficients (added mass and damping) and the impulse response function (IRF) to obtain a parametric approximation of the Cummins equation. The method and toolbox used are described in [32] and [33].

The resulting 4th order state-space approximation is shown in 2.39, 2.40, 2.41, 2.42, 2.43 and 2.44. The subscripts 1 and 2 represent the state-space approximations in surge and heave respectively.

$$A_{r,1} = \begin{bmatrix} -4.66 & -23.96 & -31.61 & -20.46 \\ 1 & 0 & 0 & 0 \\ 0 & 1 & 0 & 0 \\ 0 & 0 & 1 & 0 \end{bmatrix} \quad (2.39)$$

$$B_{r,1} = [1 \ 0 \ 0 \ 0]' \quad (2.40)$$

$$C_{r,1} = -10^4 [0.14 \ 0.56 \ 0.10 \ 0] \quad (2.41)$$

$$A_{r,2} = \begin{bmatrix} -7.71 & -42.43 & -100.00 & -78.93 \\ 1 & 0 & 0 & 0 \\ 0 & 1 & 0 & 0 \\ 0 & 0 & 1 & 0 \end{bmatrix} \quad (2.42)$$

$$B_{r,2} = [1 \ 0 \ 0 \ 0]' \quad (2.43)$$

$$C_{r,2} = -10^4 [0.28 \ 2.50 \ 2.14 \ 0] \quad (2.44)$$

2.4 Model verification

To test the theoretical model some basic tests were done with the numerical model. For example: free decay tests in surge and heave. Next, the response of the WEC under linear wave excitation is reviewed. From each response an animation can be made. This helped visualise the results and understand the motions.

The theoretical model has different outputs. All the necessary data can be reviewed. For each time step, the following states of the system are saved. See table 2.3.

Property	Unit
Surge displacement	m
Surge velocity	m/s
Heave displacement	m
Heave velocity	m/s
Pitch angle	rad
Pitch angular velocity	rad/s
Angle of the pendulum	rad
Angular velocity of the pendulum	rad/s
All the forces	N/m
All the moments	Nm/m
Produced power	W/m

Table 2.3: Theoretical model outputs

The dimensions used in the model are based on the dimensions used in the experimental tests executed by Dutch Wave Power. Some of the values are per meter because the model is only in 2D. The used parameters are shown in table 2.4. The basic model at still water level is shown in figure 2.9.

Property	Value	Unit
Radius float	0.4	m
Radius reel	0.15	m
length inside pendulum	0.35	m
Mass float	172	kg/m
Mass pendulum	32	kg/m
Mass ballast weight	80	kg/m
Still water draft	0.5	m
Water depth	6	m

Table 2.4: Parameters used in the theoretical model

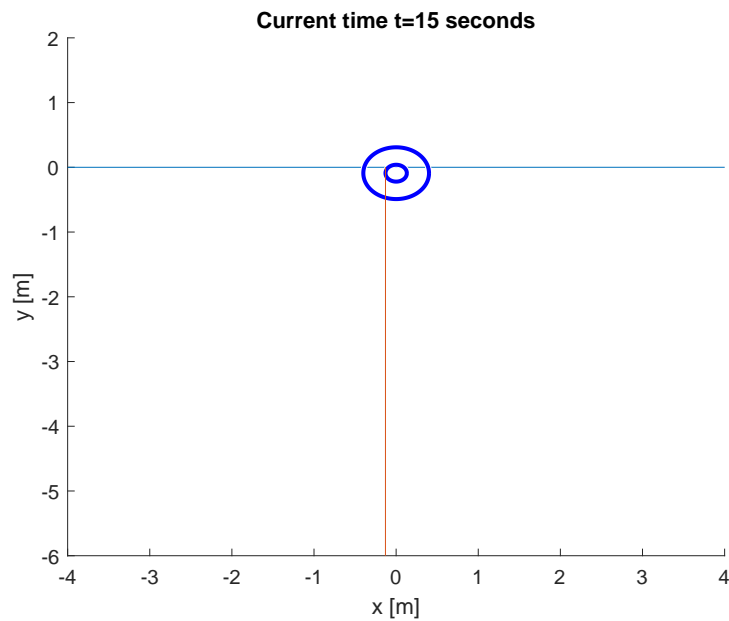


Figure 2.9: Theoretical model at SWL

2.4.1 Free decay tests

The first check that was done to test the model is a free decay test. This is done to see if the model reacts properly. The WEC is given an initial heave displacement equal to the draft and then released. Figure 2.10 shows the heave displacement over time and figure 2.11 show the resulting forces in heave. In this free decay test, the PTO damper is set to zero to ensure that no energy gets dissipated through the PTO system.

Using figure 2.10, the natural frequency of the system in heave can be estimated. The test starts with a positive displacement of 0.49m which is equal to the draft. This means that the bottom of the float just touches to water. The WEC is released at $T=0$ and moves down. What follows is an oscillating motion around the mean position $z=0$. $Z=0$ is chosen to be the still water level. After 9.2 seconds the amplitude of the displacement is smaller than 0.002m. Using the zero-crossing method it there be established that the WEC oscillates 4 times over the course of 9.2 seconds. This corresponds to a natural period of 2.3 seconds. This result can be compared with a theoretical value. The undamped natural frequency can be estimated using equation 2.45. This equation is corrected for the coupled pitch motion. Where c_{33} is the stiffness coefficient in heave, a_{33} is the added mass in heave, J is the mass moment of inertia and R_{in} is the inner radius of the WEC. c_{33} can be estimated using the water plane surface of the WEC A , the water density ρ and the gravitational acceleration g . See equation 2.46. The added mass can be estimated using equation 2.47 [27].

$$\omega_{nat} \approx \sqrt{\frac{c_{33}}{m + a_{33} + \frac{J}{R_{in}^2}}} \quad (2.45)$$

$$c_{33} \approx \rho g A \quad (2.46)$$

$$a_{33} \approx \pi \rho R^2 \quad (2.47)$$

The resulting undamped natural period is 2.9 seconds. This value is higher than the the value observed in the model. This result is expected because this theoretical value does not take damping into account. Adding a damper value will lower the natural period.

From the dynamic results, it is clear that the model handles the free decay tests properly. From the force results, it is clear that at around 1 second the WEC gets completely submerged. The model handles this fine by calculating only the maximum buoyancy force possible. This is a region where the accuracy of the model decreases, with this complete submersion multiple non-linear forces are associated that are not captured in the model. One has to watch out that with the input parameters given to the model. This behaviour is not occurring. Nevertheless, the model will give a resulting force. This is done because in irregular waves this complete submersion can occur. It is desirable that even with a short period of submersion the model can continue its calculations. But one has to keep in mind that if this happens the results around this event are less accurate. For the validation with regular waves, this behaviour is avoided. More on the results in irregular waves can be found in chapter 5.

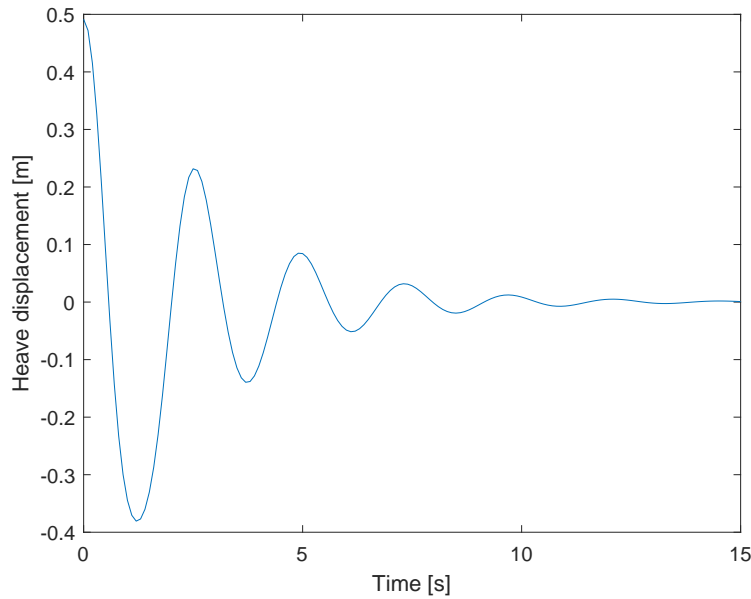


Figure 2.10: Free decay test: Heave displacement

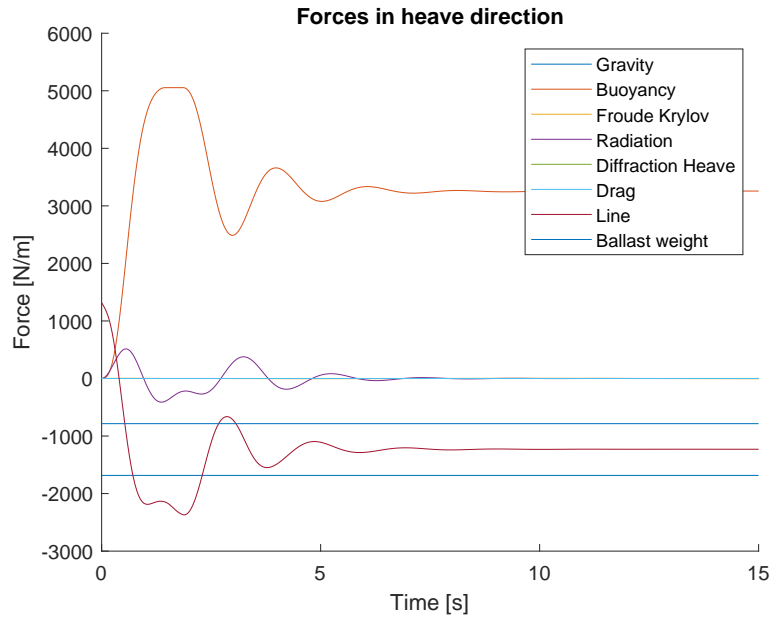


Figure 2.11: Free decay test: Resulting forces on the WEC

2.4.2 Free decay test - surge

The second test that was used to test if all the forces are modelled properly is a free decay test in surge direction. Without waves, the model is given an initial surge displacement. The WEC must return to its original still water position due to the ballast weight. The WEC is given an initial surge displacement of 3m. The results are shown in figure 2.12 and 2.13.

Using figure 2.12 it can be observed that the WEC makes 4 oscillations around the neutral position after 42 seconds. This corresponds with a surge natural period of 10.5 seconds. The second thing that is noticeable, is that the surge motions don't damp out. The amplitude of the surge motion is still 1m after 50 seconds. This is because the radiation force in surge direction is small. In real life, it is expected that the model will find its equilibrium much quicker. Probably, because there are also forces acting on the ballast weight. If the ballast weight moves through the water, drag forces are acting on it. These forces will dissipate energy from the system. These forces are neglected in the theoretical model.

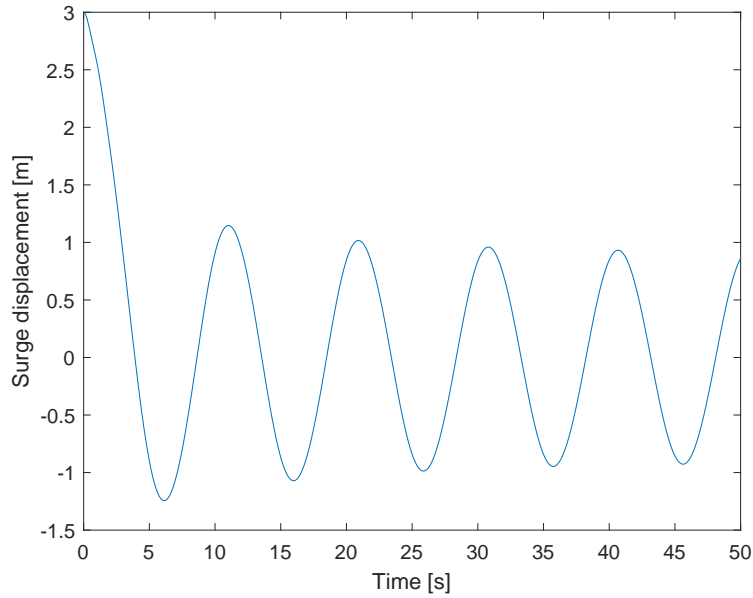


Figure 2.12: Free decay test in surge: surge motion

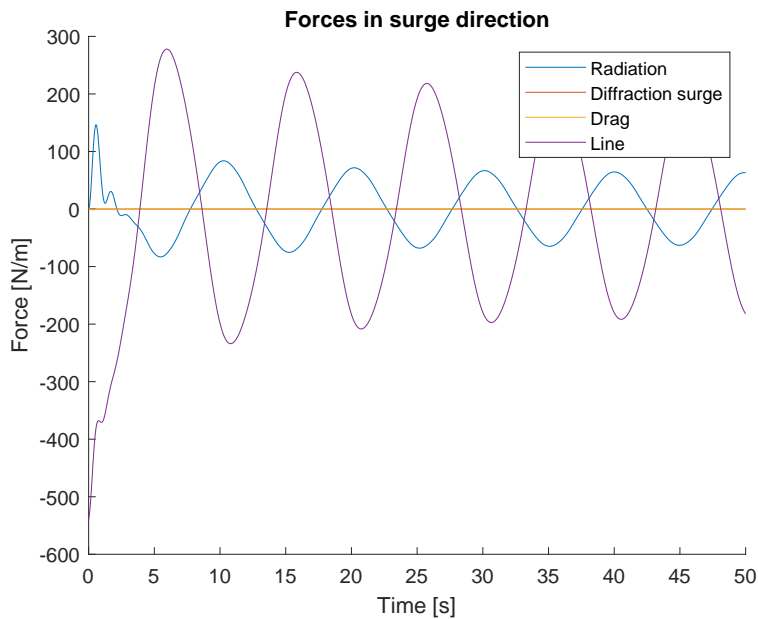


Figure 2.13: Free decay test in surge: Resulting forces on the WEC

2.4.3 Response of regular waves

The next step is to review the response of the theoretical model under regular wave loading. To describe regular waves the airy wave theory is used [27]. In the results shown here, the waves have a wave height of $1m$ ($0.5m$ amplitude) and a period T of $6.5sec$. By trying random values for the PTO damper value it is found that the desired dynamics occur with a value between 20 and $50 \frac{Nm}{rad/sm}$. The desired dynamics is when there is no slack in the ballast line and the pendulum does not make a full rotation. The value used in this test is $30 \frac{Nm}{rad/sm}$. The total simulation time is 100 seconds. The resulting dynamics are shown in figure 2.14. Figure 2.15 gives the resulting forces.

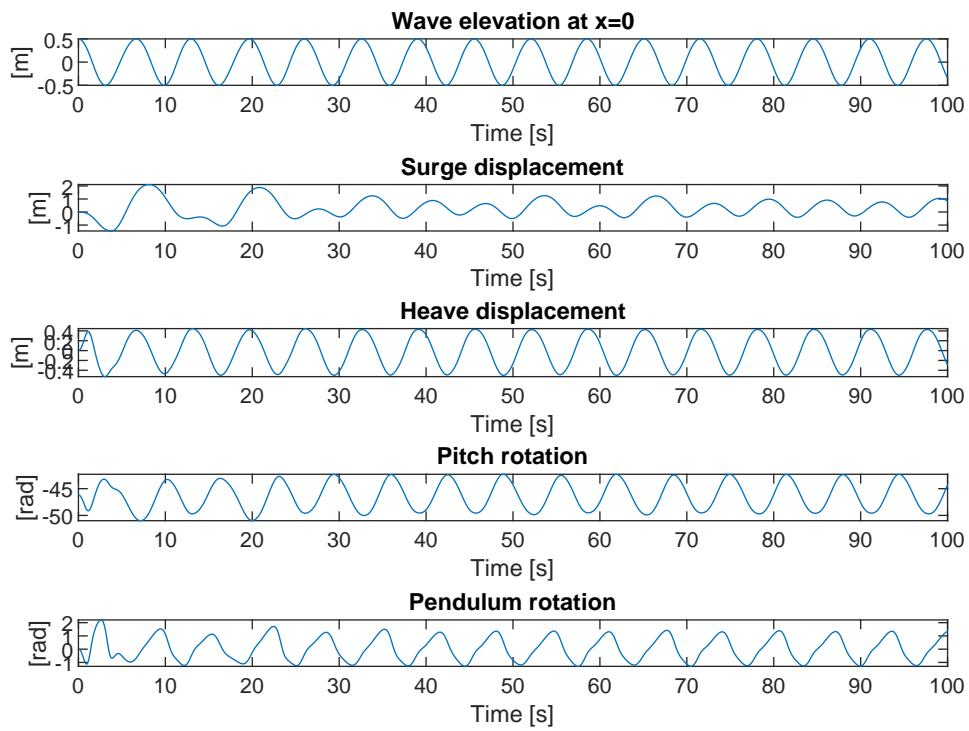


Figure 2.14: Dynamic response of a test with $H=1\text{m}$ and $T=6.5\text{s}$

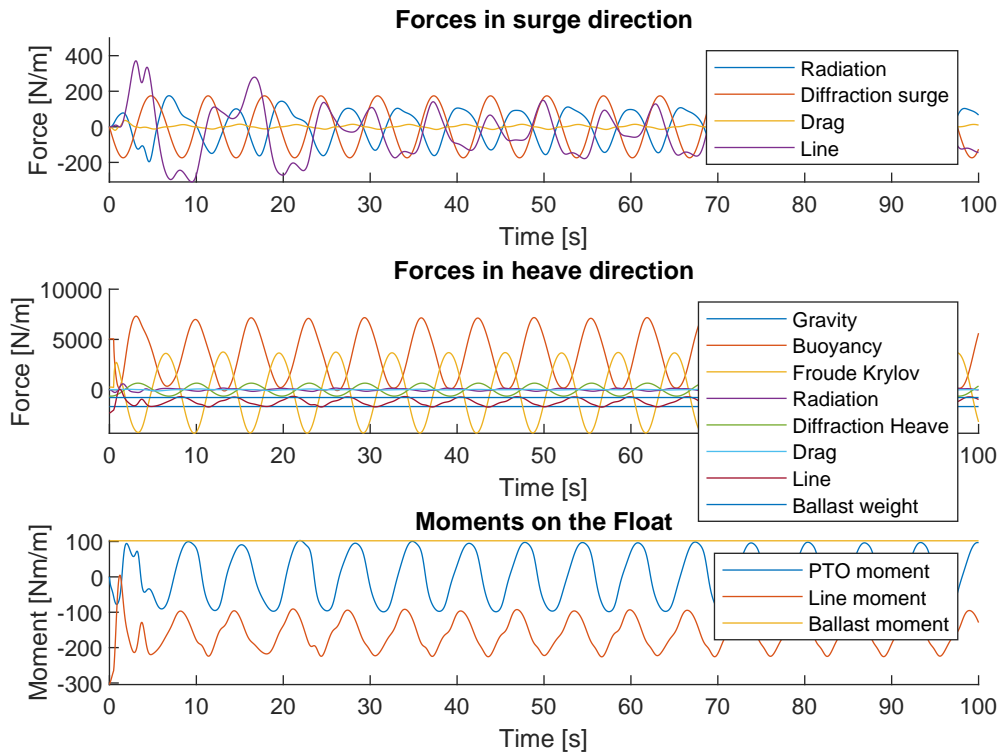


Figure 2.15: Resulting forces of a test with $H=1\text{m}$ and $T=6.5\text{s}$

From the results in figure 2.14 and 2.15 it is clear that the model needs two ramp-up waves before it reaches a steady-state response. What is also noticeable is that the surge motions never completely reach a steady state at each cycle there are small differences. The heave displacement, pitch angle and pendulum angle do reach a steady state. This means that these motions are not much influenced by the surge motion.

The forces acting on the WEC are shown in figure 2.15. From this figure it is clear that the buoyancy and Froude-Krylov force in heave are the highest and thus the most important. These are also the forces that are approximated non-linear. The forces in surge are of a smaller order. Here can be concluded that the power is mainly generated by the heaving motion. It is noted that the FK force in surge is neglected. This is discussed in section 2.5.

2.5 Discussion & limitations

The theoretical model is a simplification of the phenomenon in reality. This means that all the forces described in this chapter are approximations of reality. These simplifications come with some limitations.

The model only describes the response in 2D. In the literature, this is often done for point-absorbers. This is because a point absorber is often axis symmetric and thus this means that the directional spreading in a wave pattern is of less influence. That is why a 2D representation is . The second reason why it is convenient to describe the system in 2D is that the experimental scale tests were executed with unidirectional waves. But the WEC of Dutch Wave Power is influenced by the directional spreading of the waves because the width of the WEC is bigger than the length. Nevertheless, the 2D approximation is sufficient because this thesis is focused on the effects and working principles of this WEC.

The WEC has a large change in draft. This is described in chapter 3. But this large change in draft leads to some uncertainties in the force estimation. The hydrostatic and Froude-Krylov forces do account for this change in draft. But the radiation and diffraction forces are based on a BEM analysis which assumes a con-

stant draft. As shown in figure 2.15, the radiation and diffraction forces have a small influence compared with the buoyancy and Froude-Krylov force. That is why this linearization is a sufficient approximation.

The FK force is estimated by using the pressure at the center of the WEC. Due to this method the resulting FK force in surge is zero, because there is no pressure difference between the seaward and leeward sides of the WEC. The WEC is small wrt the wave length. This means that the pressure difference is small between the seaward and leeward side of the WEC. This means that the FK force is also expected to be small. This can be checked by using a linear FK force. The linear FK forces can be obtained from NEMOH the same way the diffraction forces are obtained. To check if the FK force in surge has an influence on the The resulting forces with the linear FK force in surge direction are showed in figure 2.16.

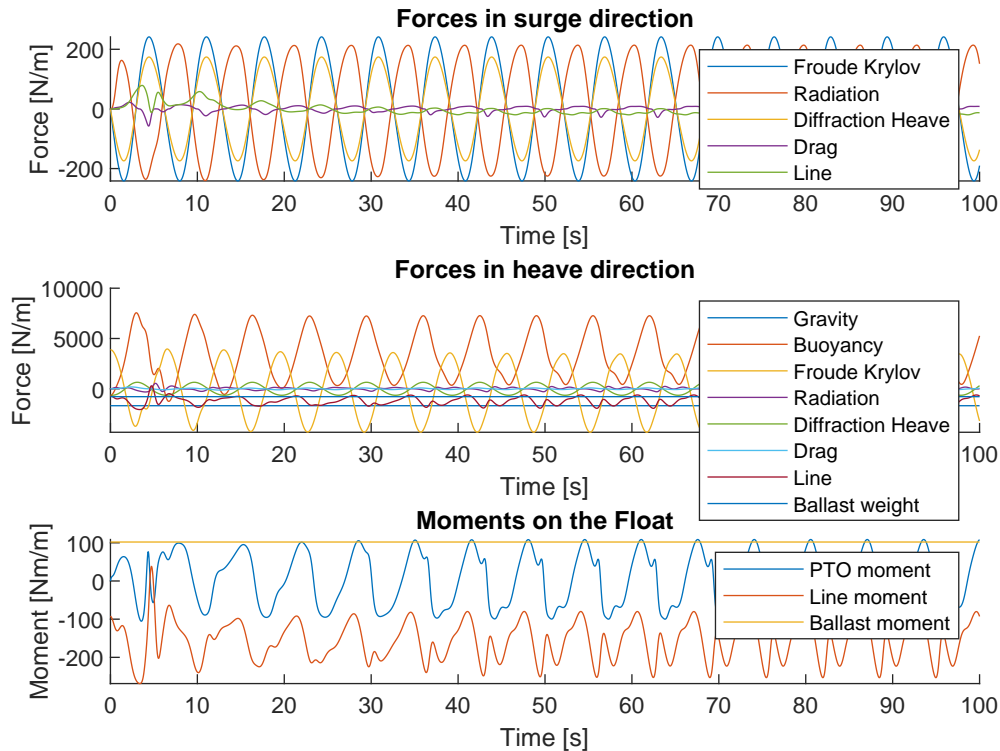


Figure 2.16: Resulting forces, with linear FK force in surge $H=1\text{m}$ and $T=6.5\text{s}$

In the top plot of figure 2.16 the resulting force components in surge direction are plotted. As shown the FK force in surge are of the same order as the radiation and diffraction forces. The resulting forces in heave are showed in the middle plot. The magnitude of the forces are of a whole different order. This is why there can be concluded that the main constitution for the power production come from the heaving motion. Nevertheless, the FK forces in surge could effect the dynamics of the WEC and inside pendulum.

The approximation of the radiation term can be improved if the 4th order of the state-space representation is increased. But this increase in order comes with a higher computation time. This is why the 4th order state-space approximation of the radiation force is sufficient.

The force in the mooring line and the ballast weight are also up for debate. For example, the ballast line is now modelled as a constant force pulling down, but it is a weight hanging on a line. This weight is not only moving up and down. It also swings. This motion also induces forces which are not captured in this model. But these motions and effects are expected to be non-linear and are expected to only have a small influence on the dynamics of the WEC. With the motions of the WEC known the forces on the ballast weight can be checked. The results described in figures 2.14 are used to check the forces on the ballast weight. The ballast weight has a length of 3m and a width of 0.19m. This results in a area of 0.61m^2 . The

drag coefficient on the ballast weight is estimated to be 0.5 [28]. The heaving velocity of the ballast weight is equal to two times the heaving velocity of the WEC. From figure 2.17 the maximum heaving velocity of the WEC is 0.45m/s. This results in a heaving velocity of the ballast weight of 0.9m/s. Using equation 2.16, the maximum drag force on the ballast weight is estimated to be 42.2 N/m. This is only at short moments at maximum velocity. In comparison, the resulting hydrostatic force due to the buoyancy and gravity force are 784N/m. This thesis is more focused on the working principle and the overall dynamics. That is why the drag forces on the ballast weight are neglected. Also the wave forces acting on the ballast weight are neglected. They are dependent of the water depth. This means that the forces are dependent of the depth of the ballast weight. In this stage of the model it is more important to gain an understanding of the working principle of the WEC, so it is chosen to neglect the wave forces on the ballast weight.

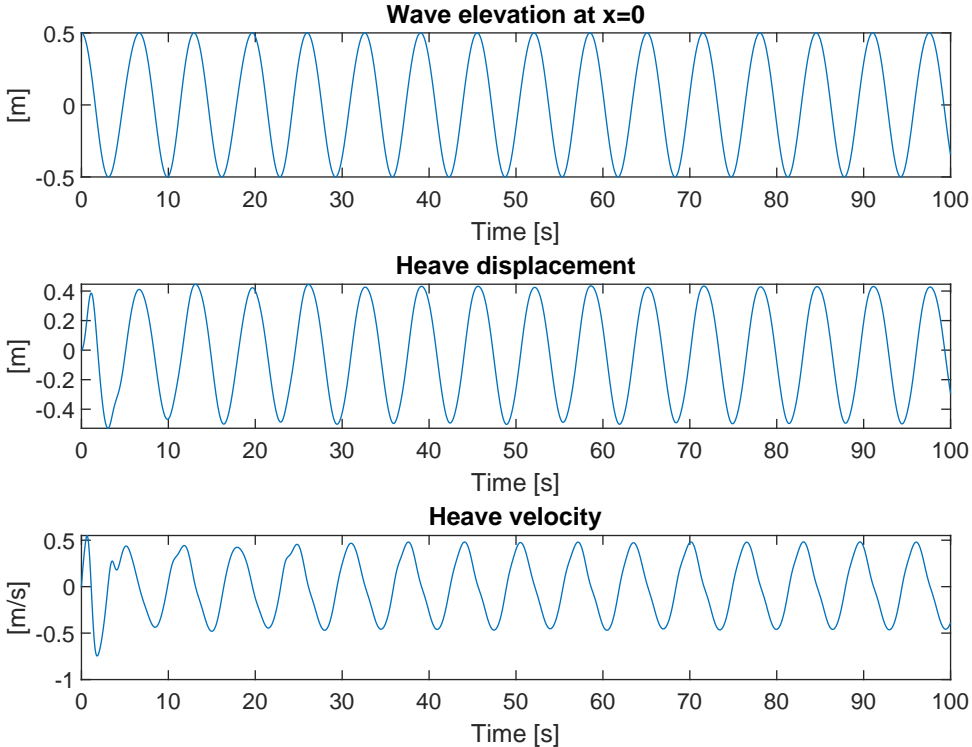


Figure 2.17: Heave displacement and velocity of the WEC H=1, T=6.5s

Chapter 3

Experimental scale tests

In this chapter are the experimental scale tests described. Section 3.1 will describe the test setup. First, the scale model and its most important parameters will be described. Secondly, a description of the wave flume and the test setup is given. It is explained how the tests are executed and what kind of data is obtained from the tests. And thirdly section 3.1 will show which kind of wave characteristics are used in the experimental tests. Section 3.2 will cover the part of the data processing. This includes the selection of useful data and the post-processing of this data. The chapter will end with section 3.3 which includes all the observations from the experimental tests.

3.1 Test setup

3.1.1 Scale model

The model tested by Dutch Wave Power is a 1:3 scale model. The model laying in the wave flume is shown in figure 3.1. The model has a width of $3m$ and a diameter of $0.8m$. The diameter of the part where the ballast weight and the mooring line are connected is $0.3m$. The total weight of the float is $515kg$ and the weight of the pendulum that is connected to the shaft inside the float is $95kg$. The weight of the ballast weight corrected for the buoyancy is $240kg$. Next, the generator is connected to the float. This means that if the float pitches the generator pitches as well. The pendulum inside the float makes sure that there is a relative velocity between the shaft and the generator. But before the shaft enters the generator, the speed gets increased by a gearbox. This gearbox has a ratio of 11.3. The generator inside the float has a given efficiency curve. This efficiency is shown in figure 3.2.

During the tests, multiple sensors are placed on the WEC these measure the movement of the float and the produced power of the generator. The movement is measured by two variables this is the pitching angle of the float and secondly the angle of the inside pendulum. During the tests, there were no wave elevation sensors present. That is why there is no record of the actual wave height. The tests were executed prior to this thesis, so the wave height/wavemaker settings must be taken for granted.

Lastly, the load on the generator could be varied. This load resembles a resistance in the electrical system. Higher resistance means less coupling in the generator and a lower resistance means more coupling in the generator. The electrical system had 3 different load options that were chosen on an educated guess. The load options for the experimental tests are 8 and 12.



Figure 3.1: Test setup in the wave flume

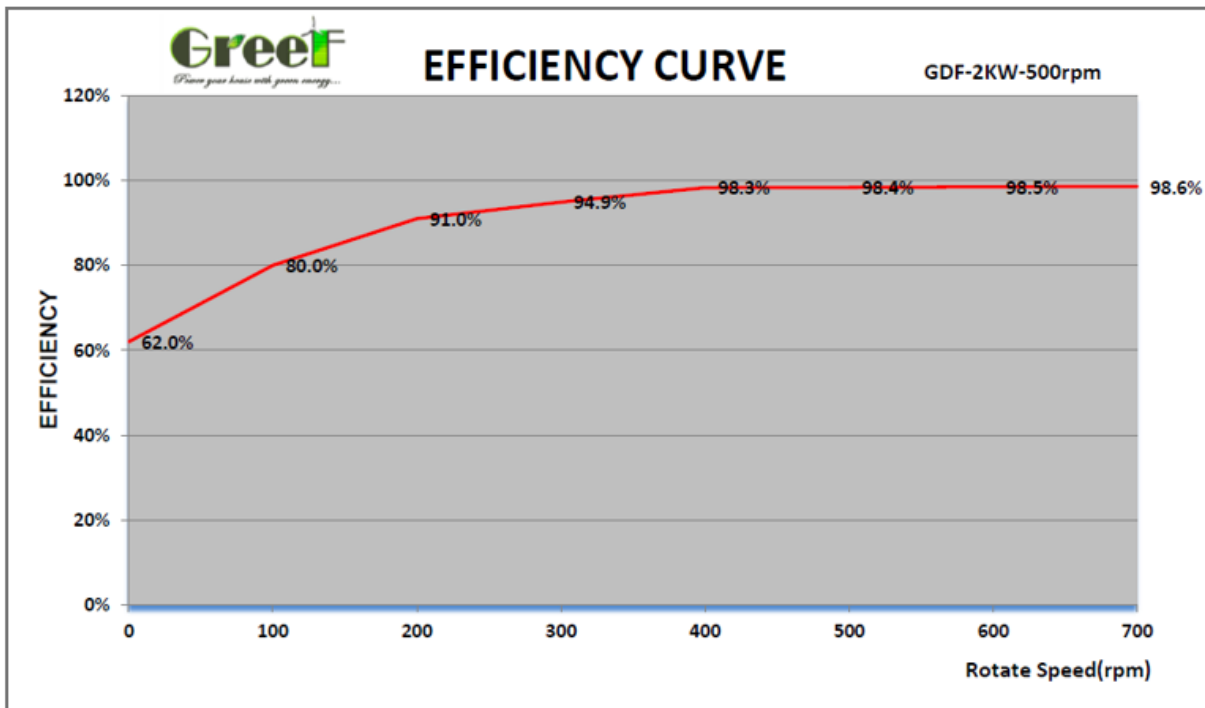


Figure 3.2: Generator efficiency curve

3.1.2 Wave flume

The experimental tests were done in the Delta flume wave flume at Deltares in Delft. The flume has a wave generator connected at the beginning and a wave absorber at the end of the flume. The total length of the flume is 300m and 5m wide. The maximum water depth is 9.5m but the depth used in the experiments is 6m. The wave generator is capable of creating both regular and irregular waves. For the experimental tests done by Dutch Wave Power, the scale model is placed in the middle of the wave flume. See figure 3.3 for a schematic view of the experimental setup. More information on the Delta flume can be found on the website of Deltares:

<https://www.deltares.nl/en/facilities/delta-flume/>

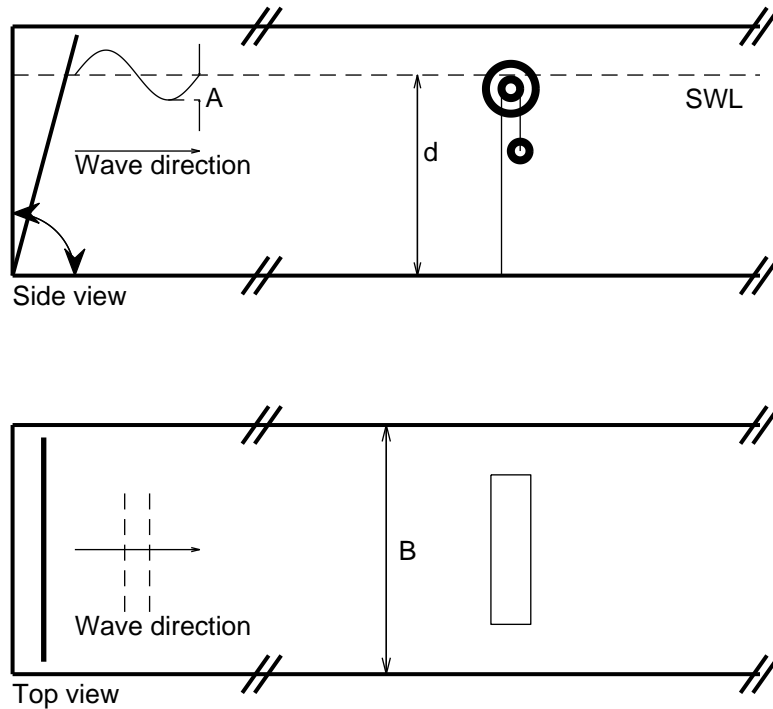


Figure 3.3: Schematic side- and top view of the experimental setup

With:

- A = Wave amplitude = Wave height/2
- d = Water depth = 6m
- B = With of the flume = 5m

3.1.3 Test parameters & wave characteristics

In the wave flume, different combinations of wave conditions and generator load were tested. Not all of the experiments turned out to be useful for this thesis. The reasons are discussed in section 3.3. In table 3.1 an overview is given of the combinations that produced clean and reliable results.

At each test, 3 outputs were measured. The pitching angle of the WEC, the angle of the pendulum and the power output of the generator. After each test, there was a waiting period to absorb all the waves left in the wave flume.

	Wave height [m]	Wave period [s]	Load on the generator [Ω]
Test 1	1	6	8
Test 2	1	6	12
Test 3	1	7	8
Test 4	1	7	12
Test 5	1	8	8
Test 6	1	8	12
Test 7	1	9	8

Table 3.1: List of experiments and parameters

3.2 Data processing

3.2.1 Correction of the raw data

The time-series data delivered by Dutch Wave Power is not complete. There is already some post-processing done by Dutch Wave Power. Unfortunately, the complete time series data is not available. It is found that there are two types of changes made to the time series results. The first one is that the data of the startup waves is deleted. And the second change that is made to the raw data is that the pitch angle of the float is sometimes corrected for a full rotation of 2π rad. The changes that were found in each individual test can be found in table 3.2 and the raw data can be found in appendix D.

	Time-step	Changes made
Test 1	3.7 - 11.3 sec	The data points between these two time-steps are missing
Test 1	24.7 sec	The data points of the ramp-up waves are missing. And at 24.7 sec the pitch angle is manually put to 0 rad
Test 2	67.2 sec	From this time step on, the pitch angle is manually put to 0 rad
Test 3	49.5 sec	From this time step on, the pitch angle is manually put to 0 rad
Test 4	38.9 - 47.0 sec	The data points between these two time-steps are missing
Test 4	75.3 sec	From this time step on, the pitch angle is manually put to 0 rad
Test 5	7.1 - 10.2 sec	The data points are wrong edited and corrected
Test 5	16.6 sec	From this time step on, the pitch angle is manually put to 0 rad
Test 6	4.4 - 11.4 sec	The data points between these two time-steps are missing
Test 6	20.6 sec	From this time step on, the pitch angle is manually put to 0 rad
Test 7	18.3 - 26.6 sec	The data points between these two time-steps are missing
Test 7	47.3 sec	From this time step on, the pitch angle is manually put to 0 rad

Table 3.2: Changes made in the raw data

3.2.2 Clean wave selection

As explained in the section 3.1 there are three outputs in each test. These are the pitch angle of the float, the angle of the pendulum and the electrical power output. To gain reliable test results that can be compared with the theoretical model, undisturbed test results are needed. The first few waves are bigger due to the ramp-up waves of the wavemaker. It is observed that the wavemaker needs two waves before it produces a steady wave height. The second reason for the limited time window is the reflected waves from the end of the wave flume. There is a wave absorber to absorb the waves. This absorber does not absorb all the waves. This means that the reflected waves are observed in the test results. In between the start-up wave and the reflected waves the test produces clean waves that can be analyzed. To select these waves the maximum pitch angle of the float is used. It is observed that after the ramp-up waves the wave flume produces 5 clean waves. These 5 waves are then used to validate the theoretical model. See figure 3.4 for the whole time series results of one test. The 5 waves selected as clean waves are indicated with the black lines in the figure. The figure shows the results of test 4. See table 3.1. The top diagram shows the angle of the float, the middle diagram shows the angle of the pendulum and the bottom diagram shows the produced power. In the following sections, the method for how to post-process the experimental data

is shown on the basis of test 4. The other tests are processed the same way. The unprocessed results of the other tests can be found in appendix D.

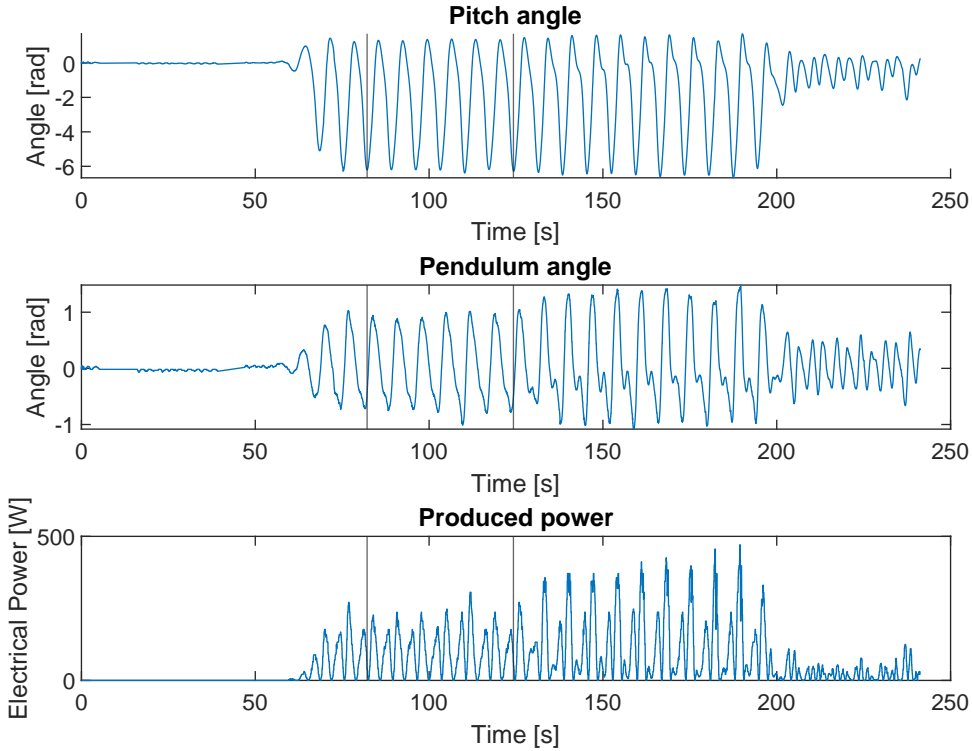


Figure 3.4: Test 4: Time series results and selected waves

After the 5 waves are selected they are corrected for the mean. This is because the ramp-up wave gives the WEC an initial displacement in the positive x-direction. This is also visible in the test results. In figure 3.4 it is clear that the float does not oscillate around 0 but somewhere around 3 rad. The reason for this is that the float makes an initial sway motion and due to the pitch angle is therefore corrected for the mean. It also makes it easier to compare the experimental results with the theoretical model in chapter 4. The results of the 5 selected clean waves corrected for the mean are shown in figure 3.5.

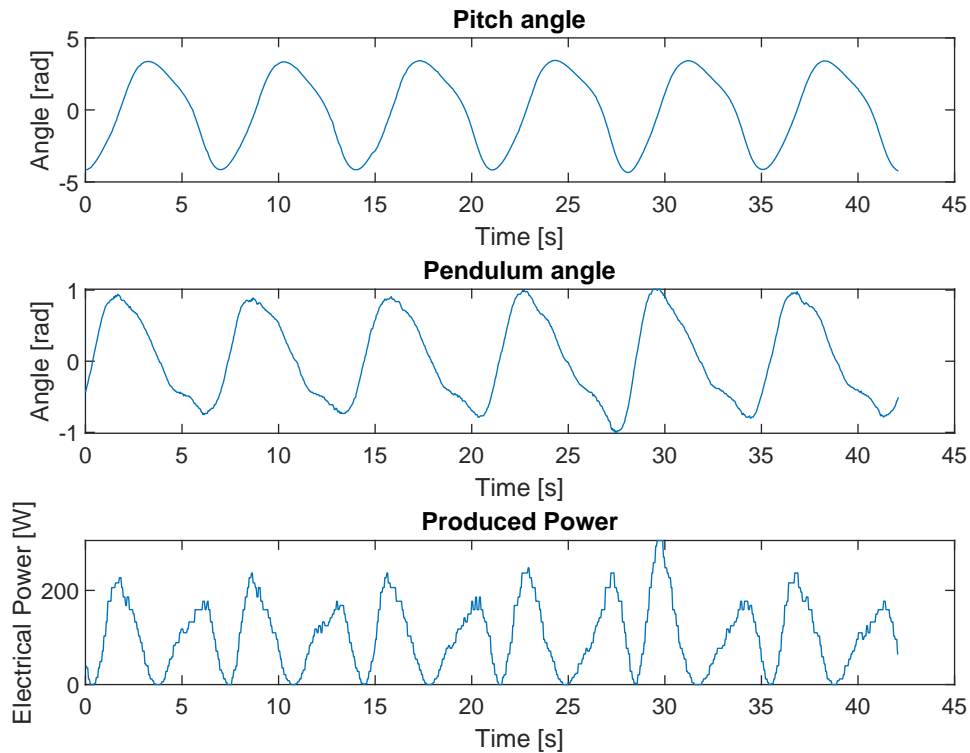


Figure 3.5: Test 4: 5 Clean waves corrected for the mean

3.2.3 Angular velocities

In the experimental tests, only the angles are measured. But it is also interesting to look at the angular velocities. This is because the electrical power is produced by the relative velocity of the generator and the shaft. These velocities are not directly measured, but they can be obtained from the measured positions. To obtain the velocities the Matlab function gradient is used. This function returns a numerical gradient of a vector. This vector must be equally spaced. This is not the case with the test results from the experimental tests. In other words. The time steps of the measurements are not all equal. The maximum time step used in the experiments is 0.096 sec, the minimum time step is 0.021 sec and a mean of 0.040 sec. To solve this the output signals of the pitch angle, the pendulum angle and the power output are re-sampled. This function in Matlab generates a new output signal that describes the same signal but with a different time vector. The new time vector that is used is the mean of the original time vector: 0.040 sec. In figure 3.6 the original signal and the re-sampled signal are compared with each other.

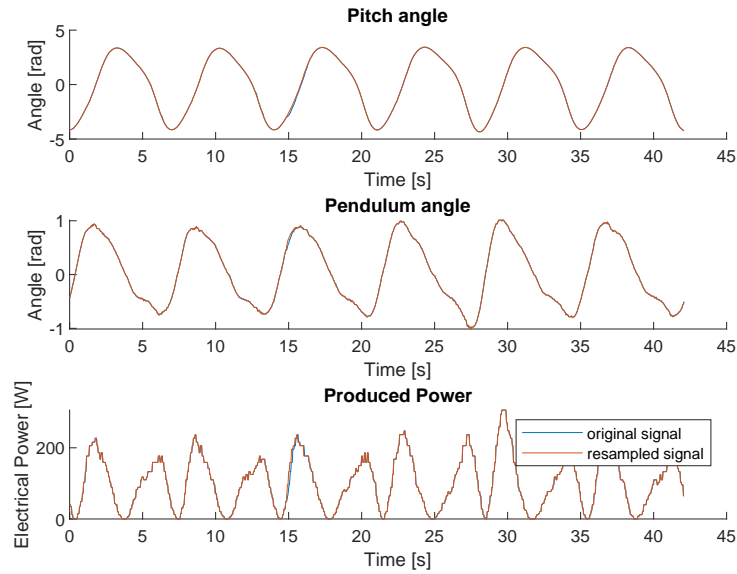


Figure 3.6: Test 4: Compare the original signal with the re-sampled signal

Now that the signals have a uniform spaced time vector the function gradient can be used. This function calculates the gradient between two points with respect to a time vector. The output corresponds to $\frac{\delta F}{\delta t}$. Where F is the re-sampled signal and dt is 0.04 seconds. The result is shown in figure 3.7. Now there is clearly some noise in the signal. To clean the signal and gain a smoother line for the velocities the signal is filtered. The Savizky-Golay filtering with a smoothness of 11 is used. The corresponding Matlab function is `sgolayfilt`. The filtered function is shown in figure 3.8.

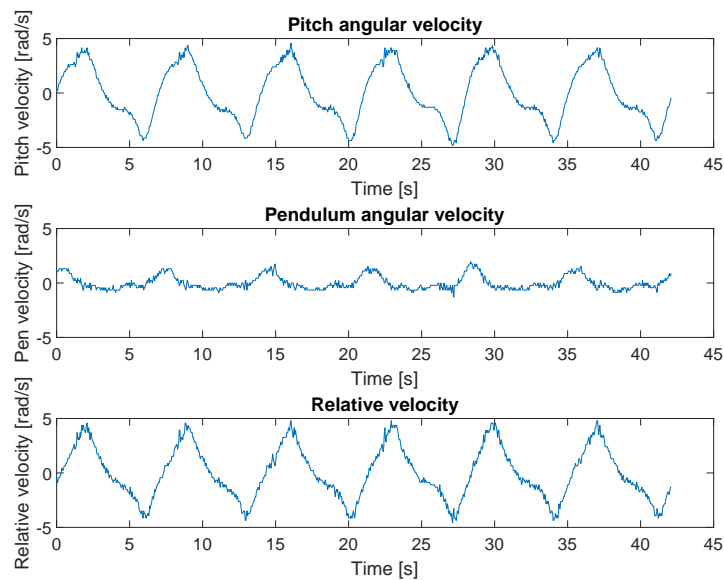


Figure 3.7: Test 4: Velocities computed with the function gradient

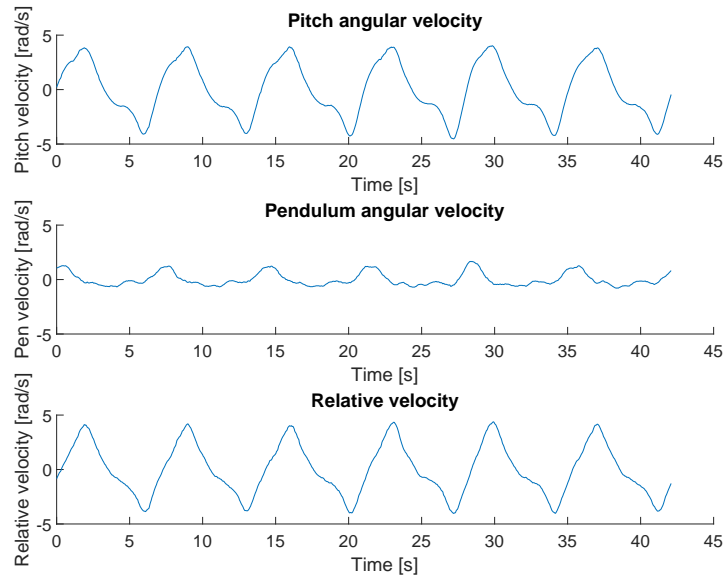


Figure 3.8: Test 4: Filtered velocities

The method that is used to obtain the velocities is numerical differentiation. This is an unreliable method if the time-steps are too small. To validate this method the filtered velocities are integrated to regain the positions. This signal is compared with the original signal in figure 3.9. As shown the signals are all most overlapping with a maximum MSE of 0.0035 for all the tests.

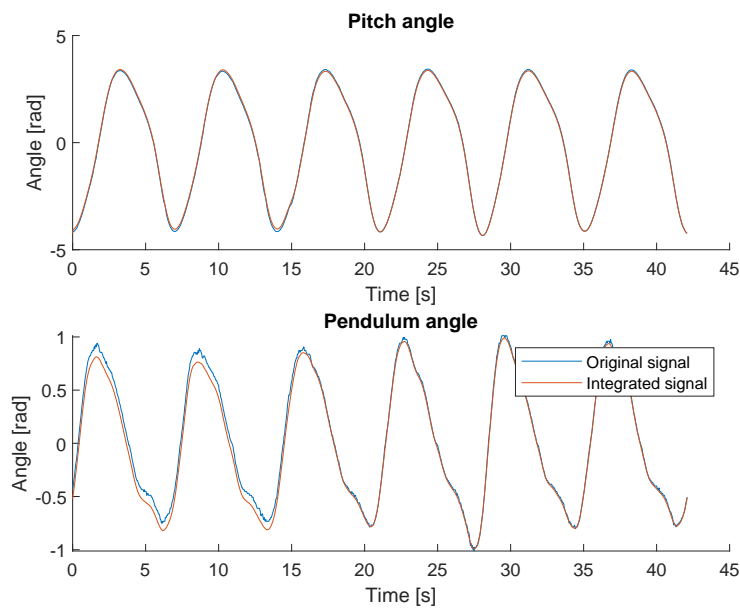


Figure 3.9: Integrated velocity signal compared with the original positions

3.3 Observations during the tests

During the experimental scale tests, it became clear that some of the tested wave conditions produced unwanted behaviour in the model. In some of the tests, this unwanted behaviour resulted in unusable results. There are three main reasons why the test results are unusable. In most tests, these effects occurred simultaneously.

3.3.1 Overtopping

The first reason is overtopping. If the change in water level is faster than the speed in heave direction or if the motion of the WEC is out of phase with the waves, then there was a chance of overtopping. This could cause moments of complete submersion of the WEC. See figures 3.10 and 3.11. This complete submersion causes high changes in the forces and thus the accelerations. These effects are not well captured in the theoretical model and that makes the tests unusable.



Figure 3.10: Unwanted behaviour during the experimental scale tests: Complete submersion 1

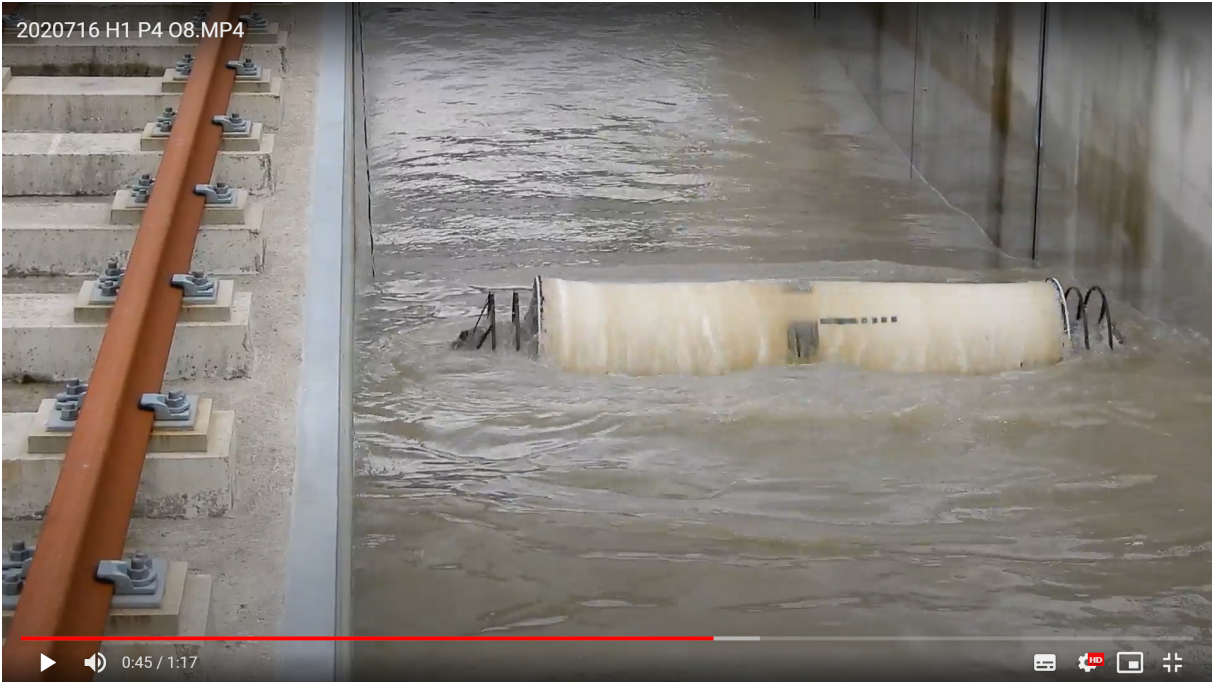


Figure 3.11: Unwanted behaviour during the experimental scale tests: Complete submersion 2

3.3.2 Slack in the ballast line

The second reason why some of the test results are unusable is because of slack in the ballast line. This slack in the ballast line is caused by the drag acting on the ballast weight. If the heave velocity of the WEC became too high the drag on the ballast weight also became high and this cause a lower downward speed of the ballast weight than that of the WEC. This caused slack in the ballast line. And secondly, if the line come under tension again, the WEC showed some shocking motions. These extreme changes in the forces are not well captured by the theoretical model and that makes these test results unusable.

3.3.3 Full rotation of the pendulum

The third unwanted behaviour of the WEC is a full rotation of the pendulum inside the WEC. This is actually a safety measure to prevent high loads on the generator. But the moments when they happen are not well estimated by the theoretical model. This is because the behaviour and forces acting on the generator are unknown and thus not well approximated. An explanation for this is given in chapter 2. Here has to be stated that although the motions of the pendulum and the produced power are not well estimated for these experiments, a good approximation can be made for the pitch motion. This is because the dynamics of the pendulum do not influence the overall behaviour of the WEC by much. This is better discussed in chapter 4.

3.3.4 Wave reflection

The last unwanted behaviour in the test results is wave reflection from the end of the wave flume. As discussed earlier in this chapter. The wave absorber at the end of the wave flume does not absorb all the waves. The reflected waves influence the dynamics of the WEC after a certain period of time. This is solved to look only at the period where the WEC is not influenced by the reflected waves. The method on how to select these clean waves is also described earlier in this chapter.

3.4 Discussion

As discussed in this chapter there are some changes made in the time series data supplied by Dutch Wave Power. There are some irregularities due to the deletion of the ramp-up data. And secondly, in all the tests the data of the pitch angle is changed to 0 rad. Because the missing data is in the ramp-up phase the tests can still be used for this thesis. For each test, there is still enough unedited data to select a section of clean waves. Secondly, because of the initial sway displacement, the pitch angle is corrected for the mean. This is why the motions can still be compared to the estimations of the theoretical model.

There is also some uncertainty in the post-processing of the data. Mainly because numerically differentiation is not always reliable. Nevertheless, it is shown that in this case it can be used because the differentiated and filtered signal still shows the same results when integrated again.

Lastly, a lot of test results are not useful for this thesis. This is because of some of the unwanted behaviour like overtopping and slack in the lines. Despite the fact that these tests are not used in this thesis these tests can be used to find the limitations of the theoretical model discussed in 2. The limitations of the theoretical model are discussed in chapter 4.

Chapter 4

Validation of the model

4.1 Comparison of the numerical model and the experimental tests

The comparison between the numerical model and the experimental tests is made based on the dynamics. This will validate the dynamic response of the numerical model. In the first part of this chapter the numerical model will be tuned to match the experimental tests. This will give certain settings for the PTO system. Secondly, in section 4.5 the settings are tuned to find the maximum power output. In the numerical model, the PTO system is based on a linear damper. In section 4.4 the choice for this linear damper is compared with the behaviour of the generator used in the experiments.

4.1.1 Input parameters for the numerical model

The results from the numerical model are compared with the results from the experiment. The only undefined force component in the numerical model is the PTO-force. This is because the right value of the PTO-damper is unknown. Figure 5.9 shows the different responses of the WEC for a wave of $1m$ wave height and a period of $7sec$. The blue line is the response of the WEC with a PTO-damper value of $20 \frac{Nm}{(rad/s)m}$, the red line with a value of $50 \frac{Nm}{(rad/s)m}$ and the yellow line $80 \frac{Nm}{(rad/s)m}$. At $20 \frac{Nm}{(rad/s)m}$ there is only a small motion in the pendulum this is desired but as explained in chapter 2 the produced power is a function of the linear damper value. This means that a higher value is desired. The value of $80 \frac{Nm}{(rad/s)m}$ is too high because the inside pendulum will make a full rotation. This is unwanted behaviour and negatively influences the power production. This means that the damper value can't be too high because the pendulum will move together with the pitch motion and there is no relative velocity and thus no power production.

As shown in figure 5.9, the PTO damper value has a significant influence on the dynamics of the pendulum. In the dynamics of the WEC itself (surge, heave and pitch) there is only a significant influence in surge motion. But the surge motions are overestimated by the numerical model as will be explained in section 4.2.3. This means that the surge motions are not a reliable output to compare the dynamics.

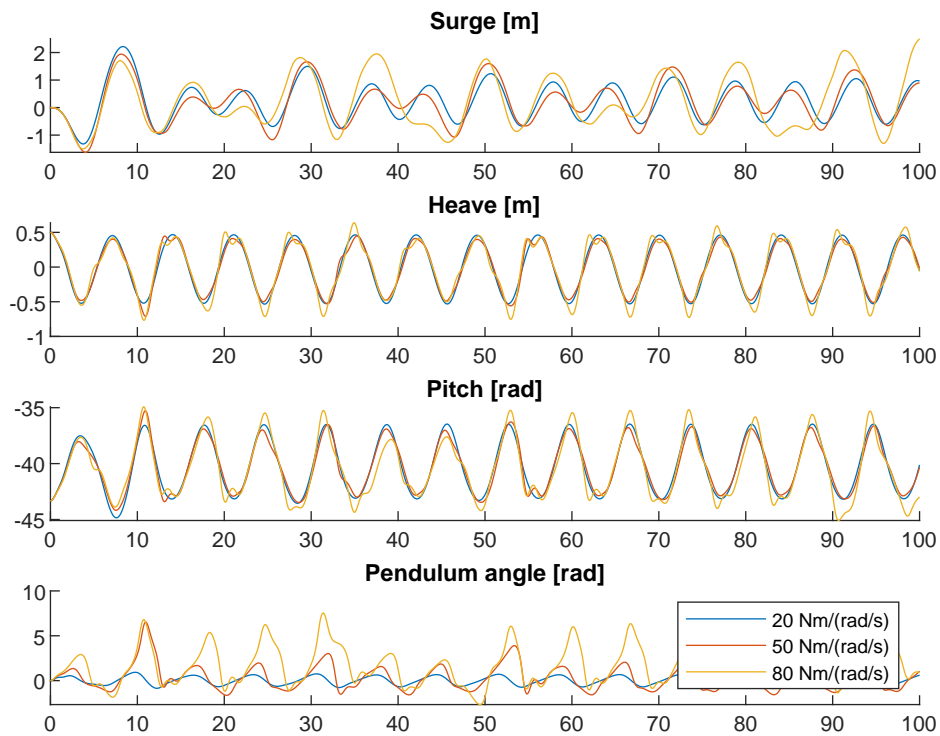


Figure 4.1: Compare the dynamic response for different PTO-damper values

4.1.2 Find the PTO-damper value to match the experiments

To match the dynamics of the numerical model and the experiments there are only two outputs that can be compared. The pitching angle and the pendulum angle. These are the only dynamic outputs of the experiments. The value that needs to be tuned to match the dynamics is the PTO-damper value. Because the pitching angle is not much influenced by the PTO-damper value, the desired PTO-damper value is found by comparing the dynamics of the pendulum. To find the optimal PTO-damper value a searching algorithm is used to find the PTO-damper value that has the lowest difference in the pendulum angle amplitude. The resulting comparison is shown in figure 4.2. This same method is used for all the experiments. The results can be found in appendix E. The numerical model does estimate the dynamics of the experiments well. The error in the pitching angle is up to 14% and the error in the pendulum angle is up to 1.4% wrt the experiments. The comparison, the used damping values and errors for each test can be found in table 4.1.

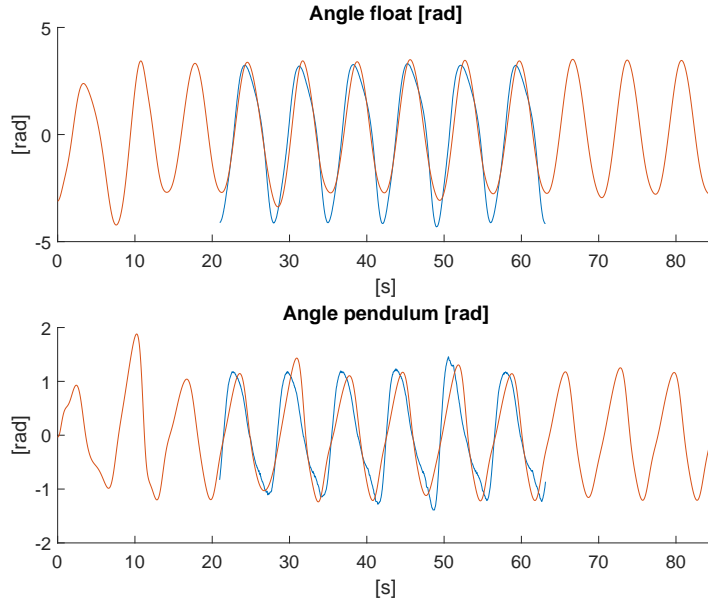


Figure 4.2: Comparison between the numerical model and the experiments

	ζ_a [m]	T [s]	Gen load [Ohm]	B_{PTO} [$\frac{Nm}{(rad/s)m}$]	Pitch amp error [%]	Pen angle amp error [%]
Test 1	0.5	6	8	42	14.0	0.4
Test 2	0.5	6	12	25	12.9	0.1
Test 3	0.5	7	8	28	10.3	1.4
Test 4	0.5	7	12	26	12.0	1.3
Test 5	0.5	8	8	34	6.8	0.6
Test 6	0.5	8	12	22	6.5	0.6
Test 7	0.5	9	8	39	8.4	0.4

Table 4.1: Errors in the dynamics with the tuned damper

4.2 Compare dynamics

4.2.1 Pitch angle

The pitch angle of the WEC is well approximated for all the different experiments. As shown in appendix E in the top left plot one can see that for all the figures the results of the pitch angle match the results within 14% accuracy. There has to be noted that in all the tests the minimum angles are underestimated. This is the moment where the float gets lifted out of the water at the top of a wave crest. This difference is properly because of the simplification in the ballast force. The difference is also visible if the velocities are compared, see figure 4.3. Here one can see that the minimum angular velocities of the experiments are lower than those of the numerical model. In the experiment, the ballast weight has some momentum. Because of this momentum, it is expected that the force in the ballast line at the wave crest is lower than estimated by the model. This could explain why the float angle gets underestimated. There has to be noted that there is no data to verify this.

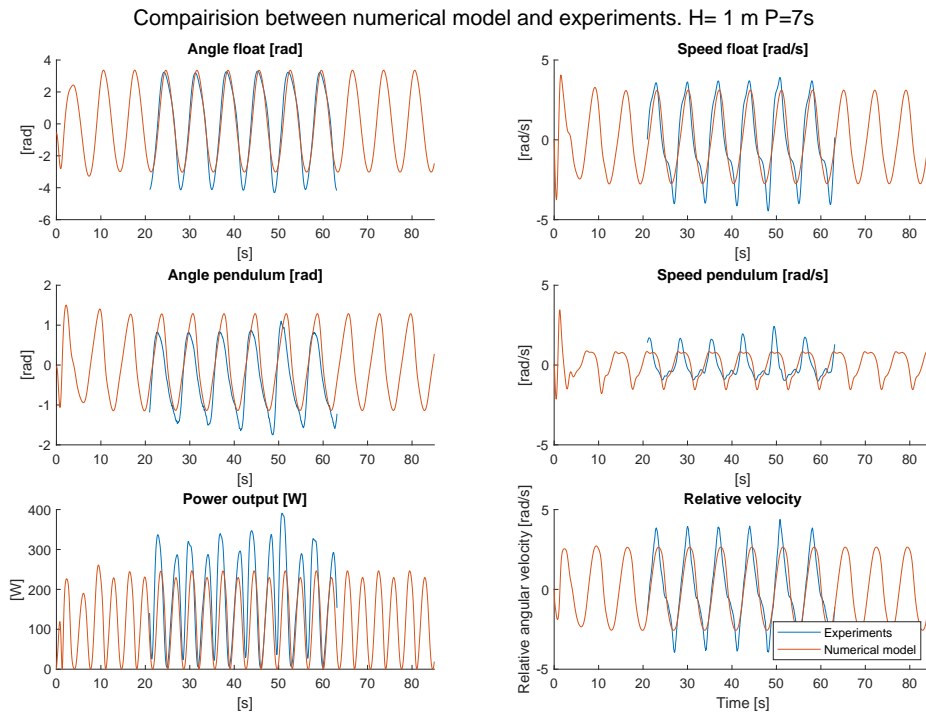


Figure 4.3: Comparison between numerical model and experiments $H=1\text{m}$, $P=7\text{s}$

4.2.2 Pendulum angle

The angle of the pendulum is influenced by the motions of the WEC. The amount of coupling between the WEC and the pendulum is determined by the load on the generator. A lower load in the generator means that there is a higher torque inside the generator, this means more coupling between the pitch motion and the pendulum angle. While a higher load on the generator means that there is less torque acting on the pendulum and also less coupling. This effect is simulated in the numerical model by using a linear damper. A higher value for this damper results in more coupling between the pitch motion and the pendulum angle, and a lower value results in a lower coupling.

4.2.3 Surge motion

The surge motion is the horizontal motion of the WEC parallel to the wave direction. Although the surge motion is not measured in the experimental tests there are videos made of the experimental tests that give an indication of the surge motion. And for the numerical model, the surge motions can be easily obtained.

In the experiments, it is clear that WEC gains a translation into the positive x-axis and oscillates around this point. This can also be concluded from the raw data of the experimental tests. In appendix D it is shown that for all the tests the pitch motion does not oscillate around zero rad, but around an angle smaller than 0. This indicates that the WEC got a translation into the positive x-axes. This translation is not found in the numerical model. This is further discussed in section 4.7.

Secondly, from the videos, the amplitude of the surge motions can be roughly estimated. These are not scientific but, they can give an indication. In figures 4.4, 4.5, 4.6 and 4.7 it is indicated how the surge motions of the experimental tests are obtained. The videos are watched and the locations in the wave flume can be compared due to the indications on the wall. It is known that the diameter of the WEC is 0.8m. This means that the amplitude of the motions can be estimated. The amplitudes of the surge motions

obtained from the videos are between the $0.5m$ and the $1.0m$, see table 4.2. The amplitudes estimated by the numerical model can be easily obtained. The amplitude of the surge motions obtained from the numerical model lay between the $1.1m$ and $2.0m$. Although there is some uncertainty in the values from the experiments because they are obtained from watching videos, it is clear that force balance in horizontal direction is off.

One of the reasons for the underestimation of the surge motion amplitude could be the ballast weight. A force is needed to pull the ballast weight through the water. The numerical model does not account for the forces on the ballast weight as it is approximated by a constant downwards pull. Despite the overestimation, it is clear that the pitch and pendulum dynamics are not so much influenced by the surge motions. As explained they are well estimated by the numerical model. And the pitch and pendulum dynamics are the ones that generate the power.

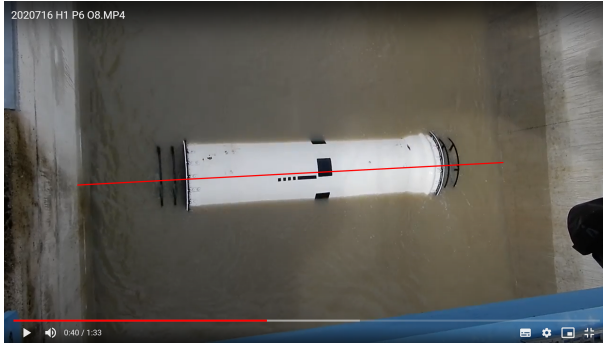


Figure 4.4: Test 1: Minimum surge



Figure 4.5: Test 7: Minimum surge



Figure 4.6: Test 1: Maximum surge



Figure 4.7: Test 7: Maximum surge

	surge amplitude experiments [m]	surge amplitude numerical model [m]
Test 1	~ 0.5	1.1
Test 2	~ 0.5	1.1
Test 3	~ 0.6	1.3
Test 4	~ 0.6	1.3
Test 5	~ 0.8	1.6
Test 6	~ 0.8	1.6
Test 7	~ 1.0	2.0

Table 4.2: Observed surge motions

4.3 Compare Produced Power

4.4 Validation of the ideal damper as a PTO-system

The numerical model does not only estimate the dynamics, it also estimates the produced power. In the bottom left plot of figure 4.2 is the produced power over time displayed and in the bottom right plot is the relative velocity over time. See appendix E for the other tests. Even though the dynamics are matched the experiments show a higher mean power output than the numerical model. What is interesting to see is that the experiments have clear peaks in the produced power. It is even noticeable that every other peak is bigger than the other. This means that the WEC reaches a higher speed and produces more power with the downward motion. This behaviour is also visible in the numerical results and becomes more visible in the tests with a lower wave period.

In wave energy, it is common to compare the produced power on the basis of the mean produced power per wave cycle. The mean produced powers per wave cycle of the experiments and the numerical model are shown in table 4.3. The numerical model underestimates the produced power up to 47%.

	Mean power output experiments [W]	Mean power output numerical model [W]	Difference [%]
Test 1	229	120	47.6
Test 2	215	142	34.0
Test 3	183	123	32.8
Test 4	154	108	29.9
Test 5	141	107	24.1
Test 6	112	85	24.1
Test 7	125	90	28.0

Table 4.3: Comparison between the mean power and maximum power of the numerical model

It is assumed that the torque and the produced power of the generator are a function of the relative angular velocity between the float and the pendulum. With an ideal damper, these relations are shown in equations 2.24 and 2.25. The exact relation in the generator is unknown, but it can be expected that both the torque and the generated power are related to this relative velocity. This relation of power and torque with the relative angular velocities is plotted in figure 4.8 and 4.9. In blue the results of the experiments and in orange the results of the numerical model. In figure 4.9 one can clearly see the behaviour of the linear damper. Also it is clear that the behaviour of the generator is not linear. The points that show the torque inside the generator for the experiments are not measured, but they are obtained by dividing the power by the relative velocity. This gives some strange behaviour around a relative velocity of 0. The result of a small power divided by something close to 0 m/s will give something large. This explains the strange behaviour of the experiments around a relative velocity of 0 m/s.

In figure 4.8 it is clear why there is an underestimation of the mean power. The numerical model underestimates the produced power for each relative velocity. The same is found in figure 4.9, the torque inside the generator is also underestimated. If a higher torque is implemented than the numerical model losses accuracy in the dynamics. This means that the area between the experiments and the numerical model in figure 4.9 are torque losses, also see equation 4.1 where M_{system} is the torque that lifts the pendulum, M_{losses} are the torque losses and $M_{generator}$, is the torque inside the generator acting on the shaft. These torque losses are not captured by the numerical model. The numerical model gives the same dynamic output, but with a lower torque on the shaft. This explains the lower produced power output of the numerical model. This means that the linear damper for the PTO can be used to estimate the dynamics. But an estimation for the torque losses needs to be included in the produced power is estimated. Nevertheless, the model can still be used to estimate the dynamics of the WEC and if changes in parameters have a positive or negative influence on the produced power. The absolute values can underestimate the produced power up to 47%.

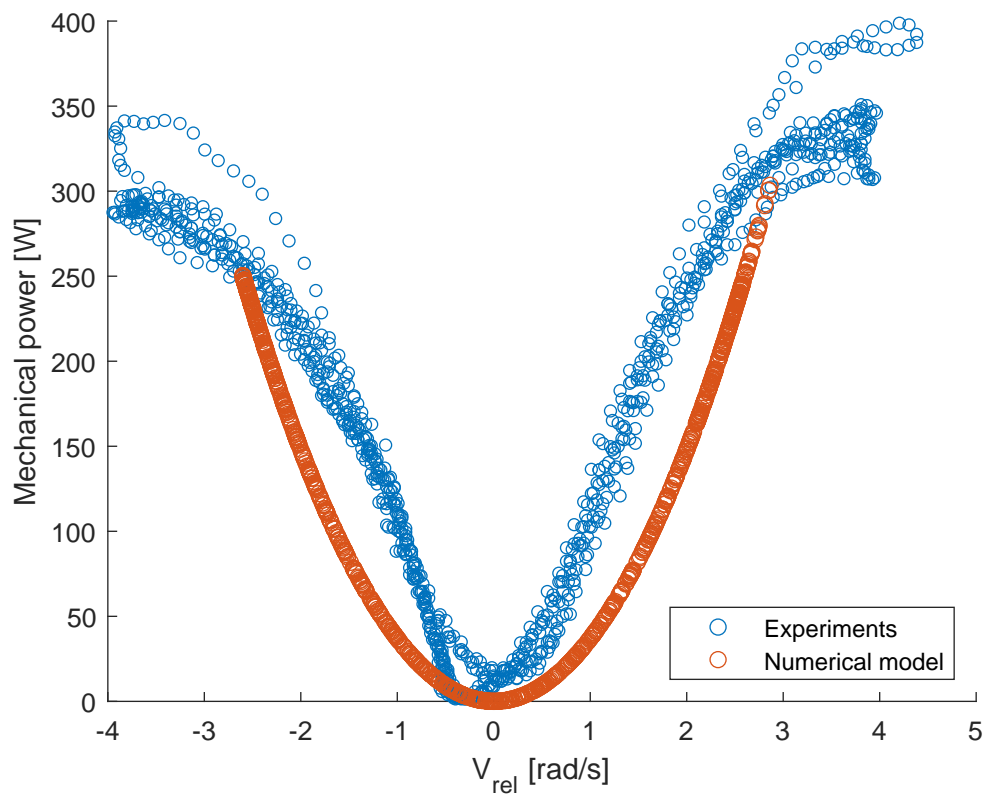


Figure 4.8: Relative velocity plotted against mechanical power $H=1m$ $T=7sec$

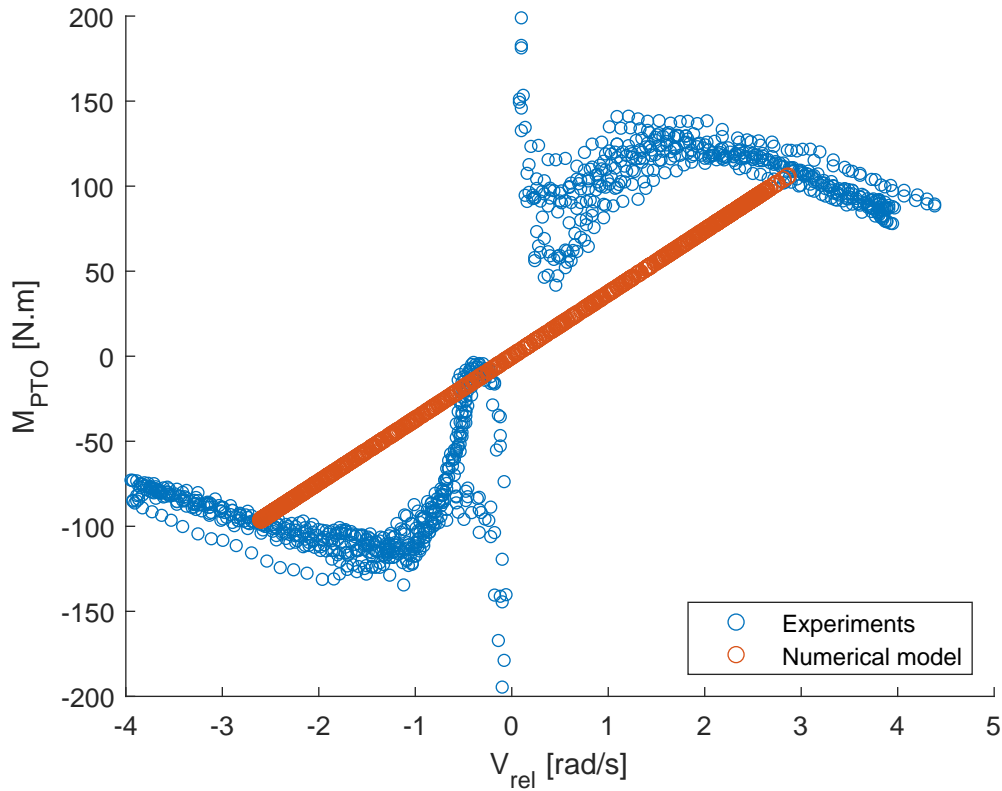


Figure 4.9: Relative velocity plotted against torque inside the generator $H=1\text{m}$ $T=7\text{sec}$

$$M_{system} + M_{losses} = M_{generator} \quad (4.1)$$

4.5 Compare generator settings with the numerical maximum

It is interesting to look at the settings of the numerical model that match the experiments, but the settings of the experiments were based on an educated guess and were executed prior to this thesis. This means that the settings used in the experiments are not the settings where the highest power is produced. As explained, the absolute values of the produced power are not so accurate, but maximizing the produced power of the numerical model gives insight into the desired dynamics at which optimal power production occurs. Furthermore, it gives an indication of how far the chosen settings of Dutch Wave Power in their experiments are from the ideal settings.

Figure 4.10 shows the mean electrical power produced for each cycle for different PTO-damper values. Each line represents a different sea-state. In this figure the regions tested by Dutch Wave Power are indicated. These are the 8 and 12 Ohm generator settings. There is not one specific damper value found that represents the different generator loads. But it is found that for each sea-state. Furthermore, it becomes clear that each regular sea-state has its own ideal PTO-damper value. The ideal PTO-damper values are given in table 4.4. Secondly, figure 4.11 shows the efficiency of the WEC. The efficiencies correspond to the points in figure 4.10. The efficiency is calculated by dividing the produced electrical power by the amount of power stored in the waves. The equation for power in waves is given in equations 4.2, 4.3 and 4.4. Deep water is assumed. The efficiency η is calculated by dividing the mean produced power by the power in the waves, see equation 4.5.

$$P_{wave} = E_{wave}c_g \quad (4.2)$$

$$E_{wave} = \frac{1}{2}\rho g\zeta_a^2 \quad (4.3)$$

$$c_g = \frac{1}{2} \sqrt{\frac{g}{k}} \quad (4.4)$$

$$\eta = \frac{P_{mean}}{P_{wave}} \quad (4.5)$$

The generator setting of 8 Ohm is near the optimal setting for the sea-state with a wave height of 1m and a period between 6 and 7 seconds. For higher periods a lower generator setting is desired. While for a higher period the load on the generator can be higher. From figure 4.10 it is clear that the choice of the PTO-damper value is specific for each sea-state. But, close to the optimum, the choice is not that sensitive. The second thing that is noticeable is that after a certain period there is a viable drop in the mean power production. This is because from that point on there is so much coupling between the float and the pendulum that the pendulum makes a full rotation. This indicates that this should be prevented. Because it significantly lowers the power production.

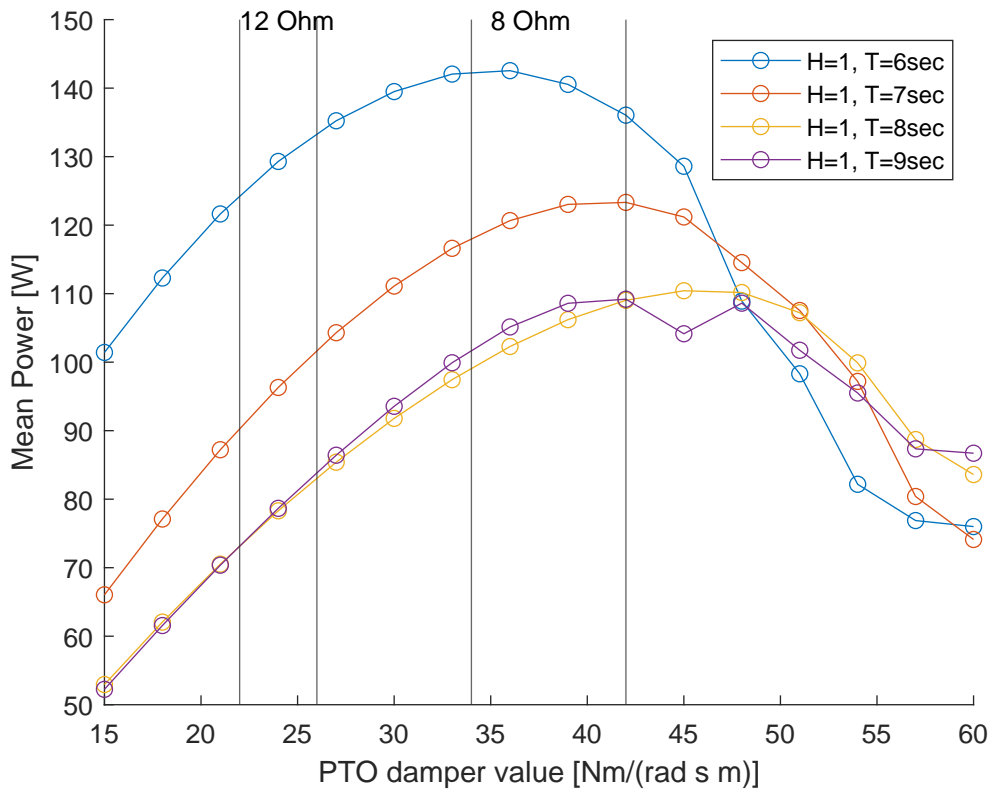


Figure 4.10: Mean power compared to different PTO-damper values

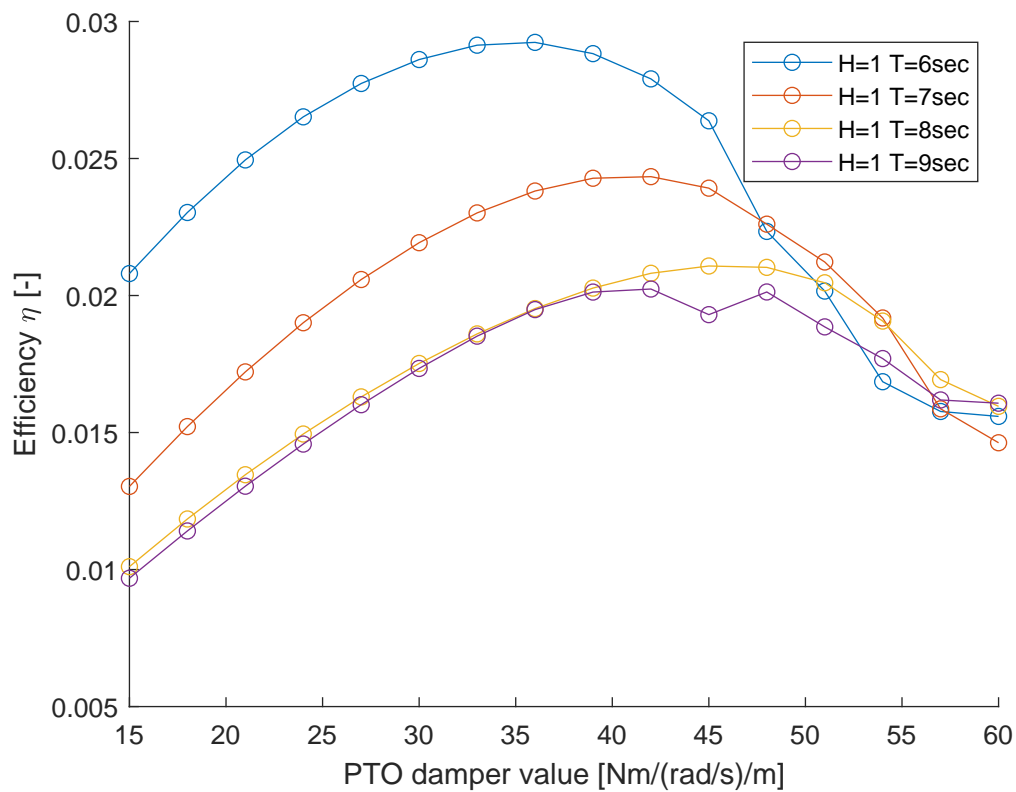


Figure 4.11: Efficiency compared to different PTO-damper values

	Optimal theoretical PTO-damper value [$\frac{Nm}{radsm}$]
H=1m, T=6sec	35
H=1m, T=7sec	40
H=1m, T=8sec	45
H=1m, T=9sec	42

Table 4.4: The optimal PTO-damper values

4.6 Improving the WEC performance

4.6.1 Pendulum Weight

One of the limitations in the power production of the WEC is the amount of torque that is acting on the shaft before the pendulum makes a full rotation. This negatively influences power production, as explained earlier. The amount of torque needed let the pendulum make a full rotation can be increased by making the weight of the pendulum heavier.

To investigate the influence of a move heavy pendulum. Mass is shifted from the WEC to the pendulum. This is done to keep the same overall mass and draft. This also means that the hydrodynamic coefficients are the same. Figure 4.12 shows the mean produced power of a sea-state with 1m wave height and a period of 7 sec at different PTO damper values. The different lines show the amount of mass that is shifted from the WEC to the pendulum mass. The original mass of the pendulum is 31.7 kg/m. This mass is increased up to 46.7 kg/m. For a higher mass, a higher PTO damper value gives the optimal power production. The mean produced power is increased regardless of the PTO damper value.

Figure 4.13 shows the difference in dynamics and produced power for the original WEC and the WEC

with a shifted weight of 15 kg in a sea-state of 1m wave height and 7sec period. There are no significant changes in the WEC dynamics, but there is an increase in mean produced power of more than 35%. Increasing the weight allows for a higher torque inside the generator. Which generates a higher power under the same dynamics. Here can be concluded that a heavier pendulum will increase the mean power output and positively influence the performance of the WEC.

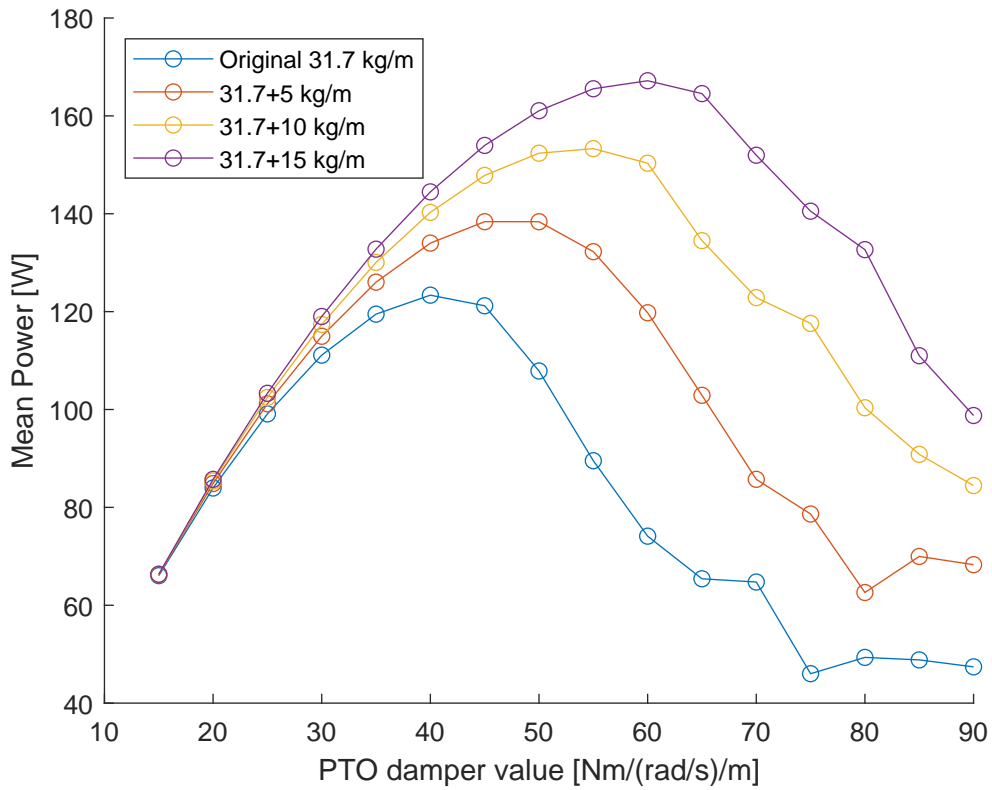


Figure 4.12: Mean produced power for different pendulum weights with a sea-state of 1m and 7sec

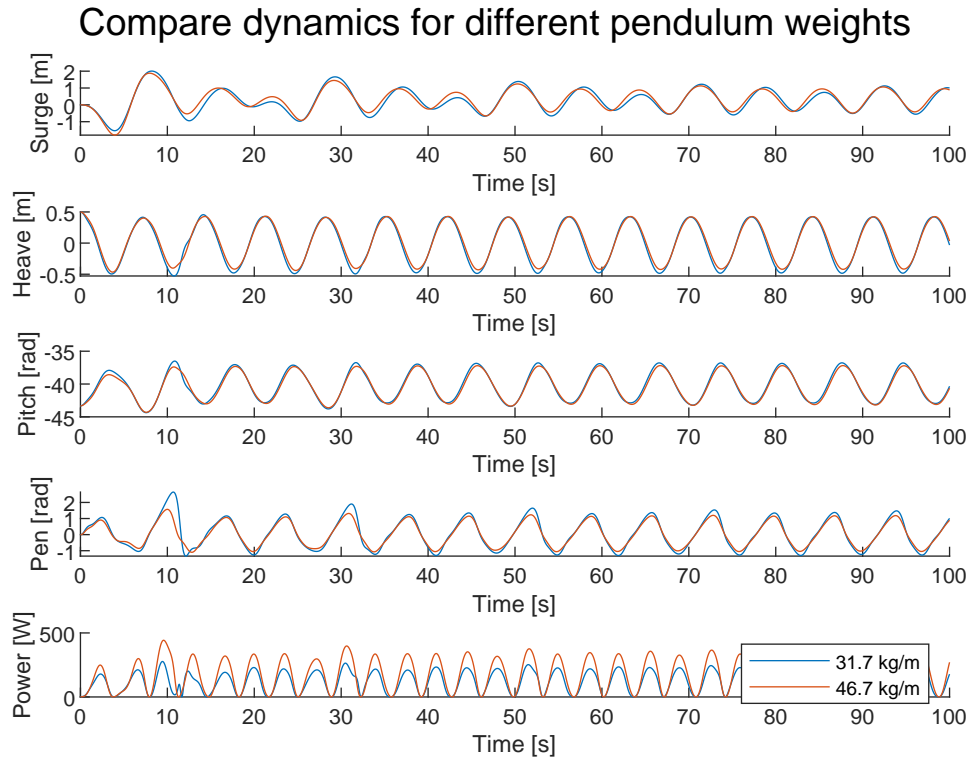


Figure 4.13: Dynamic response for different pendulum weights

4.6.2 Winding diameter

It is known that the power is generated due to the relative velocity between the pendulum and the WEC. To increase the power production it is also interesting what the effect of the diameter where the mooring and ballast lines are connected. The variation in the diameter gives higher or lower rotational speeds. The mean produced power for different diameters at different PTO damper values is shown in figure 4.14. These are the results for a sea-state of 1m wave height and a period of 7sec. This is expected, because with a smaller r_{in} the WEC needs to rotate faster for the same heaving motions. This is because these motions are coupled. For the sea-state shown in figure 4.14 up to 23% if the inner radius is decreased by 2cm. But the tuning of the PTO system becomes more important. The point where there is too much coupling and the pendulum makes a full rotation is more sensitive with a smaller diameter.

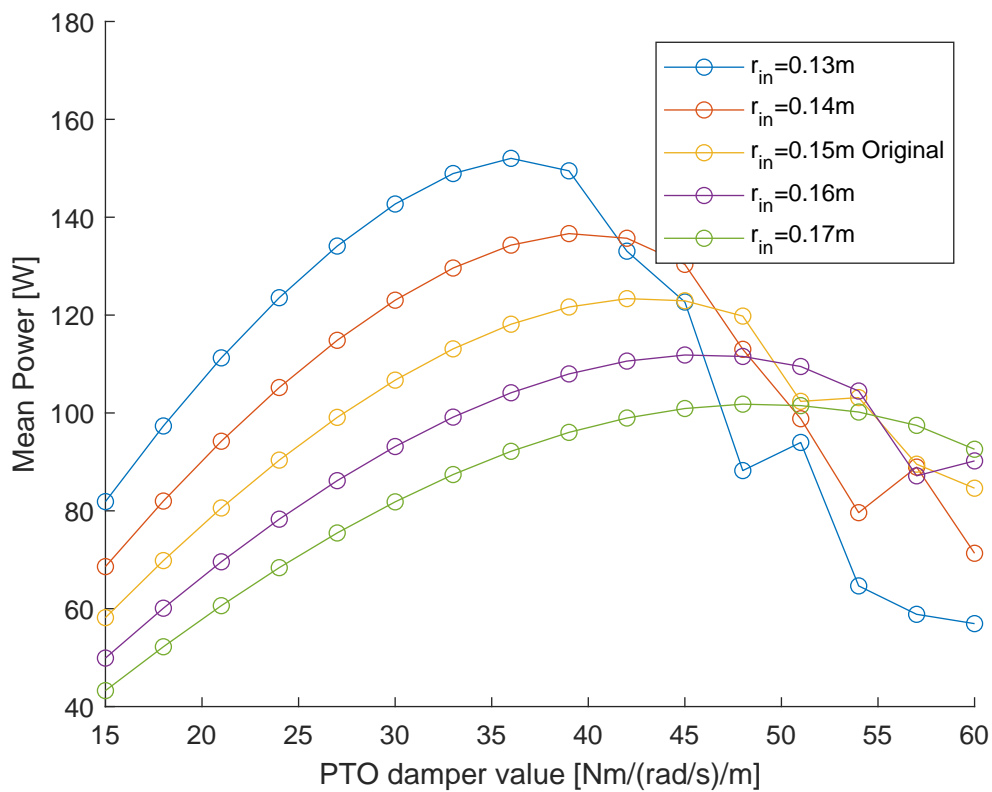


Figure 4.14: Mean produced powers for different r_{in} against different PTO damper values

In figure 4.15 the comparison in dynamics is made for two different r_{in} , one being 0.13m and the original radius of 0.15m. There are no significant differences in the heave motion and the pendulum angles. The pitching angles are increased by 16% and the mean produced power is increased by 23% for this sea-state. At the beginning of the simulations gives some unwanted behaviour. The pendulum makes a full rotation because of the start-up phase. From these results can be concluded that a decrease in r_{in} has a positive influence on the mean produced power.

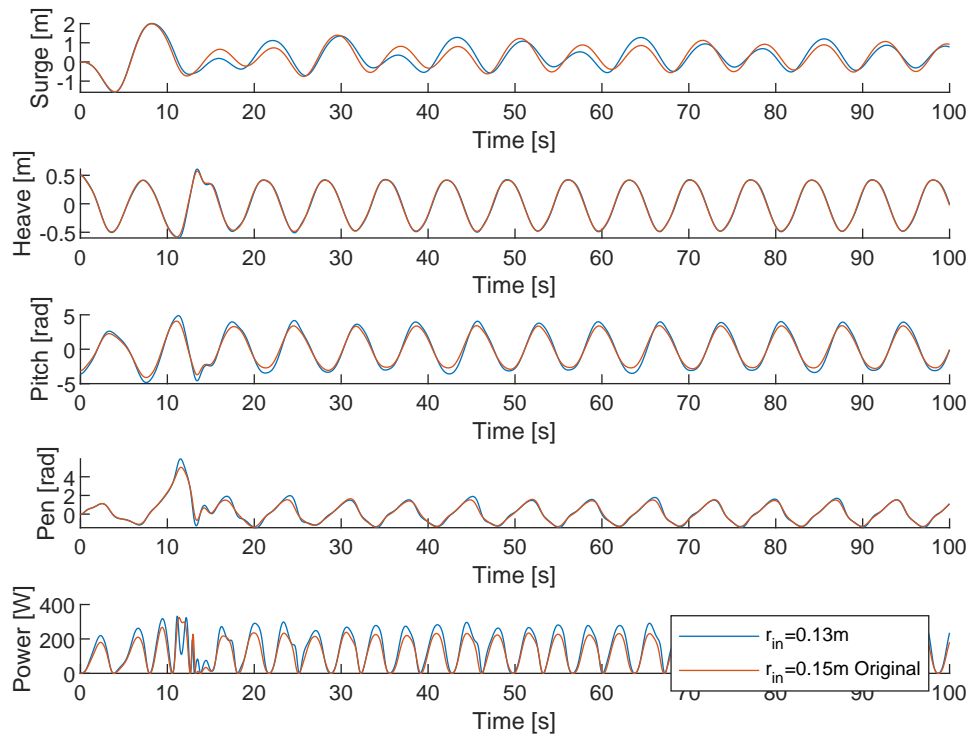


Figure 4.15: Dynamics of the WEC for different PTO damper values

4.7 Discussion and conclusion

There are some small differences in the heaving motion of the experiments and the numerical model. But there is a factor 2 difference in surge motion. If the PTO-damper is tuned the pitch dynamics of the WEC are estimated within 15% and the dynamics of the inside pendulum within 1.5%. One of the shortcomings of the numerical model is that the FK forces in surge are neglected. And secondly, the simplification of ballast weight as a constant force. The ballast weight moves through the water and influences the dynamics of the WEC itself. The forces acting on the ballast weight are neglected in the numerical model. This is why resulting surge motions will have approximately half the amplitude estimated by the numerical model.

In the experiments an initial surge transition was observed. This so called drift is not captured by the numerical model. To implement this one would need to compute the second order wave drift forces. There is chosen to not include the drift forces as this is not the focus of the thesis.

Next, the estimation of the PTO system as a linear damper also brings some uncertainties. Especially the dynamics of the pendulum and the produced power. Due to torque losses is the torque in the generator higher than in the numerical model. This higher torque also means higher power. If this same torque is modelled in the numerical model then this will mean that there is a too large coupling between the float and the pendulum. A too-large coupling between the float and the pendulum results in the pendulum making a full rotation. This is unwanted behaviour and will negatively influence the produced power. The numerical model already predicts a full rotation by torques registered in the experiments. This indicates the presence of torque losses. The ideal PTO-settings show the ideal torque on the shaft. This means that the torque in the generator will be higher than the model predicts. And with this higher torque also a higher produced power. This results in large uncertainties in the absolute values of the produced power of the numerical model. Nevertheless, the model can still be used to investigate the ideal and desired dynamics and to check if changes in parameters have a positive or negative influence on the mean produced power.

For example, one of the limitations in power production is the maximum torque on the shaft before the pendulum makes a full rotation. If the weight of the pendulum is increased, the mean produced power is also increased. Secondly, a decrease in r_{in} also gives a higher produced power. This gives an increase in pitching speed. There has to be noted that with this decrease in r_{in} the tuning of the PTO system becomes more sensitive.

Chapter 5

Irregular wave model prediction

An irregular sea-state is described as a superposition of regular wave components. This assumption gives the possibility to research the hydrodynamic response of the WEC in irregular waves. Secondly, the Froude scaling laws give the possibility to test a WEC with different scaled dimensions. This is done by scaling the waves down. This has as advantage that the hydrodynamic properties of the WEC in the numerical model don't have to be changed. The response of a WEC that is twice the size of the WEC tested in the wave flume can be derived due to the Froude scaling laws. This is done for a full range of wave height and period combinations to construct a power matrix.

5.1 Irregular waves

5.1.1 Wave spectrum

In nature, a regular sea-state does not occur. The waves present in the real world are presented by an irregular sea-state. Also referred to as a random sea. An irregular sea-state can be composed as a summation of sinusoidal regular waves, see equation 5.1 and figure 5.1 [34]. The number of wave components (n), also called partial waves, that need to coincide depends on the total simulation time. This is to prevent the sea-state from repeating itself. The number of partial waves can be calculated using equation 5.2. Each partial wave has its own wave frequency. Equation 5.2 is used to calculate the maximum step size for the wave frequency.

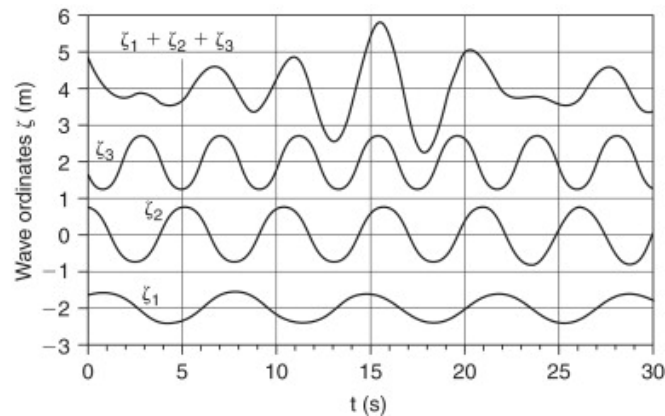


Figure 5.1: Irregular waves from the sum of regular waves

$$\eta(x, t) = \sum_{i=1}^n \zeta_i \cos(k_i x - \omega_i t + \epsilon_i) \quad (5.1)$$

$$T_{simulation} = \frac{2\pi}{\Delta\omega} \quad \text{and} \quad \Delta f = \frac{\Delta\omega}{2\pi} \quad (5.2)$$

The parameters for the partial waves can be obtained from a wave spectrum $S_\zeta(\omega_n)$. This wave spectrum shows how the energy in the waves is divided. From this wave spectrum, the wave amplitudes of the partial waves can be obtained see equation 5.3 and figure 5.2 [27].

$$S_\zeta(\omega_n)\Delta\omega = \sum_{\omega_n}^{\omega_n+\Delta\omega} 1/2\zeta_{a_n}^2(\omega) \quad (5.3)$$

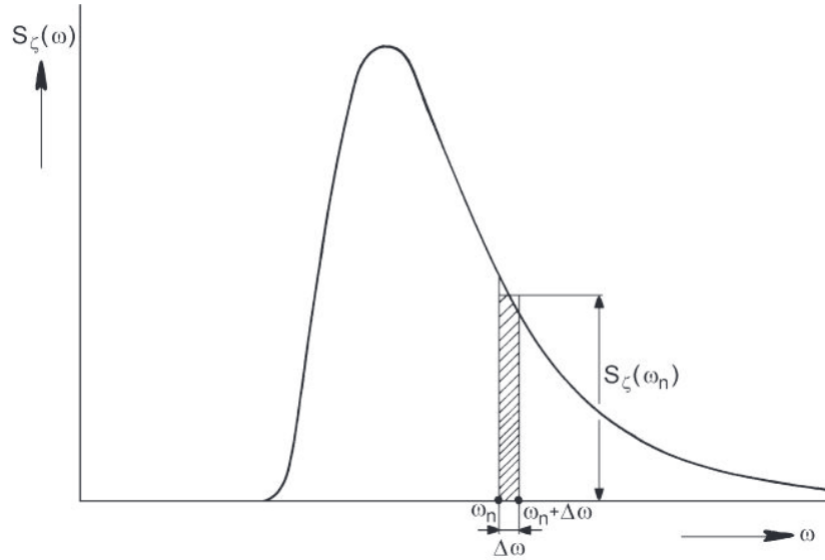


Figure 5.2: Wave spectrum

5.1.2 JONSWAP spectrum

The irregular sea-states used in this thesis are based on the JONSWAP spectrum. This is short for the Joint North Sea Wave Program. A JONSWAP spectrum is used to describe a sea-state that is not fully developed. A JONSWAP spectrum can be constructed using equation 5.4 [27] [34] [35]. An example of a JONSWAP spectrum with a significant wave height of 1m and a peak period of 5 sec is given in figure 5.3.

$$S(\omega) = \frac{\alpha g^2}{\omega^5} \exp\left(-\frac{5}{4}\left(\frac{\omega_p}{\omega}\right)^4\right) \gamma \exp\left(-\frac{(\omega - \omega_p)^2}{2\sigma^2\omega_p^2}\right) \quad (5.4)$$

$$\begin{aligned} \alpha &= 0.076\left(\frac{U_{10}^2}{F_g}\right)^{0.22} \\ \omega_p &= 22\left(\frac{g^2}{U_{10}F}\right)^{1/3} \\ \gamma &= 3.3 \\ \sigma &= \begin{cases} 0.07\omega \leq \omega_p \\ 0.09\omega > \omega_p \end{cases} \end{aligned}$$

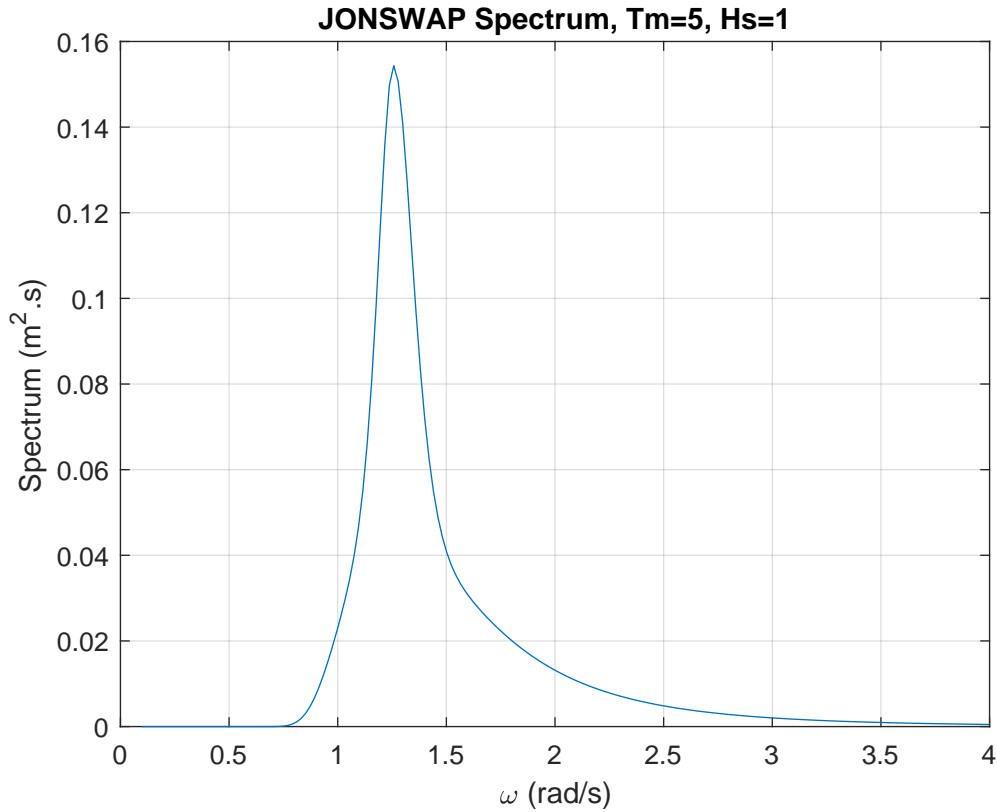


Figure 5.3: Example of a JONSWAP spectrum

5.2 Adaptation of the model for irregular waves

If the theoretical model wants to estimate the response of irregular waves. Some improvements need to be made. There are 3 parts of the model that need to be improved to adapt the model for irregular waves. This is the wave input, the Froude-Krylov forces and the diffraction forces.

5.2.1 Wave input and ramp-up time

As described in the previous section, an irregular sea-state can be described as a summation of multiple regular waves. Each component has its own amplitude ζ_i , wave frequency ω_i and phase shift η_i . The wave parameters are estimated based on a JONSWAP spectrum with as inputs the significant wave height H_s and the peak period T_p . The amount of wave parameters N is dependent on the total simulation time. The resulting wave elevation is now described in equation 5.1.

Because the wave height of an irregular sea is shifted by a random phase shift, it is not possible to know the wave elevation at $t = 0$. To ensure a smooth start-up phase of the model a ramp function is used. This ramp function gradually increases the wave elevation and forces. The ramp-up time is 20 seconds.

5.2.2 Froude-Krylov force

The Froude-Krylov force is adapted for the theoretical model using the same superposition principle as for the wave components. The pressure contribution of each wave component gets integrated over the wet surface of the WEC. The Froude-Krylov force is the summation of all the different wave components. See equation 5.5 and 5.6. The integral for each wave component is simplified and solved as described in section 2.3.2.

$$F_{FK} = \sum_{i=1}^N \iint_S P_{dyn,i} n dS \quad (5.5)$$

$$P_{dyn,i} = \rho g \zeta_i \cos(k_i x(t) - \omega_i t + \eta_i) e^{k_i z} \quad (5.6)$$

5.2.3 Diffraction force

The diffraction forces can also be adapted by using the superposition principle. Each wave component has its own period. From this period a force coefficient can be obtained from figure 2.8. For each wave component the diffraction force is calculated using the method used in section 2.2.3 The total diffraction force is now the summation of the diffraction force components. See equation 5.7.

$$F_{Diff} = \sum_{i=1}^N \zeta_i C_{diff,123,i} \cos(k_i x(t) - \omega_i t + \eta_i + \epsilon_{123,i}) \quad (5.7)$$

5.2.4 Results

The resulting outputs of the model to irregular wave loading are shown in figure 5.4 and 5.5. In this specific test the significant wave height H_s is 1m and the peak period T_p is 6.5 seconds. The total simulation time is 100 seconds and that corresponds to 63 wave components N .

From figure 5.4 it is clear that after the changes are made the model also handles irregular waves. Here has to be noted that sometimes complete submersion occurs. This happens only at big wave components like the one around 19 seconds and 40 seconds. This means that around these moments the output is less accurate and non-linear forces are expected. Nevertheless, even in higher waves, the model gives an estimation of the dynamics. See 5.6 and 5.7

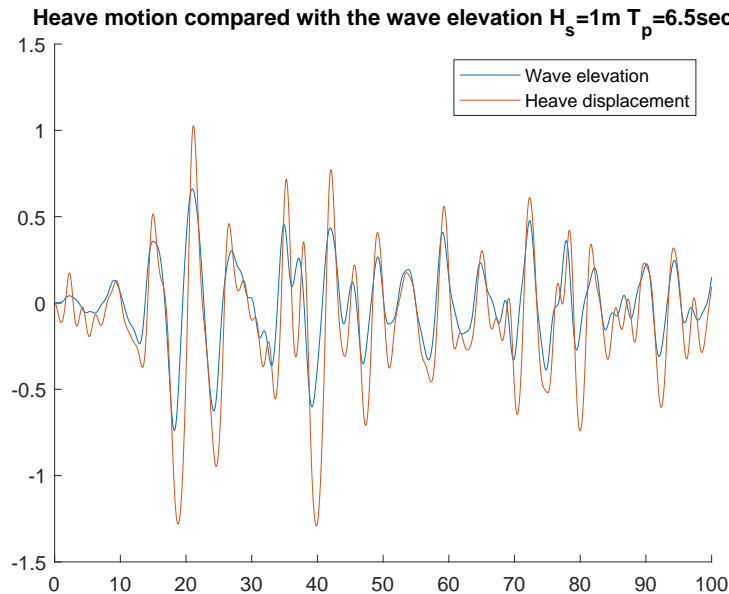


Figure 5.4: Irregular waves: Heave motion and Wave elevation $H_s = 1m$ $T_p = 6.5sec$

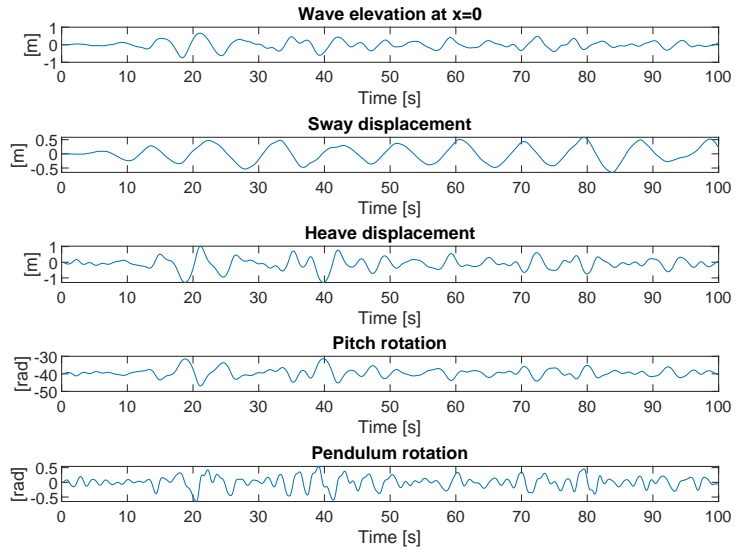


Figure 5.5: Irregular waves: model output $H_s = 1m$ $T_p = 6.5sec$

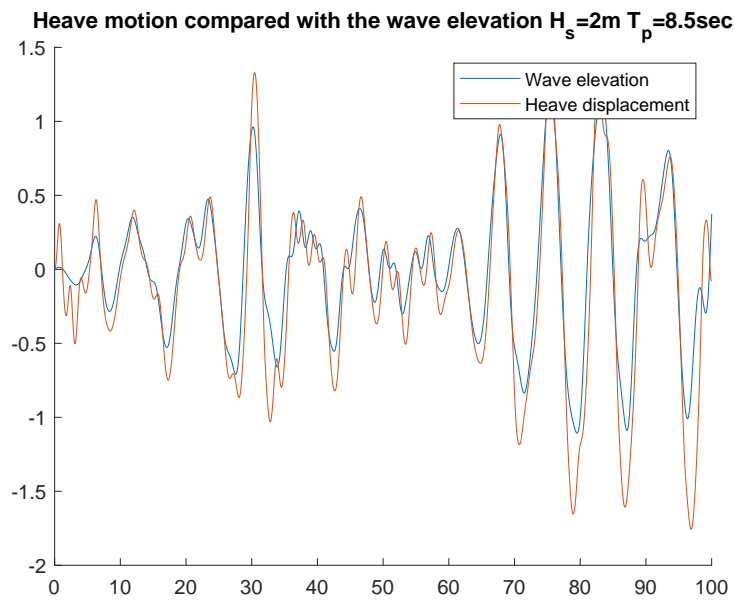


Figure 5.6: Irregular waves: Heave motion and Wave elevation $H_s = 2m$ $T_p = 8.5sec$

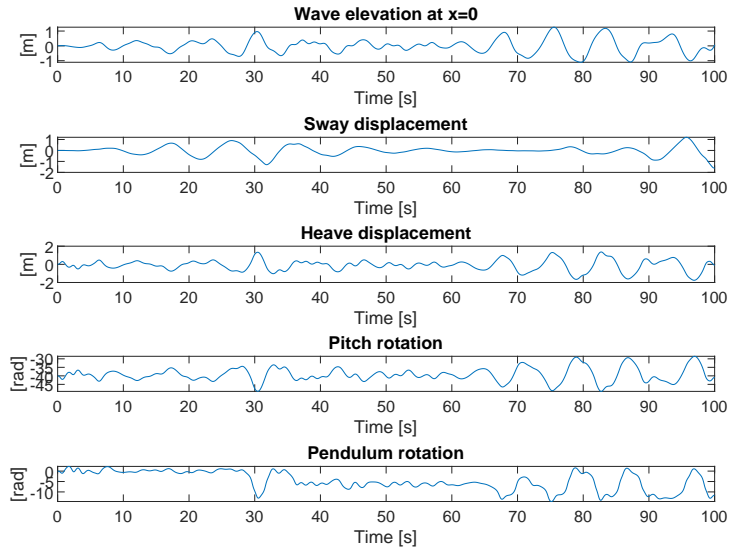
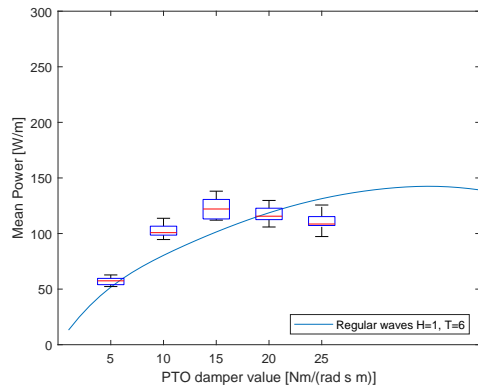


Figure 5.7: Irregular waves: model output $H_s = 2m$ $T_p = 8.5sec$

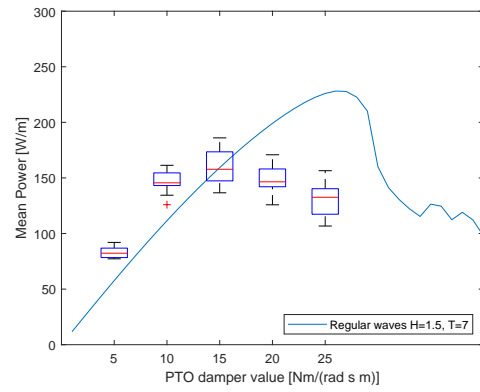
5.3 Optimizing the PTO damper for irregular waves

In regular waves, the model reaches a steady-state. For this steady-state, the PTO-damper can be optimized. In irregular waves it is harder to find the ideal PTO-damper value. Irregular waves are random, and if the simulation time is too short the produced power can be biased. To find the ideal PTO-damper value for a wave-height/period combination. Multiple simulations of 10 times the peak period were simulated. Each run is based on the same spectrum, but the phase shifts of the wave components are random each time. This is done for 5 different PTO damper values. Figure 5.8 shows the mean produced power of irregular waves based on the PTO setting and compares them with the ideal PTO-damper value for regular waves. This is done for 3 different sea-states. The blue lines are the resulting mean powers for regular waves and the box plots show the results of 10 simulations of each 10 times the peak period. For each new simulations new phase shifts are used.

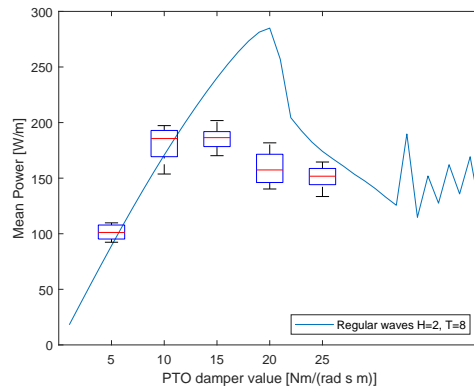
There are a few things that are noticeable from these figures. The first thing is that the mean power of the irregular waves is lower than that of the regular sea-states. That is logical because the power stored in an irregular sea is spread out in a range of frequencies. While the power in a regular sea-state is stored in one frequency. This means that the PTO-damper can be easily tuned to capture that power. This is not the case with irregular waves. The second thing that is noticeable is that the curve of the regular waves starts smooth and dips after a certain point. This is the point where the moment on the pendulum becomes too large and the pendulum starts making full rotations. This makes the behaviour of the pendulum hard to estimate and negatively influences the produced power. Lastly, the optimal PTO-damper value for irregular waves has a different, lower, value than that for the regular wave.



(a) $H_s=1\text{m}$ $T_p=6\text{sec}$



(b) $H_s=1.5\text{m}$ $T_p=7\text{sec}$



(c) $H_s=2\text{m}$ $T_p=8\text{sec}$

Figure 5.8: Mean power for different PTO-damper values for regular and irregular waves

To better understand the effect of a high or low PTO-value on the WEC, one wave pattern is created based on a sea-state of $H_s = 1\text{m}$ and $T_p = 6.5\text{sec}$. The model is run to generate the response of the WEC for 2 different PTO-damper values, 5 and $15 \frac{\text{Nm}}{(\text{rad/s})\text{m}}$. From the first it is known that it is under the optimal setting, and from the second it is known that it is close to the optimal. The results are given in figure 5.9.

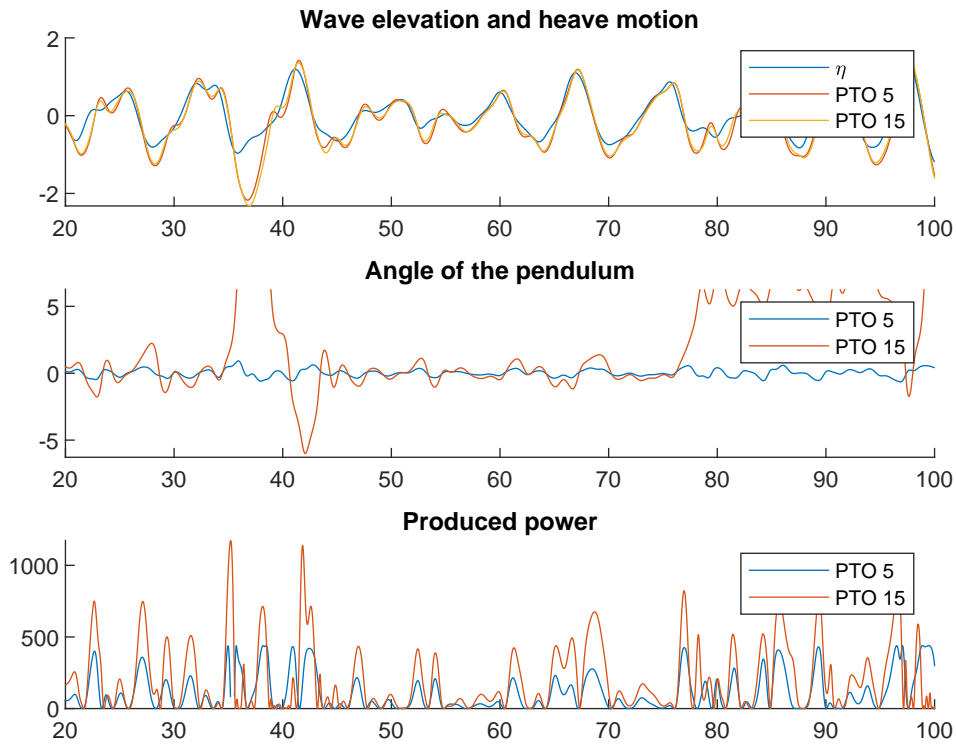


Figure 5.9: Compare two PTO settings

In the top plot of figure 5.9 is the wave elevation η shown together with the heave for both damper values. As expected, there is not much difference in heave motion. Just as with regular waves. The heave motion is not much affected by the damper value. In the middle plot is the angle of the pendulum plotted. And in the bottom plot, the produced power. If the angle of the pendulum becomes larger or smaller than 2π , it means that the pendulum made a full rotation. If we compare the power output and the angle of the pendulum it becomes clear that it is not a problem if the pendulum makes a full rotation with a high wave. There is also a spike in the produced power.

5.4 1:2 Scale model predictions

5.4.1 Froude scaling

Now that the hydrodynamic model is ready, it can be used to estimate the performance of a WEC with another scale. To obtain the results, the Froude scaling laws are used, see table 5.1 for the scaling laws. [27].

In the model, all the dimensions are scaled with the factors below. For example if one is interested in the heave motions of the WEC with a scale factor of $\lambda = 2$ and $\lambda = 3$. The wave height and length are scaled with a factor λ . The other parameters are kept equal. Then the response of the theoretical model also has to be scaled. For example, the heave output has to be scaled up with the factor λ , but also the power output has to be scaled but with a factor of $\lambda^{3.5}$.

Quantity	Scaling
Wave height and length	λ
Wave period	$\lambda^{.5}$
Wave frequency	$\lambda^{-.5}$
Linear displacement	λ
Angular displacement	1
Linear velocity	$\lambda^{.5}$
Angular velocity	$\lambda^{-.5}$
Linear acceleration	1
Angular acceleration	λ^{-1}
Mass	λ^3
Force	λ^3
Torque	λ^4
Power	$\lambda^{3.5}$
Linear damping	$\lambda^{2.5}$
Angular damping	$\lambda^{4.5}$

Table 5.1: Froude Scaling Laws

5.4.2 Power matrix

To gain an idea of the performance of the WEC a power matrix is constructed. A power matrix shows the expected generated mean power per meter width of the device in kW/m for an irregular sea-state with a significant wave height H_s and a peak period T_p . The absolute values in the power matrix have some uncertainties because of the uncertainties in the theoretical model. But as explained the theoretical model can give an indication if changes to the parameters of the WEC are an improvement for the produced power or not. Secondly finding the ideal PTO-damper value for each sea-state takes a lot of computation time. That is why the PTO-damper value is optimized for an irregular sea-state with $H_s = 1m$ and $T_p = 6.5sec$. This is the most frequent sea-state found at the L9 platform, as shown in figure 5.10. Next the waves are made smaller to review the responce of a bigger WEC. This is done for 3 different scale factors $\lambda = 1$, $\lambda = 2$ and $\lambda = 3$.

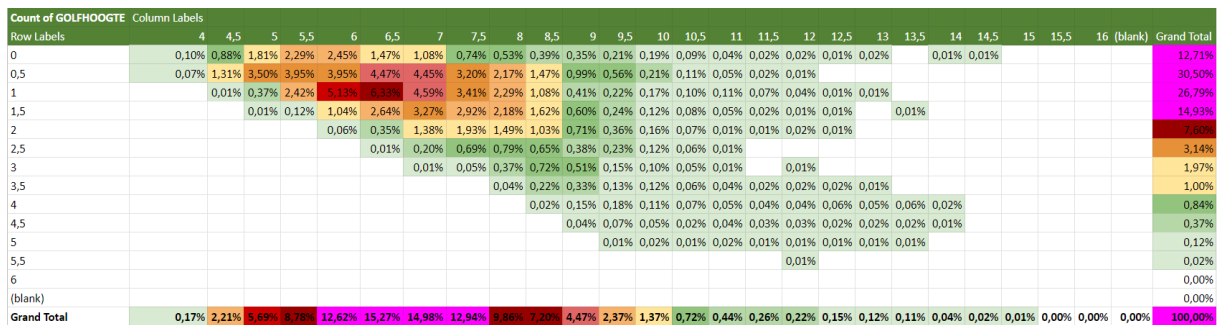


Figure 5.10: Wave scatter data for the L9 platform in the North Sea

Next to the power matrix is a matrix given that shows the energy capture ratios. This matrix indicates how much of the energy stored in waves is generated into electrical power. The amount of energy stored in an irregular sea per meter wave crest P_{wave} is expressed in equation 5.8, H_s is the significant wave height and T_p is the peak period or energy period. Deep water is assumed [27]. The energy capture ratio is the ratio between the power generated into electricity divided by the available power in the waves, see equation 5.9. This gives an indication of the efficiency of the WEC at different sea-states. Again the absolute values don't hold much value, but this does indicate what the optimal conditions are for the WEC to operate.

As shown in the figure 5.11, the highest produced powers are, as expected, obtained in the highest wave. These waves hold the most energy. But the highest energy capture ratios are found for the lowest waves with a low period. This indicates that the WEC is not optimized. Ideal would be if the highest energy capture ratios are found at the sea-states most frequent present in the wave scatter diagram shown in figure 5.10.

$$P_{wave} = \frac{\rho g^2}{64\pi} H_s^2 T_p \quad (5.8)$$

$$\eta = \frac{P_{mean}}{P_{wave}} \quad (5.9)$$

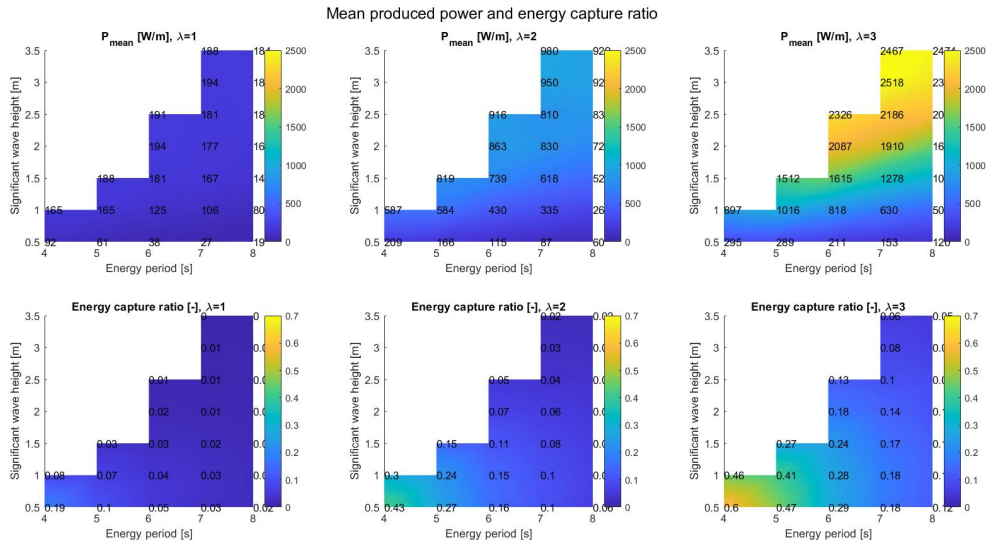


Figure 5.11: Mean produced power and the energy capture ratios for an irregular sea-state and different scale factors

5.4.3 Discussion

By using the theoretical model and the Froude scaling laws the power matrix of the Dutch Wave Power WEC is derived. It has to be noted that some of the wave-height/peak period combinations from this matrix will almost never occur in the real world. Secondly, the theoretical model has no real physical limitations. The lines are infinitely long and the WEC can make infinite full rotations. In real life, this is limited by the device put offshore.

Then there are some uncertainties in the average produced powers given in the power matrix. First, there is the uncertainty of the PTO system. The PTO system is estimated using a linear damper. As discussed in 4, this estimation gives some uncertainties. Also, the PTO values are estimated using regular waves. These values are close to the optimal value of irregular waves, but they can be optimized. This is not done because finding the optimal PTO value for irregular waves is a time-intensive process. Secondly, the average powers are estimated in simulations with 10 simulations, each 100 seconds. This only adds up to 1000 seconds of simulation for each significant wave height/peak period combination. This only adds up to 16min40sec. Due to the randomness of the irregular waves, this can still give some fluctuations in the average power. This can be solved by running longer simulations, but due to time restrictions, this was not possible. Thirdly, the powers given in the power matrix are in W per meter. The powers will probably go down if the WEC becomes longer. This is because the waves are not unidirectional. The longer the WEC becomes, the more this will negatively influence the performance of the WEC.

The power matrix indicates how much power is obtained from the waves according to the theoretical model. The energy capture ratios say something about the efficiency of the WEC at each specific sea-state.

The WEC with scale factor $\lambda = 3$ is already better tuned to capture the energy in a real sea-state than the original. This indicates that a bigger floater can give an increase in produced power. But more research is needed to find the optimal sizing for the WEC. Optimization is not the objective of this thesis.

Chapter 6

Conclusions & Recommendation

6.1 Conclusions

Wave energy converters are a source of renewable energy with a lot of potential, but they are underdeveloped with respect to more mature renewable energy technologies like solar and wind. Dutch Wave Power is one company that tries to bridge this knowledge gap and is developing a new type of WEC. The objective of this thesis was to understand the working principle and the effects influencing the dynamics and power production of their concept. This is done by constructing a numerical time domain model.

The numerical model is constructed with an analytical non-linear Froude-Krylov force approximation to capture the large change in draft of the model. The results of the numerical model have an error of 14% in pitching amplitude with respect to the experimental tests for a wave period of 6 seconds and the accuracy goes up for waves with a higher wave period. The dynamics of the inside pendulum can be estimated with an error of less than 2% for the angle of the pendulum. This is done with use of a linear damper that represents the PTO-system. The value of the linear damper is first tuned to match the experiments. Secondly, the linear damper is tuned to find the maximum power extraction.

After analyzing the results it is found that the main driver for the pitching motions and thus the power production come from the heaving motions. The surge motions have little influence on the power production. The surge motions are also overestimated with an error of more than 50%. It is expected that the reason for this is that the ballast weight is estimated as a downward pulling force and the forces acting on the ballast weight itself are neglected. Secondly, one of the driving forces in the surge direction is neglected. The FK forces in surge are neglected due to the analytical estimation. The resulting pressure at the seaward and leeward sides of the WEC are equal to each other. Nevertheless, it is expected that this will only influence the dynamics, because it is shown that the forces in surge are of a different, smaller, order than the driving forces in heave.

The numerical model lends itself to research whether changing design parameters of the WEC improves or worsens power production, although the mean produced power is not well estimated. The linear damper used as estimation for the generator is capable of estimating the dynamics, but not in estimating the produced power. This is due to the torque losses in the shaft.

The two parameters that were studied are the weight of the pendulum and the inner radius of the float. Firstly, increasing the weight of the pendulum also increases the maximum torque inside the generator before the pendulum makes a full rotation. This higher torque gives a higher power output in return. The model predicts an increase in mean produced power of 35% if the pendulum is made 15kg/m heavier and if the PTO damper is tuned correctly. Secondly, decreasing the inner radius of the float, increases the rotational pitching velocity. This higher velocity results in a higher power output. It has to be noted that the system becomes more sensitive to high torques and a full rotation occurs faster. This means that the tuning of the PTO system becomes even more important. If the PTO damper is tuned, the model predicts up to 23% higher mean produced power according to the model and for the sea states tested.

Lastly, the numerical model is adapted to capture the response in irregular waves. For irregular waves,

three sizes of the WEC are tested. The dimensions and parameters are scaled according to the Froude scaling laws. The scaling factors used are $\lambda = 1$, $\lambda = 2$ and $\lambda = 3$. Optimizing the PTO-system for an irregular sea-state is a time-consuming task. That is why for each scale factor the PTO system is tuned for only one sea-state. Increasing the size of the WEC with a scale factor of $\lambda = 3$ increases the produced power with a factor between 3 and 14.

6.2 Recommendations

To conclude this thesis, some recommendations are made. The recommendations can be split into 2 parts. One are recommendations to improve the numerical model. The other are recommendations for further research.

6.2.1 Recommendations - numerical model

The biggest improvement for the numerical model can be gained by improving the PTO-system. The linear damper works if only the dynamics are estimated, but evenly important is the produced power. It would already be an improvement to implement some torque losses, but it would be even better to find a model that could capture the non-linear behaviour of the generator.

The second improvement in the numerical model can be made by estimating the forces balance in surge. There is a 50% error in the amplitude of the surge motion and one of the main driving forces, the FK force, in surge direction is neglected. Furthermore, the ballast weight moving through the water is expected to influence the surge motion.

6.2.2 Recommendations - Further research

It would be interesting to see the effects of wave spreading to the WEC. How is the response influenced by incoming waves under an angle? And how is this effect influenced by the length of the float?

Secondly, further research is needed to find the optimal dimensions of the WEC, including the desired weights of the float and pendulum. This optimizing must go hand in hand with designing the PTO-system and is dependent of the location where the WEC will be installed.

Bibliography

- [1] J. Falnes, “A review of wave-energy extraction,” 10 2007.
- [2] G. Mørk, S. Barstow, A. Kabuth, and M. T. Pontes, “Assessing the global wave energy potential,” in *Proceedings of the International Conference on Offshore Mechanics and Arctic Engineering - OMAE*, vol. 3, pp. 447–454, 2010.
- [3] M. A. U. Amir, R. M. Sharip, M. A. Muzanni, and H. A. Anuar, “Wave energy convertors (WEC): A review of the technology and power generation,” in *AIP Conference Proceedings*, vol. 1775, American Institute of Physics Inc., 10 2016.
- [4] Y. Li and Y. H. Yu, “A synthesis of numerical methods for modeling wave energy converter-point absorbers,” 8 2012.
- [5] L. Rodrigues, “Wave power conversion systems for electrical energy production,” *Renewable Energy and Power Quality Journal*, vol. 1, pp. 601–607, 3 2008.
- [6] A. De Andres, E. Medina-Lopez, D. Crooks, O. Roberts, and H. Jeffrey, “On the reversed LCOE calculation: Design constraints for wave energy commercialization,” *International Journal of Marine Energy*, vol. 18, pp. 88–108, 6 2017.
- [7] E. Rusu and F. Onea, “A review of the technologies for wave energy extraction,” 6 2018.
- [8] T. Aderinto and H. Li, “Ocean Wave energy converters: Status and challenges,” 2018.
- [9] J. Aubry, H. Ben Ahmed, B. Multon, A. Babarit, and A. Clément, “Wave energy converters. Bernard Multon. Marine renewable energy handbook,” 2011.
- [10] P. Ricci, “Time-Domain Models,” in *Numerical Modelling of Wave Energy Converters*, pp. 31–66, Elsevier, 2016.
- [11] A. S. Zurkinden and M. M. Kramer, “Numerical time integration methods for a point absorber wave energy converter,” tech. rep.
- [12] A. Babarit, J. Hals, M. J. Muliawan, A. Kurniawan, T. Moan, and J. Krokstad, “Numerical benchmarking study of a selection of wave energy converters,” *Renewable Energy*, vol. 41, pp. 44–63, 2012.
- [13] B. Bosma, T. K. Brekken, H. T. Özkan-Haller, and S. C. Yim, “Wave energy converter modeling in the time domain: A design guide,” in *2013 1st IEEE Conference on Technologies for Sustainability, SusTech 2013*, pp. 103–108, 2013.
- [14] R. G. Coe and V. S. Neary, “REVIEW OF METHODS FOR MODELING WAVE ENERGY CONVERTER SURVIVAL IN EXTREME SEA STATES,” tech. rep., 2014.
- [15] M. Alves, “Frequency-Domain Models,” in *Numerical Modelling of Wave Energy Converters*, pp. 11–30, Elsevier, 2016.
- [16] M. P. Retes, G. Giorgi, and J. V. Ringwood, “A Review of Non-Linear Approaches for Wave Energy Converter Modelling,” tech. rep., 2015.
- [17] A. S. Zurkinden, F. Ferri, S. Beatty, J. P. Kofoed, and M. M. Kramer, “Non-linear numerical modeling and experimental testing of a point absorber wave energy converter,” *Ocean Engineering*, vol. 78, pp. 11–21, 3 2014.

- [18] G. Giorgi and J. V. Ringwood, “Analytical formulation of nonlinear froude-krylov forces for surging-heaving-pitching point absorbers,” in *Proceedings of the International Conference on Offshore Mechanics and Arctic Engineering - OMAE*, vol. 10, American Society of Mechanical Engineers (ASME), 2018.
- [19] G. Giorgi and J. V. Ringwood, “Computationally efficient nonlinear Froude–Krylov force calculations for heaving axisymmetric wave energy point absorbers,” *Journal of Ocean Engineering and Marine Energy*, vol. 3, pp. 21–33, 2 2017.
- [20] D. Josh and C. Ronan, “Efficient nonlinear hydrodynamic models for wave energy converter design-A scoping study,” 1 2020.
- [21] Cummins WE, “The impulse response function and ship motions,” *Hydromechanics laboratory research and development report*, 1962.
- [22] Z. Yu and J. Falnes, “State-space modelling of a vertical cylinder in heave,” tech. rep., 1995.
- [23] C. Liu, Q. Yang, and G. Bao, “State-space approximation of convolution term in time domain analysis of a raft-type wave energy converter,” *Energies*, vol. 11, 1 2018.
- [24] R. Taghipour, T. Perez, and T. Moan, “Hybrid frequency-time domain models for dynamic response analysis of marine structures,” *Ocean Engineering*, vol. 35, pp. 685–705, 5 2008.
- [25] J. A. Armesto, R. Guanche, F. Jesus, A. Iturrioz, and I. J. Losada, “Comparative analysis of the methods to compute the radiation term in Cummins’ equation,” *Journal of Ocean Engineering and Marine Energy*, vol. 1, pp. 377–393, 11 2015.
- [26] M. A. Bhinder, A. Babarit, L. Gentaz, and P. Ferrant, “Assessment of viscous damping via 3D-CFD modelling of a Floating Wave Energy Device Assessment of the Viscous Damping via 3D-CFD Modelling of a Floating Wave Energy Device,” tech. rep., 2011.
- [27] J. M. J. Journée, W. W. Massie, and R. H. M. Huijsmans, “OFFSHORE HYDROMECHANICS Third Edition,” tech. rep., 2015.
- [28] A. H. Tanis, *The Ocean Cleanup Barrier: A hydro-elastic model for fatigue lifetime assessment of The Ocean Cleanup barrier*. PhD thesis, 2016.
- [29] Senan NAF, “A brief introduction to using ode45 in MATLAB,”
- [30] “SALOME-platform,” 2022.
- [31] F. Kalofotias, “Manual for the open source potential solver: NEMOH Derivation of potentials and drift forces for a semi-submersed heaving sphere,” tech. rep., 2017.
- [32] T. Duarte, A. Sarmento, M. Alves, J. Jonkman, and A. Sarmento, “State-Space Realization of the Wave-Radiation Force within FAST: Preprint,” tech. rep., 2013.
- [33] T. Perez and T. I. Fossen, “A Matlab toolbox for parametric identification of radiation-force models of ships and offshore structures,” *Modeling, Identification and Control*, vol. 30, no. 1, pp. 1–15, 2009.
- [34] Anthony F. Molland, “Chapter 1 - The marine Environment,” tech. rep., 2008.
- [35] Pecher A and Kofoed JP, *Handbook of ocean wave energy*. 2017.

APPENDICES

Appendix A

Equations of motion of the WEC

Equation of motion in the x-direction:

$$m_1 \ddot{x} = \sum F_x - \sin(\alpha) F_T \quad (\text{A.1})$$

Equation of motion in the z-direction:

$$m_1 \ddot{z} = \sum F_z - \cos(\alpha) F_T \quad (\text{A.2})$$

Kinetic constraints:

$$\sigma(t) = -l(t)r_{in} \quad (\text{A.3})$$

$$\dot{\sigma} = -\dot{l}r_{in} \quad (\text{A.4})$$

$$\ddot{\sigma} = -\ddot{l}r_{in} \quad (\text{A.5})$$

With:

$$l(t)^2 = x(t)^2 + (l_0 + z(t))^2 \quad (\text{A.6})$$

$$\frac{d}{dt}[l(t)^2] = 2l(t)\dot{l} = 2x(t)\dot{x} + 2(l_0 + z(t))\dot{z} \quad (\text{A.7})$$

$$\frac{d^2}{dt^2}[l(t)^2] = 2\dot{l}^2 + 2l(t)\ddot{l} = 2\dot{x}^2 + 2x(t)\ddot{x} + 2\dot{z}^2 + 2(l_0 + z(t))\ddot{z} \quad (\text{A.8})$$

This can be rewritten as:

$$l(x) = \sqrt{x(t)^2 + (l_0 + z(t))^2} \quad (\text{A.9})$$

$$\dot{l} = \frac{2x(t)\dot{x} + 2(l_0 + z(t))\dot{z}}{2l(t)} \quad (\text{A.10})$$

$$\ddot{l} = \frac{2\dot{x}^2 + 2x(t)\ddot{x} + 2(l_0 + z(t))\ddot{z} - 2\dot{l}^2}{2l(t)} \quad (\text{A.11})$$

The angle alpha:

$$\tan(\alpha) = \frac{x(t)}{l_0 + z(t)} \quad (\text{A.12})$$

Appendix B

Derivation of the pendulum angle θ

Equation of motion for the angle θ . Lagrangian derivation of a pendulum on a moving support.

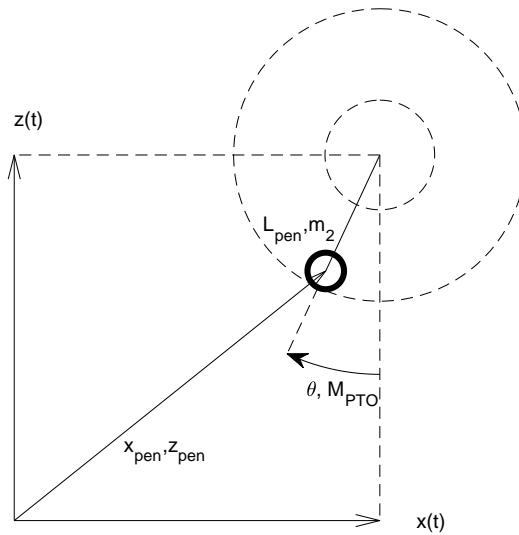


Figure B.1: Pendulum on a moving support

A pendulum with mass m_2 and length L_{pen} , is connected to a support that can move in the x, z plane. The position of the pendulum is described by θ . The x and z positions of pendulum are:

- $x_{pen} = x(t) - L_{pen} \sin(\theta) \rightarrow \dot{x}_{pen} = \dot{x} - L_{pen} \dot{\theta} \cos(\theta)$
- $z_{pen} = z - L_{pen} \cos(\theta) \rightarrow \dot{z}_{pen} = \dot{z} + L_{pen} \dot{\theta} \sin(\theta)$

Now the kinetic energy of the system is:

$$T = 1/2 m_1 (\dot{x}^2 + \dot{z}^2) + 1/2 m_2 (\dot{x}_{pen}^2 + \dot{z}_{pen}^2) \quad (\text{B.1})$$

And the potential energy is:

$$V = m_1 g z + m_2 g z_{pen} \quad (\text{B.2})$$

and to include the external force:

$$R = 1/2 B_{PTO} (\dot{\theta} - \dot{\sigma})^2 \quad (\text{B.3})$$

Now find the equation of motion for θ :

$$L = T - V \quad (\text{B.4})$$

$$\frac{d}{dt} \frac{\partial L}{\partial \dot{\theta}} - \frac{\partial L}{\partial \theta} + \frac{\partial R}{\partial \dot{\theta}} = 0 \quad (\text{B.5})$$

$$\frac{d}{dt} \frac{\partial L}{\partial \dot{\theta}} = m_2 L_{pen} \frac{d}{dt} [-\dot{x} \cos(\theta) + \dot{z} \sin(\theta) + L_{pen} \dot{\theta}] \quad (\text{B.6})$$

$$\frac{d}{dt} \frac{\partial L}{\partial \dot{\theta}} = m_2 L_{pen} (-\ddot{x} \cos(\theta) + \dot{x} \sin(\theta) \dot{\theta} + \ddot{z} \sin(\theta) + \dot{z} \cos(\theta) \dot{\theta} + L_{pen} \ddot{\theta}) \quad (\text{B.7})$$

$$\frac{\partial L}{\partial \theta} = m_2 L_{pen} (\dot{x} \sin(\theta) \dot{\theta} + \dot{z} \cos(\theta) \dot{\theta} + g \sin(\theta)) \quad (\text{B.8})$$

$$\frac{\partial R}{\partial \dot{\theta}} = B_{PTO} (\dot{\theta} - \dot{\sigma}) \quad (\text{B.9})$$

Fill in into equation B.5:

$$m_2 L_{pen} (-\ddot{x} \cos(\theta) + \ddot{z} L_{pen} \sin(\theta) + L_{pen}^2 \ddot{\theta} - g \sin(\theta) + B_{PTO} (\dot{\theta} - \dot{\sigma})) = 0 \quad (\text{B.10})$$

Rewrite the equation B.10 gives the equation of motion for θ :

$$\ddot{\theta} = \frac{\ddot{x} \cos(\theta)}{L_{pen}} + \frac{(g - \ddot{z}) \sin(\theta)}{L_{pen}} - \frac{B_{PTO} (\dot{\theta} - \dot{\sigma})}{m_2 L_{pen}} \quad (\text{B.11})$$

Appendix C

Derivation Line Tension

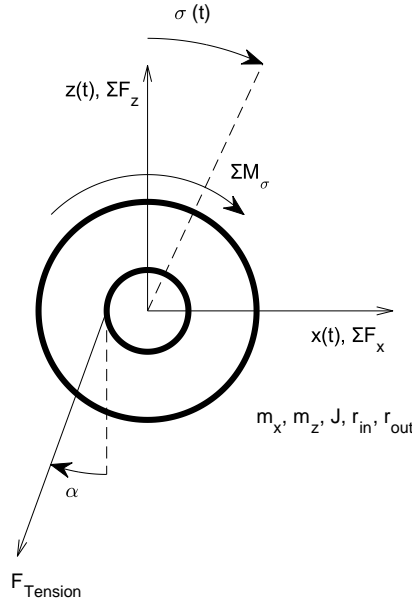


Figure C.1: Solve the F_T in 2D

There are 3 equations of motion

$$m_x \ddot{x} = \sum F_x - \sin(\alpha) F_T \quad (\text{C.1})$$

$$m_z \ddot{z} = \sum F_z - \cos(\alpha) F_T \quad (\text{C.2})$$

$$J \ddot{\sigma} = \sum M_\sigma - F_T r_{in} \quad (\text{C.3})$$

And the constraint

$$\ddot{\sigma} = -\frac{\ddot{l}}{r_{in}} \quad (\text{C.4})$$

where $l(t)$ is the length of the line.

$$l(t) = \sqrt{x(t)^2 + (l_0 + z(t))^2} \quad (\text{C.5})$$

In the equations A.9 too A.11 \dot{l} is know. Substitute equation A.11 into the constraint (equation C.4) and substitute the constrain into equation C.3. Next isolate the tension force F_T to obtain the following expression:

$$F_T = \frac{\sum M_\sigma l(t) r_{in} m_x m_z - J \dot{l}^2 m_x m_z + J \dot{x}^2 m_x m_z + J \dot{z} m_x m_z + J x(t) \sum F_x m_z + J z(t) \sum F_z m_x + l_0 J \sum F_z m_x}{l(t) m_x m_z r_{in}^2 + J \cos(\alpha) m_x z(t) + J \sin(\alpha) x(t) m_z + l_0 J \cos(\alpha) m_x} \quad (\text{C.6})$$

Appendix D

Experimental Test results - Unprocessed data

	Wave height [m]	Wave period [s]	Load on the generator [Ω]	Figure	Comments
Test 1	1	6	8	D.1	
Test 2	1	6	12	D.2	
Test 3	1	7	8	D.3	
Test 4	1	7	12	D.4	
Test 5	1	8	8	D.5	
Test 6	1	8	12	D.6	
Test 7	1	9	8	D.7	

Table D.1: List of experimental tests, parameters and corresponding figures

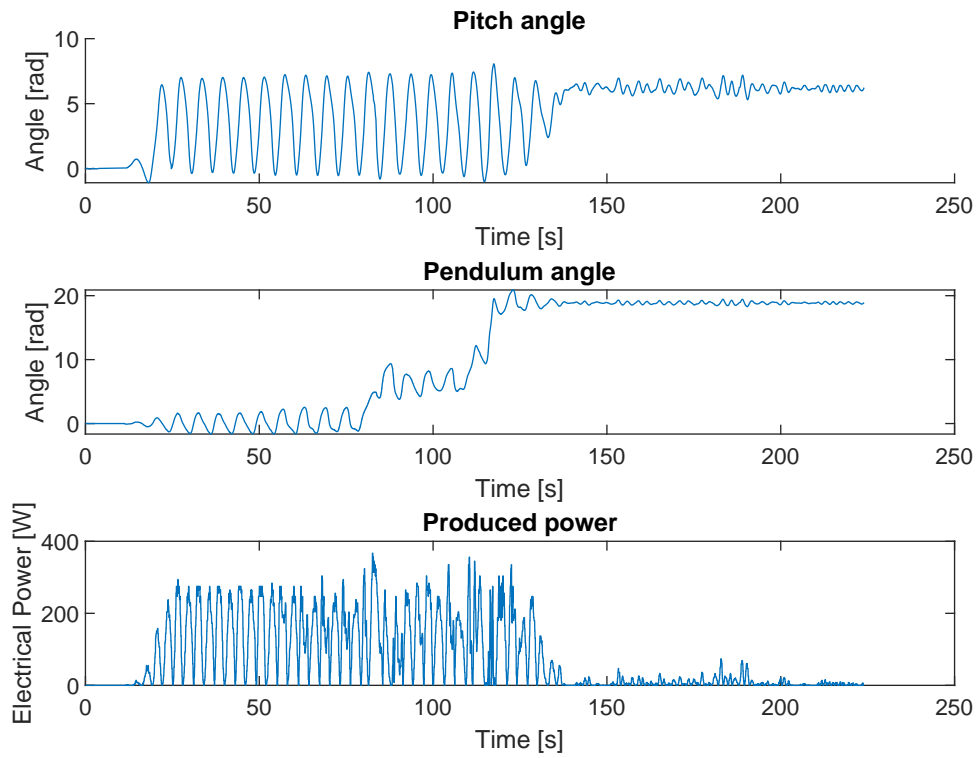


Figure D.1: Unprocessed data Test 1: $H=1\text{m}$ $T=6\text{sec}$ Load=80Ohm

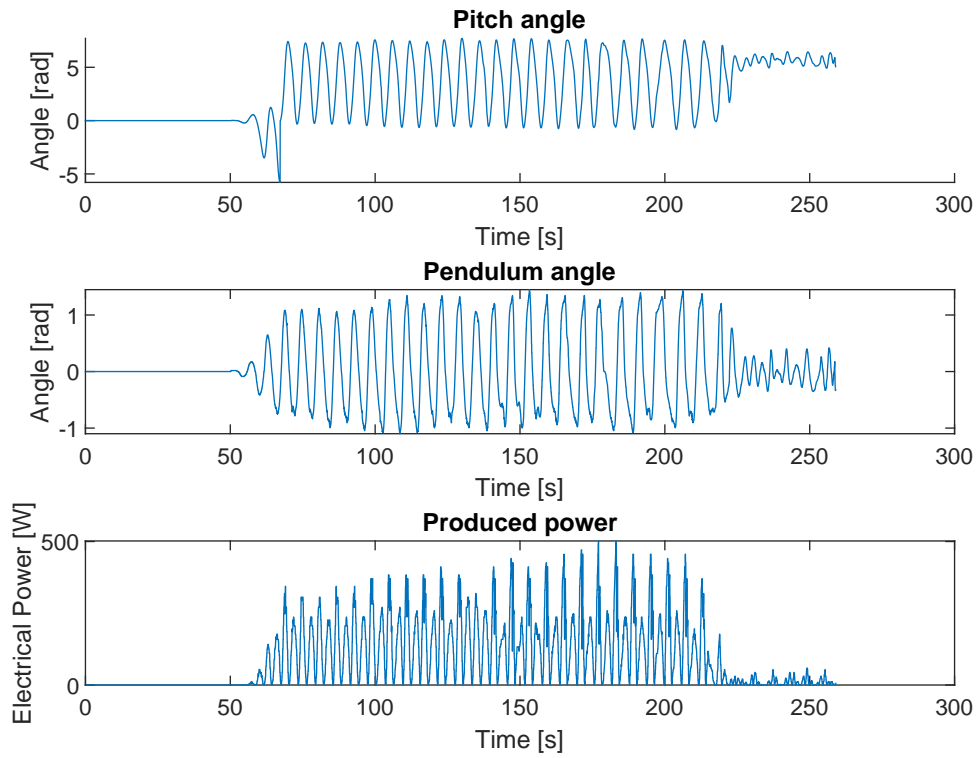


Figure D.2: Unprocessed data Test 2: $H=1\text{m}$ $T=6\text{sec}$ Load=120Ohm

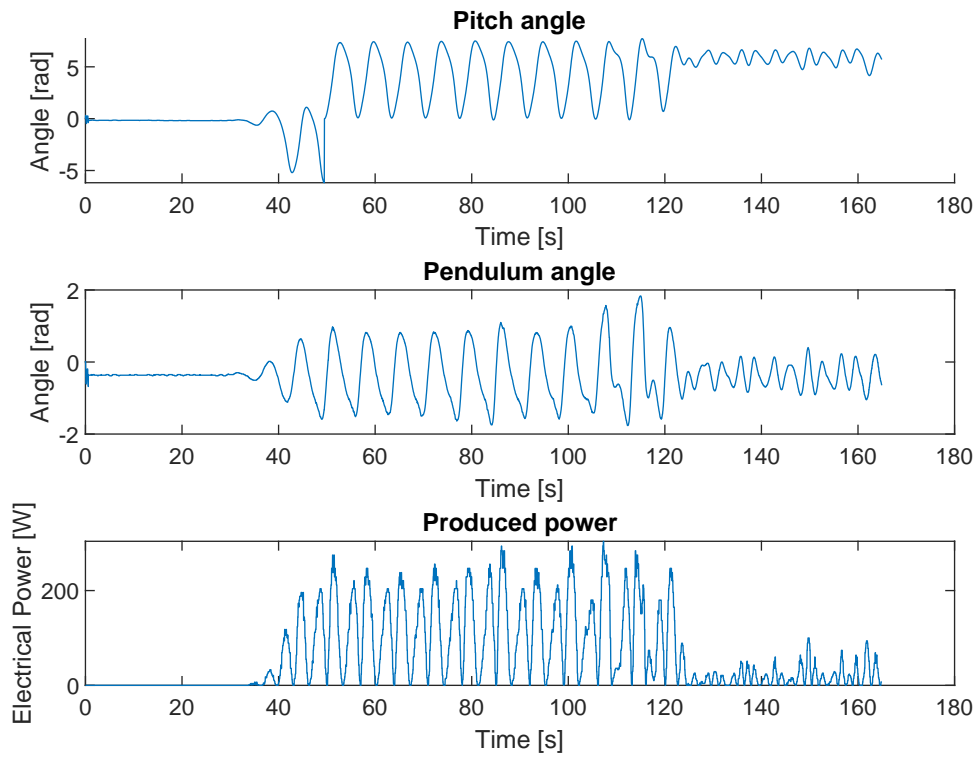


Figure D.3: Unprocessed data Test 3: H=1m T=7sec Load=80hm

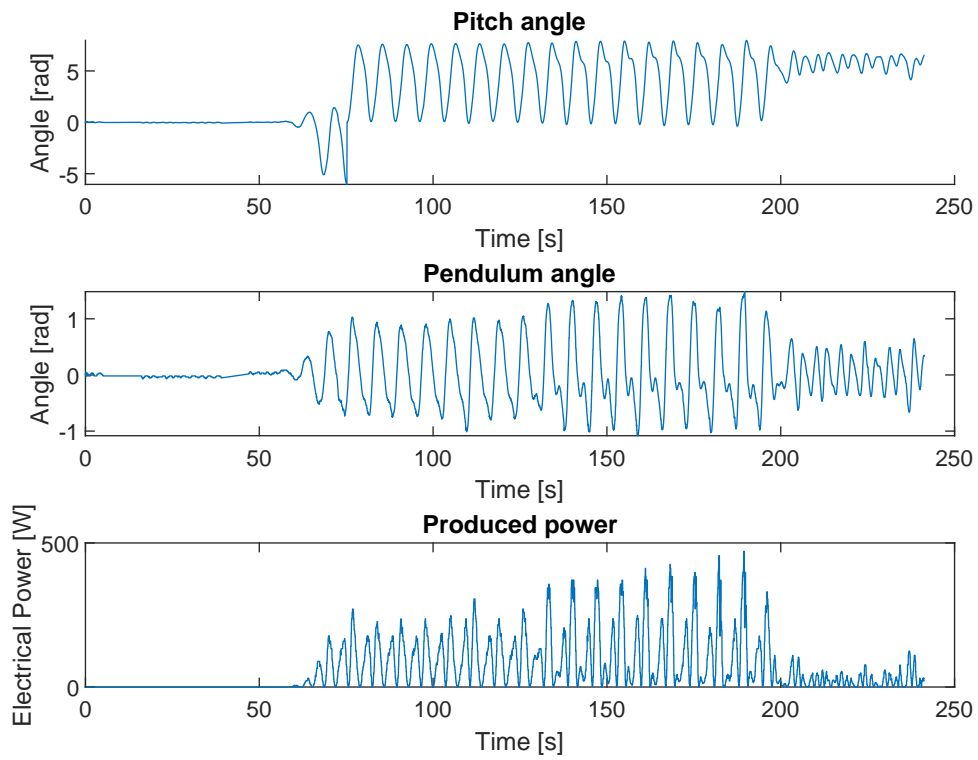


Figure D.4: Unprocessed data Test 4: H=1m T=7sec Load=120hm

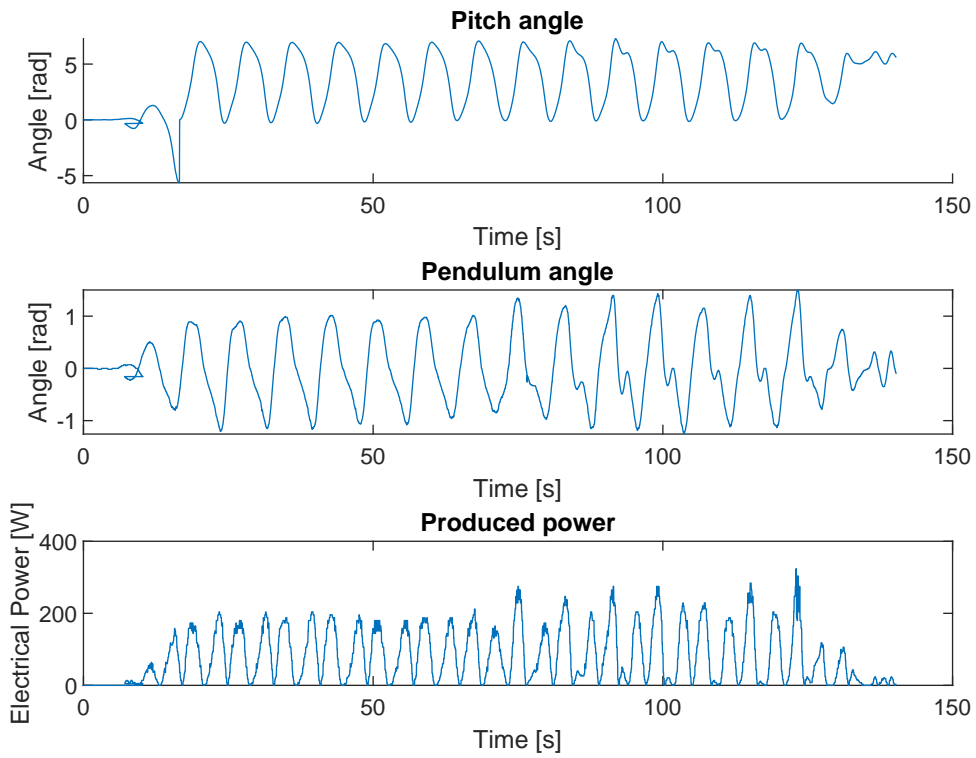


Figure D.5: Unprocessed data Test 5: H=1m T=8sec Load=80Ohm

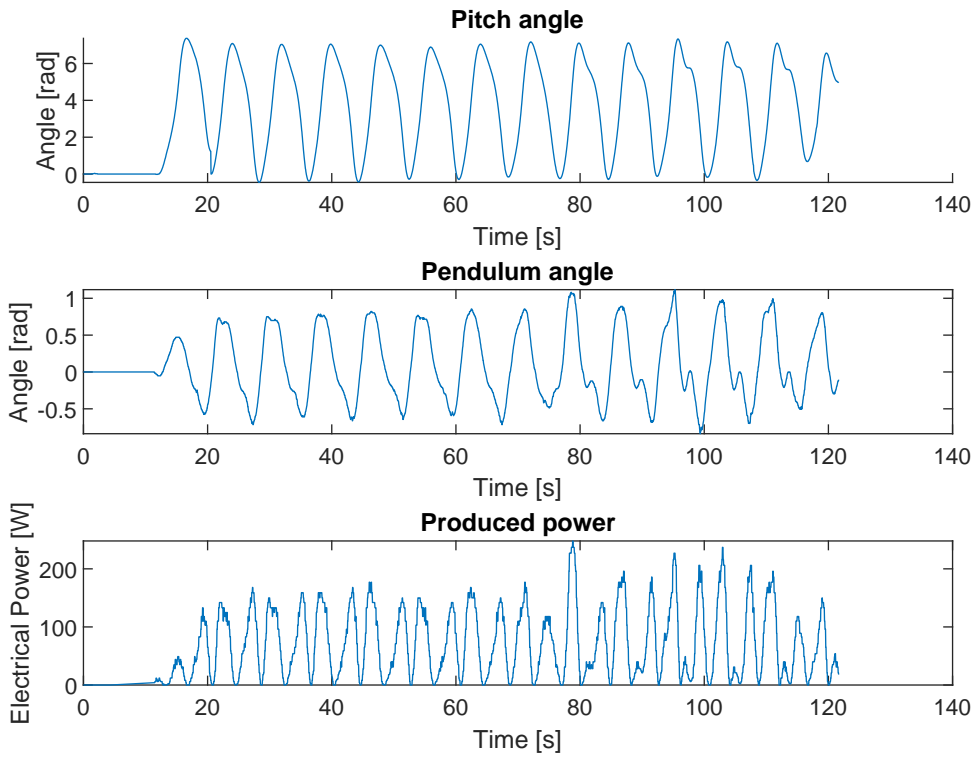


Figure D.6: Unprocessed data Test 6: H=1m T=8sec Load=120Ohm

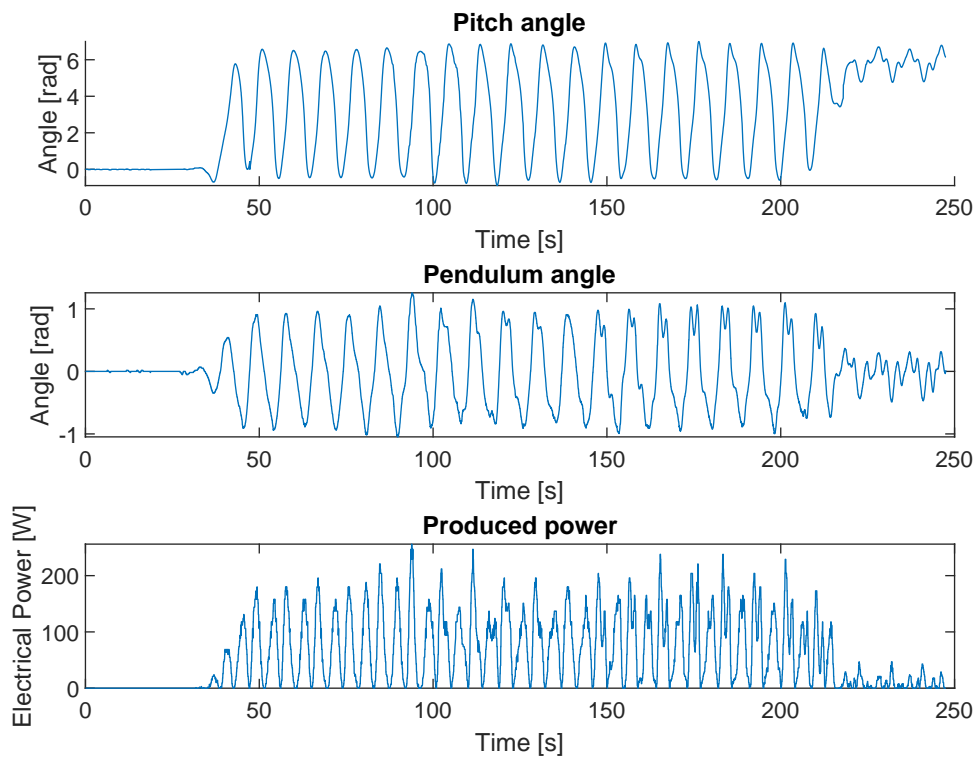


Figure D.7: Unprocessed data Test 7: H=1m T=9sec Load=80hm

Appendix E

Experimental Test results - Comparison with the theoretical model

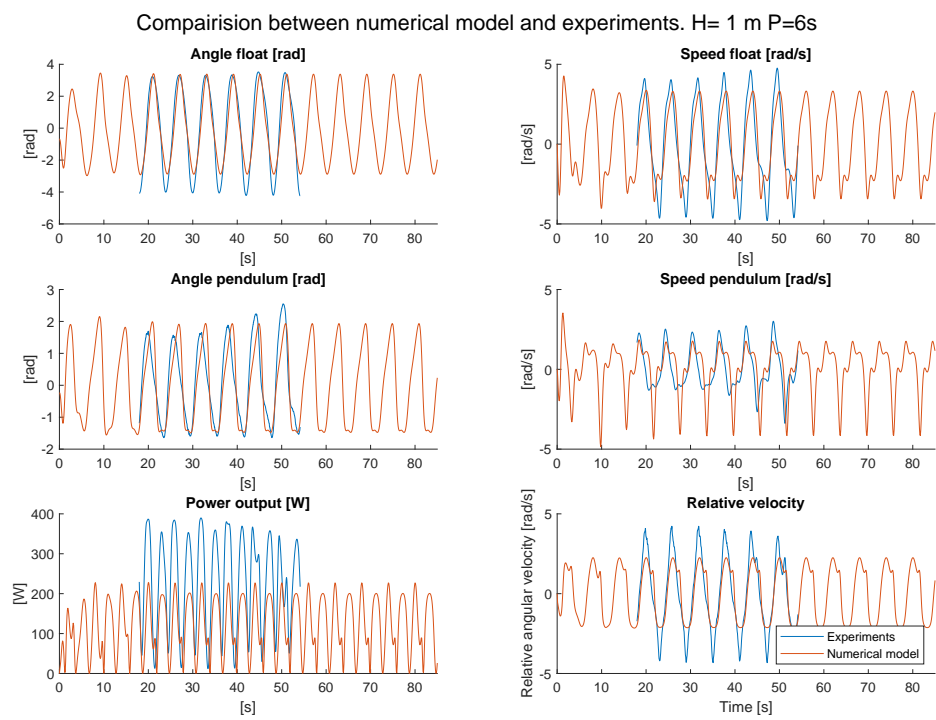


Figure E.1: Comparison of Test 1 with the theoretical model

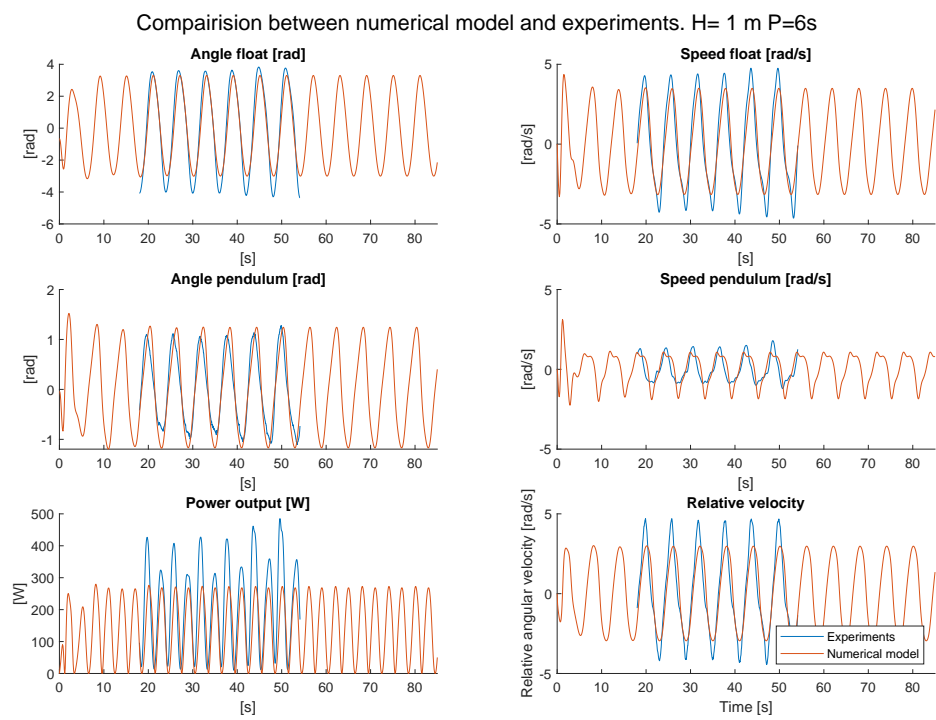


Figure E.2: Comparison of Test 2 with the theoretical model

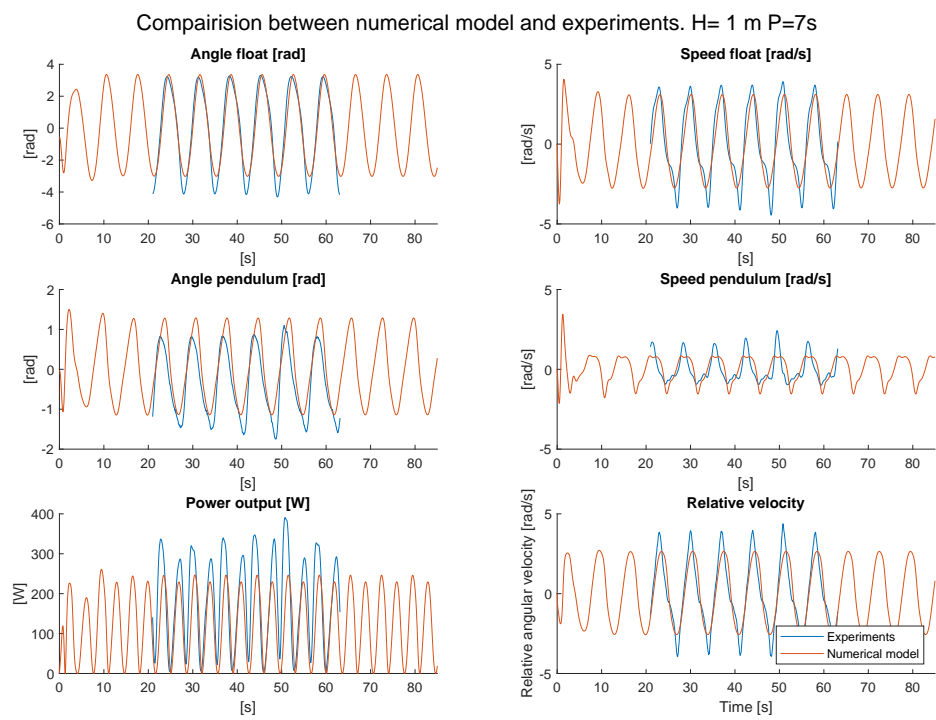


Figure E.3: Comparison of Test 3 with the theoretical model

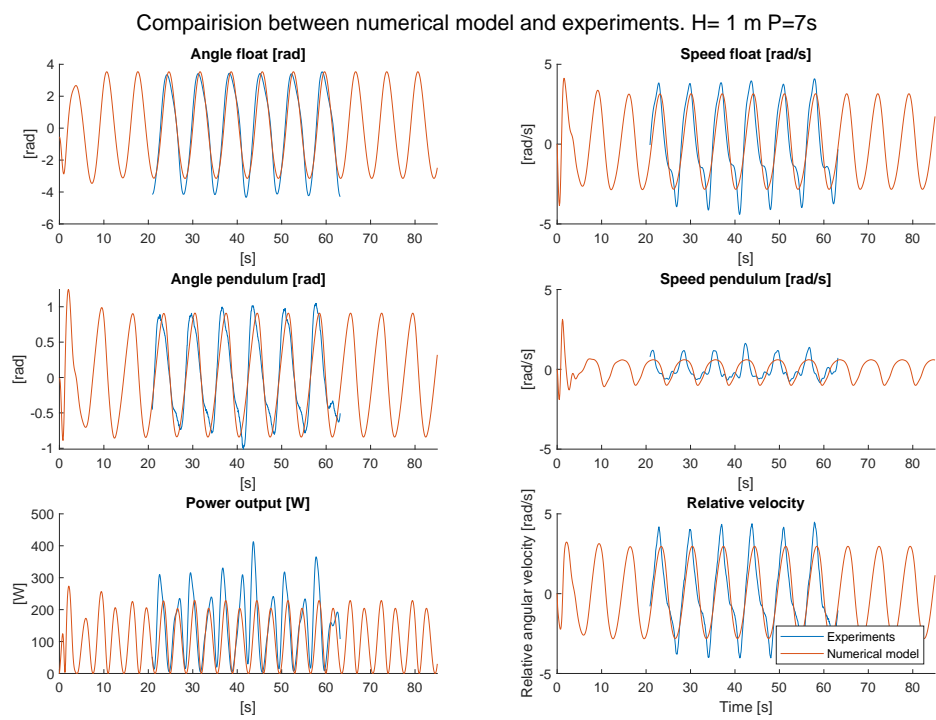


Figure E.4: Comparison of Test 4 with the theoretical model

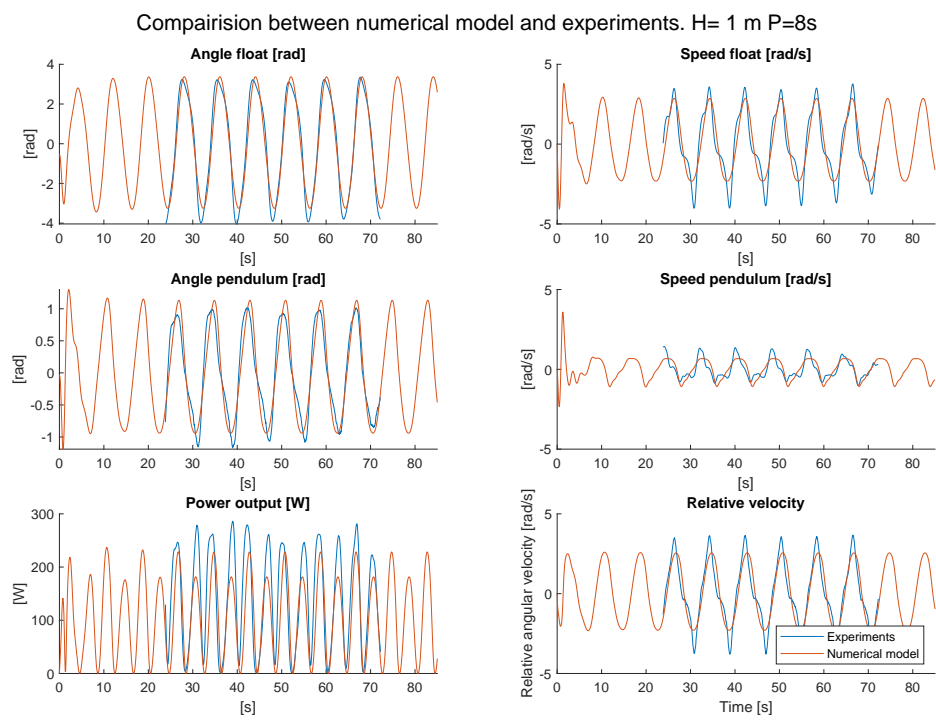


Figure E.5: Comparison of Test 5 with the theoretical model

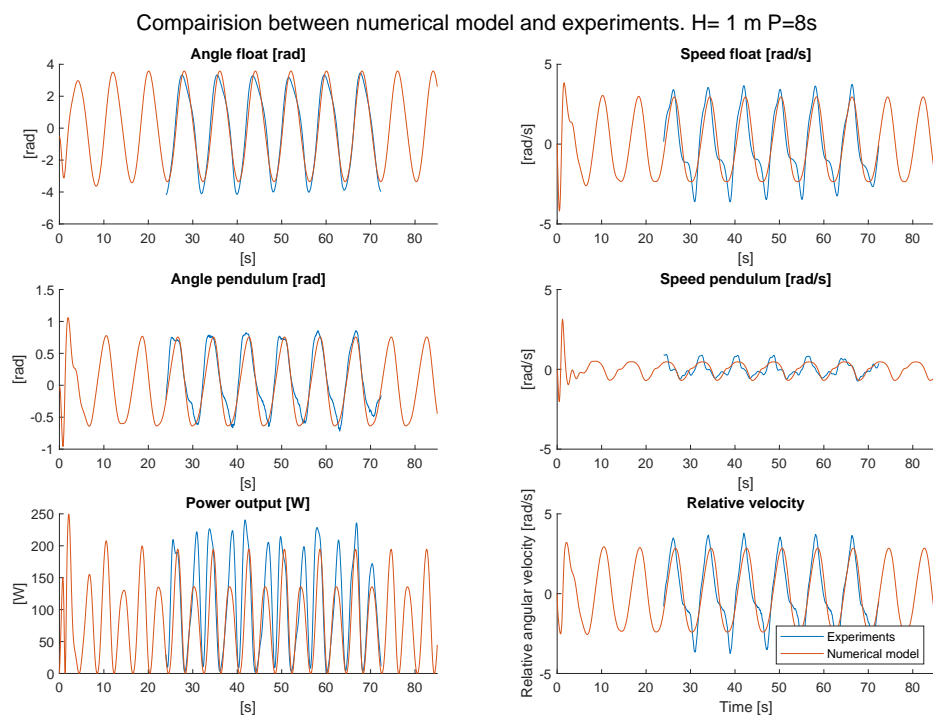


Figure E.6: Comparison of Test 6 with the theoretical model

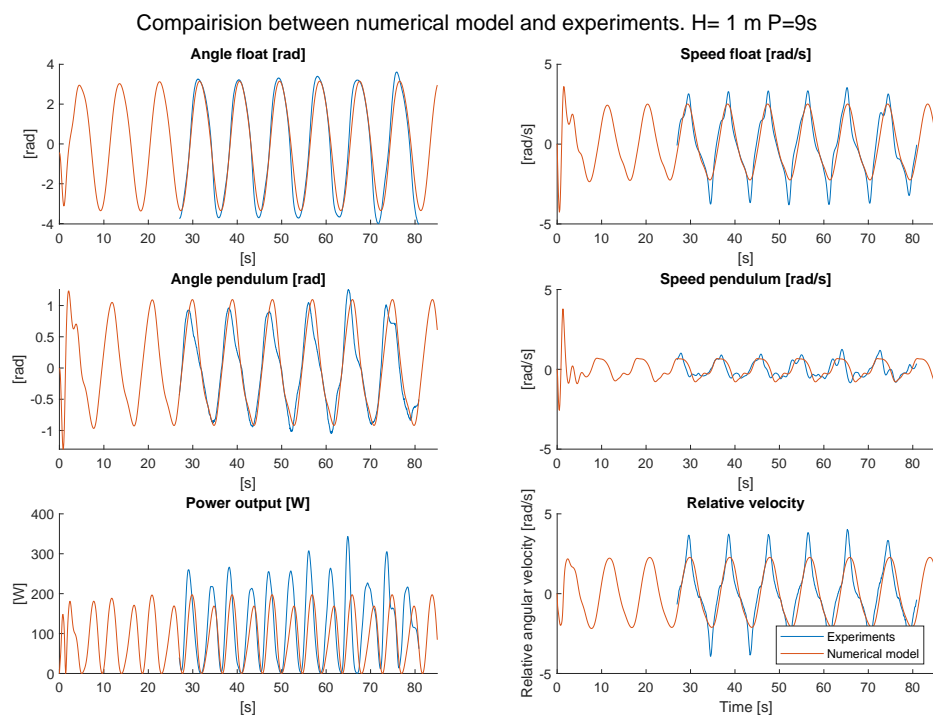


Figure E.7: Comparison of Test 7 with the theoretical model